UNIVERSITÀ
DEGLI STUDI
FIRENZE

DOTTORATO DI RICERCA
INTERNATIONAL DOCTORATE IN STRUCTURAL BIOLOGY

CICLO XXXIII

COORDINATOR Prof. Lucia Banci

Functional and structural elucidation of the mitochondrial Fe/S protein network

Settore Scientifico Disciplinare CHIM/03

PhD student
Dott. *Dafne Suraci*

Tutor
Prof. *Lucia Banci*

Coordinator
Prof. Lucia Banci

2017 – 2020

This thesis has been approved by the University of Florence, the University of Frankfurt and the Utrecht University

Universiteit Utrecht

CERM Firenze

FRANKFURT AM MAIN

Rare sono le persone che usano la mente, poche coloro che usano il cuore e uniche coloro che usano entrambi

Rita Levi-Montalcini

A mia madre

CONTENTS

1 INTRODUCTION

1.1 THE ROLE OF IRON-SULFUR CLUSTERS IN HUMAN CELLS

Billions of years ago organisms evolved using various systems to protect themselves through anaerobic and aerobic atmosphere. Iron sulfur clusters (ISCs) are one of the oldest cofactors known in biology and these clusters have been proposed to have had a critical role in the formation of early metabolic pathways used by primitive organisms[1]. To maintain these cofactors after transformation of the atmosphere into an oxidative and aerobic one (which does not support the formation, neither the stability of ISCs) the organisms evolved a whole set of proteins to coordinate a safe, efficient and specific biogenesis of these metal cofactors. Indeed, metabolism in nowadays living organisms is strictly dependent on a large share of enzymes which coordinate metal ions in their active site, not only to carry out their functions, but also to maintain tertiary/quaternary structures and to mediate protein-protein interactions[2,3]. ISCs versatile chemical properties have fostered their pervasive use in all organisms to execute an impressive number of reactions in fundamental cellular processes such as respiration, photosynthesis, metabolism and nitrogen fixation[4]. Eukariotic organisms feature complex and quite sophisticated mechanisms conserved from *Saccharomyces cerevisiae* to humans, which regulate metals homeostasis and trafficking between and inside living cells. Each individual essential metal has specific and very selective transport systems, i.e. shuttle proteins called chaperones, that ensure proper metal delivery to target apoproteins[5,6]. The amount of readily available metal ions in the cell, in the form of free aquo-complexes or labily bound to small molecules, is highly controlled and maintained in low concentration, or, in some instances, approximately to zero[7,8]. Otherwise, it is possible that improper biogenesis of ISCAs and presence of free metal ions may produce highly toxic reactive oxygen species (ROS)[9].

The iron ion of the ISC clusters is typically coordinated by the sulfur of protein-bound cysteine residues or by the nitrogen of histidine residues, but in rare cases other amino acid residues or cofactors such as S-adenosylmethionine (SAM) or Glutathione (GSH) are used as coordinating ligands[10]. These cofactors are composed of iron and inorganic sulfur, most frequently found in a rhombic [2Fe-2S] and a cubane [4Fe-4S] cluster forms. The first ones are present in enzymes such as mammalian ferrochetalase, in mitochondrial respiratory complexes I and II, in ferredoxins and Rieske proteins and are involved in electron transfer reactions, participate in catalytic and regulatory processes[11]. The tetranuclear [4Fe-4S] clusters have essential roles in several metabolic pathways, e.g. mitochondrial aconitase of the tricarboxylic acid cycle (TCA). In addition, [4Fe-4S] proteins have been found to

function as sensors, as in the bacterial FNR and IscR protein, and in mammalian IRP1, which regulates cytosolic iron metabolism in mammalian cells[12,13]. Recently, the redox switch in the oxidation state of [4Fe-4S] clusters was also found to modulate the DNA-binding affinity of enzymes that processing DNA, such as glycosylases, helicases and primases[14,15]. In mammalian cells, Fe-S clusters are synthesized in both mitochondria and the cytosol, in contrast to yeast, in which it is asserted that *de novo* Fe-S cluster biogenesis occurs solely in mitochondria[16].

1.2 MITOCHONDRIAL IRON SULFUR TARGET PROTEINS

Mitochondria are the major iron-consuming subcellular organelles. The metal is imported into mitochondria by mitoferrin and is subsequently assembled into Fe-S clusters or heme groups[17]. The main function of this organelle is linked to energy production via ATP synthesis, converting glucose to carbon dioxide. ATP molecules can be produced via three main pathways in mitochondria: the glycolysis, the citric acid cycle/oxidative phosphorylation, and beta-oxidation. The first two are components of the process known as cellular respiration, the third is the catabolic metabolism of fatty acids. As *energy farm*, mitochondria require transition metal ions or cofactors for many physiological aspects and for this purpose, Fe-S clusters are highly conserved due to their ability to donate or accept single electrons (**Tab. 1**) [18]. These electrons create an essential flow in the last part of the cellular respiration, by which ATP is produced. For example, in mitochondrial complex I, seven Fe-S clusters form a wire-like pathway, along which electrons ascend with gradually increasing reduction potentials. Thus, the ability of Fe-S clusters to maintain low reduction potentials (i.e. low affinity for electrons) facilitates efficient capture of chemical energy from NADH as electrons move progressively through respiratory chain complexes[19]. Some proteins or protein complexes can contain more than one cluster. Respiratory complex II, involved in electron transfer chain, contains a [2Fe-2S], a [3Fe-4S] and a [4Fe-4S] cluster[20]. The mitochondrial request of iron and its transport inside the organelles is a crucial step; once iron is transported into the mitochondrion it can then be used for heme synthesis, ISC synthesis, or stored in mitochondrial ferritin (Ftmt). As already said, it is essential that mitochondrial iron is maintained in a safe form to prevent oxidative damage, due to the fact that mitochondria are a major source of cytotoxic ROS[21].

Function	Type of Cluster	Protein
Electron transfer	[2Fe-2S] [3Fe-4S] [4Fe-4S]	Ferredoxins High-potential iron–sulfur
Catalysis of a nonredox reaction	[4Fe-4S]	Aconitase
Catalysis of redox reactions	[4Fe-4S]	Sulfite reductase
Stabilization of protein structure for DNA repair	[4Fe-4S]	Endonuclease III, MutY
Sensing and regulation: (i) Oxygen sensors: loss of original cluster and of Activity	[4Fe-4S] [4Fe-4S]/[2Fe-2S] [4Fe-4S]/[3Fe-3S]	Aconitase
(ii) Sensor of O2 and NO: redox-regulated control of transcription	[2Fe-2S]	SoxR protein
(iii) Iron sensor: posttranscriptional regulation	[4Fe-4S]	Iron regulatory protein aconitase
Redox-mediated generation of free radicals	[4Fe-4S]	Biotin synthase

Table 1. The (Fe-S) clusters proteins play a central role in different processes

1.3 STRUCTURE OF THE FeS CLUSTERS

The simplest form of a Fe-S protein contains one iron coordinated by four protein ligands. The most common ligand is cysteine, as iron has a high affinity for thiolate groups, followed by histidines and aspartates. The most frequently found clusters in nature are [2Fe-2S], [3Fe-4S] and [4Fe-4S] (**Fig. 1**). More complex clusters derive from metal substitutions and fusions of the simpler clusters[22]. Fe-S clusters can exist in different oxidation states, which are related to the total formal oxidation state of the iron (Fe^{2+}or Fe^{3+}) and sulphides (S^{2-}) ions present, without taking into consideration the coordinating ligands. The cluster oxidation states are referred to as the oxidised or the reduced form of the Fe-S cluster. Apart from a few exceptions, the all-ferrous and all-ferric states of an Fe-S cluster are not present in nature. In general, only two oxidation states differing by a single electron are taken by the clusters [2Fe-2S] (2+/ 1+), [4Fe-4S] low potential (2+/ 1+) and [4Fe-4S] high potential (3+/ 2+). For some of the $[3Fe\text{-}4S]^{1+/0}$clusters a third all-ferrous state is naturally occurring (2-)[11]. Overall, any type of cluster exchanges one electron only. Fe-S clusters cover a wide range of redox potentials from around -0.6 to +0.45 V. This makes them excellent electron donors or acceptors[3]. Some enzymes even contain several Fe-S clusters, which serve as an "electric wire" through the enzyme. One example is fumarate reductase, which contains three Fe-S clusters with a typical spacing of 10-14 Å. The electrons are transferred from the membrane-bound menaquinone to cytosolic fumarate by electron hopping between the clusters.

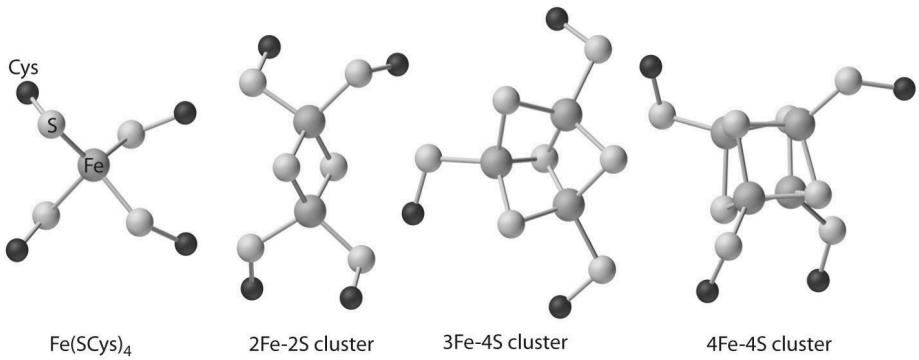

Figure 1. Ligand geometries and arrangement of iron and sulfide ions in clusters.

1.4 BIOGENESIS OF ISCS AND MITOCHONDRIAL ISC ASSEMBLY MACHINERY

Despite the chemical simplicity of Fe-S clusters, their biosynthesis is rather complex and requires more than two dozen components in eukaryotes[16]. Notably, in mammalian cells, accumulating evidence suggested that several key Fe-S cluster biogenesis proteins are present not only in mitochondria but also in cytosolic and/or nuclear compartments, whereas their yeast counterparts are alleged to reside only in mitochondria (with the exception of cysteine desulfurase)[23].

The most extensive studies available on iron sulfur cluster biogenesis were focused on bacteria (*Escherichia coli* and *Azetobacter vinelandii*) and yeast *Saccharomyces cerevisiae*. Three different systems were identified for the biogenesis of bacterial Fe-S proteins: the NIF system, for specific maturation of nitrogenase in azototrophic bacteria; the ISC assembly and the SUF systems, for the generation of housekeeping Fe-S proteins under normal and oxidative-stress conditions, respectively. The first studies to establish the details about the Fe-S cluster biosynthesis pathways in eukaryotes were performed on *S. cerevisiae* as model organism. Recent investigations in human cell culture and other model systems have shown that the process is highly conserved from yeast to human. In general Fe-S proteins are synthesized in their apo-state and obtain their ISC cofactor from a dedicated pathways and protein machineries. Three distinct protein machineries are required in the (non-plant) eukaryotic cells for the biogenesis of the Fe-S clusters and their insertion into apo proteins (**Fig. 2**):

- the ISC assembly machinery located in mitochondria (inherited from bacteria during evolution);
- the ISC export machinery located in the mitochondrial inter membrane space;
- the cytosolic ISC assembly (CIA) machinery, located in the cytosol.

The ISC export and CIA machineries are specifically involved in the maturation of cytosolic and nuclear ISC proteins, whereas the mitochondrial ISC assembly machinery is required for the generation of all cellular Fe-S proteins[24–26]. The mitochondrial ISC assembly and export systems, in addition to their function in extra-mitochondrial Fe-S protein maturation, are crucially involved in the regulation of cellular iron homeostasis. Eukaryotic cells apparently use the efficiency of mitochondrial Fe-S protein assembly as

an important sensor of the intracellular iron status[27,28]. This regulatory task of the mitochondrial ISC system is present in yeast, fungi, and vertebrates, but the mechanisms used for regulating iron homeostasis in these organisms are radically different, *i.e.* transcriptional in yeast-fungi and post-transcriptional in higher eukaryotes. In both cases, nuclear or cytosolic Fe-S proteins are implicated in this regulatory task and need the mitochondrial ISC systems for their own maturation.

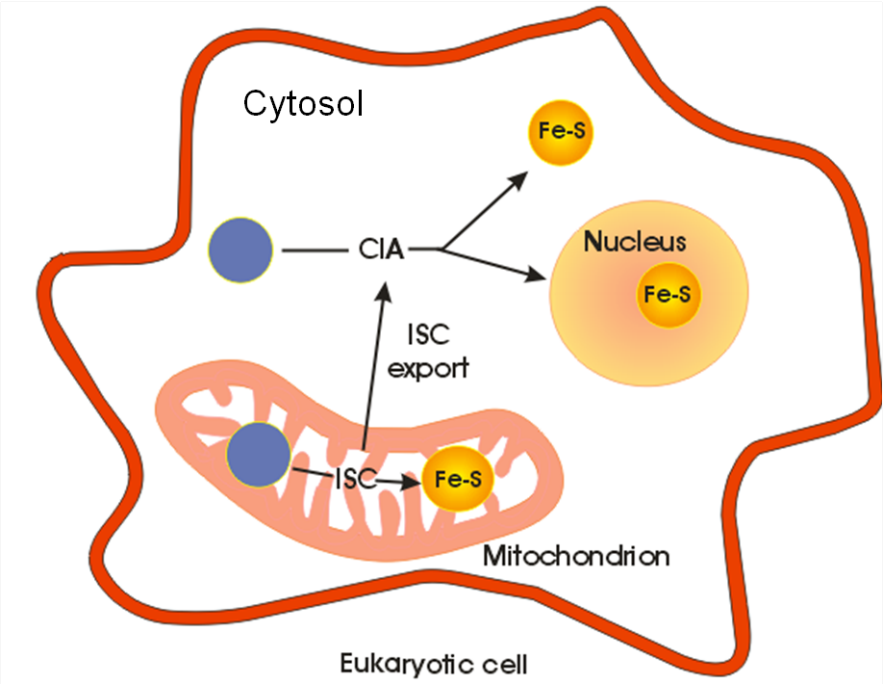

Figure 2. Schematic representation of ISC assembly in eukaryotic cell

1.4.1 MITOCHONDRIAL ISC ASSEMBLY MACHINERY

The mitochondrial *ISC assembly machinery*, which was inherited from the bacterial endosymbiont during evolution, encompasses 17 known proteins[16]. The mitochondrial machinery (**Fig. 3**), isn't only needed for the generation of mitochondrial Fe-S proteins, but has a role also in the maturation of cytosolic and nuclear Fe-S proteins, many of which perform essential cellular functions[29]. The biogenesis process inside mitochondria can be divided into three major functional steps: (i) the *de novo* assembly of a [2Fe–2S] cluster on the scaffold protein, ISCU, (ii) cluster transfer from ISCU to glutaredoxin 5 (GLRX5) followed by of its delivery to mitochondrial [2Fe–2S] proteins, and (iii) the synthesis of [4Fe–4S] clusters followed by their target-specific insertion into recipient apoproteins (**Fig 3**). The mitochondrial components required for Fe-S cluster formation in higher organisms are similar to the bacterial ISC proteins and apparently were inherited from a prokaryotic progenitor[30]. To accomplish *de novo* cluster formation on the scaffold protein ISCU, sources of iron and sulfur are needed. The sulfur required for this process is provided by conversion of cysteine to alanine by the desulfurase complex, NFS1–ISD11, in human cells[31]. Additionally, the sulfur has to be reduced to sulphide in order to be combined with ferrous iron (Fe^{2+}) to form a [2Fe–2S] cluster on ISCU. This task is accomplished by the electron transfer chain composed by a ferredoxin and ferredoxin reductase, which receives the electron from NADH[32,33]. Ferrous iron is imported into the mitochondrion by the intermembrane transporters Mitoferrin1/2 (Mrfn1/2),and is delivered to the scaffold by Frataxin, which was shown to interact with yeast IscU *in vivo* and *in vitro* in an iron-stimulated fashion[34]. In the second step, the Fe-S cluster is released from the scaffold protein to the monothiol glutaredoxin GLRX5, an event that is mediated by a dedicated chaperone system. Here, the [2Fe–2S] cluster can be directly handed over to [2Fe–2S] target proteins. In the third step, the [2Fe–2S] is converted into [4Fe–4S] cluster by the ISCA1-ISCA2 complex and transferred to the late acting factors of the pathway, i.e. NFU1. In the final step NFU1 lead the cluster to target apo proteins, such as lipoate synthase (LIAS)[35,36]. Mitochondrial and cytosolic Fe-S cluster protein maturation strictly depends on the function of the ISC machinery, which drives the cluster formation from mitochondria to the cytoplasm through the ISC export machinery, within the cytosolic Fe-S cluster pathways.

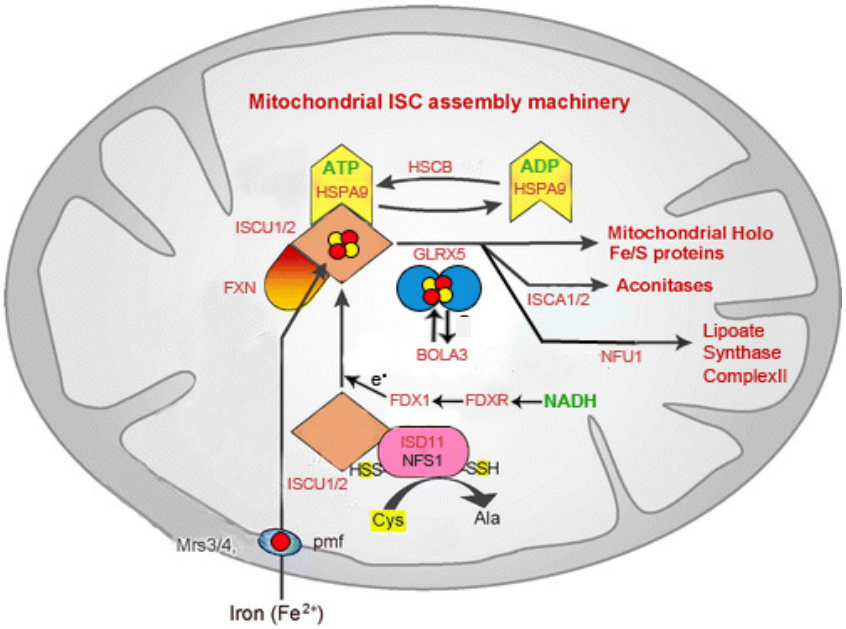

Figure 3. Mitochondrial ISC assembly machinery components and pathway.

1.5 HUMAN DISEASES ISC RELATED

I previously summarized that numerous proteins require Fe-S clusters as cofactors to become functionally active in a wide range of activities, from electron transport to DNA repair. Defective Fe-S cluster synthesis not only affects activities of many iron-sulfur enzymes, such as aconitase and succinate dehydrogenase, but also alters the regulation of cellular iron homeostasis, causing both mitochondrial iron overload and cytosolic iron deficiency. Thus, defects in the iron-sulfur cluster biogenesis pathway could underlie many human diseases. Studies on patients largely contributed to the identification and clarification of the biochemistry underlying mammalian Fe–S cluster biogenesis. The most common inherited iron-related disorder is Friedreich's ataxia, caused by a triplet expansion in intron 1 of the *frataxin* gene[24,26]. The severity of the phenotype caused by Friedreich's ataxia correlates with the length of this triplet expansion. Frataxin is located in mitochondria and the related disorder is characterised by accumulation of iron within the mitochondria and by Fe-S cluster protein deficiency. The disease causes slow progressive degeneration of the nervous system leading to an inability of voluntary muscle movement (ataxia) and compromises the heart conditions [37].

The recent discovery of one patient exhibiting recurrent myoglobinuria and slowly progressive muscle weakness augmented the number of diseases associated to altered Fe–S cluster biogenesis. The adolescent onset myopathy in a daughter from a consanguineous family is caused by a homozygous missense mutation in the first codon of the *FDX1L* gene encoding mitochondrial ferredoxin 2 (FDX2) protein. The mutation disrupts the ATG translation initiation site, resulting in undetectable protein levels of FDX2 in muscle and fibroblasts. The patient displayed severely decreased activity levels of the Fe–S cluster-containing respiratory chain complexes I, II and III as well as of aconitase and PDH complex. The malfunction of GLRX5 was found in a patient who had microcytic anemia. In GLRX5-deficient cells, ISC biosynthesis was impaired which lead to high activity of IRP1, increased levels of IRP2, cytosolic iron depletion, and mitochondrial iron overload[38]. A myopathy with exercise intolerance, intracellular iron overload, and deficiencies in succinate dehydrogenase and aconitase activity were connected with the splicing mutation in the gene encoding the central component of the ISC assembly machinery in mitochondria – the scaffold protein ISCU[39].

1.5.1 MULTIPLE MITOCHONDRIAL DYSFUCTION SYNDROME (MMDS)

Multiple mitochondrial dysfunctions syndromes (MMDSs) have recently emerged as a group of mitochondrial diseases that are inherited in an autosomal recessive manner. Six different types of MMDSs have been described so far. Clinical and biochemical investigations on patients revealed that symptoms are related to single point mutations in *NFU1*, *BOLA3*, *IBA57*, *ISCA1* or *ISCA2* genes. All these proteins are involved in the late steps of iron sulfur cluster biogenesis, and studies of MMDSs suggested that the transfer of ISCs to secondary carriers represents a mechanism for specifically delivering Fe-S cofactors to subsets of recipients, which may explain the distinctive phenotypes associated with the different disease gene mutations (**Tab. 2**).

Multiple mitochondrial dysfunctions syndromes are characterized by general impairment of mitochondria. The signs and symptoms of this severe disease begin early in life, and affected individuals usually do not live past infancy. Typically, the patients present brain dysfunction (encephalopathy), which can contribute to weak muscle tone (hypotonia), seizures, and delayed development of mental and movement abilities (psychomotor delay). These infants often have difficulties in growing and gaining

weight at the expected rate (failure to thrive). Most affected babies have a buildup of lactic acid in the body (lactic acidosis), which can be life-threatening. Careful phenotyping of humans with problems caused by defects in Fe-S cluster biogenesis should help to clarify aspects of the pathway, particularly those regarding how target Fe-S proteins are identified, that have remained elusive in studies of bacteria and yeast model systems. Determining why these diseases affect some tissues, but not others, is an important challenge that will probably be resolved by detailed studies of molecular pathophysiology. Insights into the pathophysiology of these diseases depends on gaining a better understanding of Fe-S cluster biogenesis and its regulation in eukaryotic cells, particularly in mitochondria.

Disease	Affected gene (protein)	Affected process
1) Fe/S diseases associated with mitochondrial iron accumulation		
1.1.) Friedreich's ataxia (FRDA)	*FXN* (Frataxin)	Core ISC assembly
1.2.) Hereditary Myopathy with Lactic acidosis (HML)	*ISCU*	Core ISC assembly
1.3.) Mitochondrial muscle myopathy with deficiency of ferredoxin 2	*FDX1L* (ferredoxin 2)	Core ISC assembly
1.4.) Combined oxidative phosphorylation defect with ISD11 deficiency	*LYRM4* (ISD11)	Core ISC assembly
1.5.) Sideroblastic anemias		
1.5.1.) Inherited sideroblastic anemias		
1.5.1.1.) Sideroblastic anemia with deficiency of glutaredoxin 5	*GLRX5*(Glutaredoxin 5)	Cluster transfer
1.5.1.2.) X-linked sideroblastic anemia with cerebellar ataxia (XLSA/A)	*ABCB7*	ISC export
1.5.2.) Acquired sideroblastic anemias		
1.5.2.1.) Refractory anemia with ring sideroblasts (RARS)	*ABCB7*	ISC export
1.5.2.2.) Refractory anemia with ring sideroblasts and isodicentric (X)(q13) chromosome	*ABCB7*	ISC export
2) Fe/S diseases without mitochondrial iron accumulation		
2.1.) Multiple mitochondrial dysfunction syndromes		
2.1.1.) Juvenile encephalomyopathy with deficiency of IBA57 (MMDS3)	*IBA57*	[4Fe–4S] assembly
2.1.2.) Multiple mitochondrial dysfunction syndrome with functional NFU1 deficiency (MMDS1)	*NFU1*	[4Fe–4S] assembly
2.1.3.) Multiple mitochondrial dysfunction syndrome with functional BOLA3 deficiency (MMDS2)	*BOLA3*	[4Fe–4S] assembly
2.2.) Mitochondrial encephalomyopathy with deficiency of IND1	*NUBPL* (IND1)	Complex I assembly
3) Variant erythropoietic protoporphyria with abnormal expression of mitoferrin 1	*SLC25A37*(Mitoferrin 1, MFRN1)	Mitochondrial iron import

Table 2. Human proteins associated with Fe-S disease

1.6 CYTOSOLIC AND MITOCHONDRIAL NFU1 PROTEIN

In 2003 the group of Tracy A. Rouault showed that human NFU1 is able to assemble a labile [4Fe-4S] cluster coordinated by two NFU1 monomers *via* a highly conserved C-terminal CXXC motif [40]. In agreement with the plant and bacterial data available at the time, it was suggested that NFU1 could act as a *scaffold* for the [4Fe-4S] clusters. Analyses of human genomic DNA and transcripts indicated that an alternative mRNA splicing results in translation of two NFU1 isoforms with distinct subcellular localizations. Isoform I of NFU1 is localized in the mitochondria, while isoform II remains in the cytosol. The mitochondrial isoform looses the first 58 residues at the N-terminus, because, as mitochondrial targeting sequence, it is processed by peptidases (**Fig.4**). *In vivo* studies showed that human NFU1 is required for the proper assembly of a subset of mitochondrial [4Fe-4S] proteins, which include components of respiratory complexes I and II, and lipoyl synthase[41,42]. A recent structural characterization of a construct of human NFU1 showed that the apo protein is monomeric in solution and adopts a dumbbell-shaped structure with well-structured N- and C-domains connected by a linker (Fig4), and that chemically reconstituted mitochondrial NFU1 binds a [4Fe-4S] cluster[43]. In 2011 two groups reported on patients carrying mutations in the NFU1 gene[41,42,44]. In the first case a non-sense mutation resulted in abnormal mRNA splicing and complete loss of the protein, while in the second, a G-C point mutation led to glycine- to-cysteine change just next to the active-site (CXXC) of NFU1. Affected individuals were born on time with no evident symptoms, but fast developed severe developmental retardation, brain abnormalities and pulmonary hypertension, eventually leading to death from about 3 months to one year after birth (MMDS1). The biochemical analyses of these patients showed a phenotype similar to that observed in BOLA3-mutant patients (MMDS3), with normal activities of aconitase but massive decrease in complexes I and II activities [45]. Additionally, strong defects in lipoic acid-containing proteins, pyruvate dehydrogenase (PDH), and α-ketoglutarate dehydrogenase (KGDH), together with hyperglycinemia and an increase in organic ketoacids were detected. This phenotype was explained by a defect of the Fe-S cluster-containing protein lipoate synthase. RNAi-depletion of NFU1 in human cell cultures gave the same phenotype as that observed in patients, pointing to a role of NFU1 in the assembly of complex Fe-S proteins (respiratory complexes I

and II and lipoate synthase containing eight, three or two Fe-S clusters, respectively)[28]. Despite the progresses made in the analyses of human patients, little is still known about exact role of NFU1 protein in Fe-S cluster biogenesis and possibly other processes in the cell.

```
        10         20         30         40         50
GSFTMFIQTQ DTPNPNSLKF IPGKPVLETR TMDFPTPAAA FRSPLARQLF
        60         70         80         90        100
RIEGVKSVFF GPDFITVTKE NEELDWNLLK PDIYATIMDF FASGLPLVTE
       110        120        130        140        150
ETPSGEAGSE EDDEVVAMIK ELLDTRIRPT VQEDGGDVIY KGFEDGIVQL
       160        170        180        190        200
KLQGSCTSCP SSIITLKNGI QNMLQFYIPE VEGVEQVMDD ESDEKEANSP
```

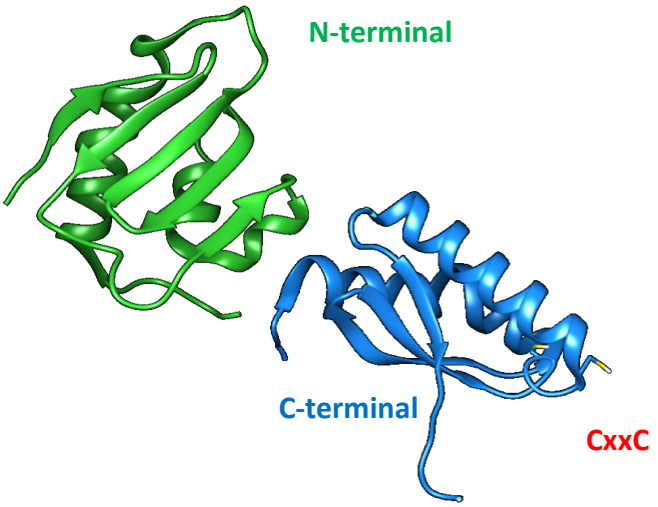

Figure 4. Human NFU1 sequence and 3D solution structure of the N-terminal (PDB ID 2LTM) and C-terminal (PDB ID 2M5O) domains, green and blue respectively.

1.7 MITOCHONDRIAL BOLA3 PROTEIN

In eukaryotes, after the [2Fe-2S] cluster is assembled on a scaffold protein in mitochondria, the cluster is released to monothiol glutaredoxin 5 (GLRX5), which mediates its transfer to several target proteins[46]. In this frame BolA-like proteins, which are generally grouped into three functionally divergent subfamilies designated BolA1-, BolA2-, and BolA3-like proteins, have recently emerged as novel players [22,47]. The BolA-like protein family is widely conserved from prokaryotes to eukaryotes and includes the eponymous member of the family, namely *E. coli* BolA. Bacterial BolA1 is a putative transcriptional regulator that plays a role in stress response via control of genes involved in the maintenance of cell morphology. Unlike BolA1 proteins, BolA2- and BolA3-like proteins are found exclusively in eukaryotes[48]. In *S. cerevisiae, S. pombe*, and *H. sapiens* BolA1 and BolA3 proteins are located in the mitochondria, while BolA2 in the cytosol. Similarly to *S. cerevisiae* BolA3, human BOLA3 is located in the mitochondria and mutation in the gene expressing this protein, is associated with multiple mitochondrial dysfunction syndrome 2 (MMDS2)[41]. Another link for BOLA3 to mitochondrial Fe-S protein biogenesis is provided by the fact that BOLA3 interacts with monothiol glutaredoxins (GLRX5) forming a [2Fe-2S] cluster heterodimer, that play a critical role in Fe-S protein biogenesis[50]. On the other hand, the interaction between yeast NFU1 and BOLA3 homologues was not experimentally observed in mitochondrial lysates and not clearly identified in pulldown experiments[45]. Thus, while the BOLA3 behavior in the first stage of iron sulfur cluster biogenesis has been described in detail, how BOLA3 may facilitate [4Fe-4S] cluster dissociation and transfer from NFU1 to apo target proteins remains unclear.

1.8 AIMS AND TOPICS OF THE RESEARCH

Within my PhD studies, I addressed some structural and functional aspects of human metalloproteins involved in iron-sulfur cluster (ISC) biogenesis. Previous work allowed to divide the maturation pathway of mitochondrial Fe-S proteins into three distinct major steps. The general function of many ISC assembly machinery components involved in those steps is quite well described in the literature. However, mechanistic details of several steps of the Fe-S clusters assembly are not yet described at the molecular level [16]. Hence, the aims of my work focused on a better understanding of the late steps of the Fe-S cluster biogenesis, after its synthesis and before insertion into target apo-proteins. During the three years of my PhD program, I focused my attention on the expression, purification and characterization of mitochondrial human proteins that have been implicated in iron metabolism but whose functions, at the beginning of my PhD, were still not clearly defined. I characterized these proteins at a structural and biochemical level, as well as investigated their interactions with partner proteins. The results obtained by these studies contributed to define the mitochondrial Fe-S protein maturation pathways at atomic level. It has been already demonstrated that one protein from the BOLAs family, BOLA3, can interact with GLRX5, forming a [2Fe-2S]-bridged heterodimeric complex, but no information was available on the possible protein partners. Furthermore, the [4Fe-4S] cluster formation and delivery remained not defined. Mutations in genes encoding proteins involved in ISC maturation, such as NFU1, BOLA3, ISCA2 and IBA57, have been related to MMDSs. In particular, BOLA3 and NFU1 deficiency causes MMDS types 2 and 3, resulting in the reduced functionality of the respiratory complexes I and II as well as of lipoic acid-dependent enzymes. Similar clinical and biochemical phenotypes in patients with mutations in the late acting factor protein (NFU1), suggested a functional correlation between the two proteins in the late step of the mitochondrial Fe-S protein maturation, even if detailed biochemical investigations of their molecular role in mitochondria have not been reported yet. MMDS5 has recently been described in a clinical case report of patients carrying a mutation in *ISCA1*, but with no further analysis.

In my PhD studies, I characterized [4Fe-4S] NFU1 and how the [2Fe-2S] GLRX5/BOLA3 complex cooperates in the assembly of the [4Fe-4S] cluster on NFU1. Lately, the work was focused on the *in vitro* interaction and cluster transfer between NFU1 and ISCA1/ISCA2 complex. The current prevailing model, largely based on studies in *S. cerevisiae*, proposes that NFU1 receives a [4Fe-4S] cluster assembled on the ISCAs proteins system and then

transfers it to selected apo target proteins with the assistance of BOLA3. Based on this model, we detailed the molecular interactions between the [4Fe-4S] ISCA2 dimer or/and the ISCA1/ISCA2 complex with NFU1, all involved in [4Fe-4S] cluster transfer to targets enzymes. Finally, I characterized an heterozygous variant of BOLA3 gene, not previously analyzed (c.176G>A, p.Cys59Tyr)[51]. This mutation is associated with a novel phenotype of MMDS2. The tyrosine substitution affects an highly conserved amino acid, the p. Cys59 residue, that has been identified as one of the two Fe/S cluster ligands in BOLA3. It is possible that the tyrosine substitution at p. Cys59 results in a protein with partial activity, imparting a milder phenotype, also considering the functional association with the [2Fe-2S] GLRX5 *in vivo* and *in vitro*.

REFERENCES

(1) Klotz, M. G.; Schmid, M. C.; Strous, M.; Op Den Camp, H. J. M.; Jetten, M. S. M.; Hooper, A. B. Evolution of an Octahaem Cytochrome c Protein Family That Is Key to Aerobic and Anaerobic Ammonia Oxidation by Bacteria. *Environ. Microbiol.* **2008**. https://doi.org/10.1111/j.1462-2920.2008.01733.x.

(2) Banci, L.; Bertini, I.; Calderone, V.; Della-Malva, N.; Felli, I. C.; Neri, S.; Pavelkova, A.; Rosato, A. Copper(I)-Mediated Protein-Protein Interactions Result from Suboptimal Interaction Surfaces. *Biochem. J.* **2009**. https://doi.org/10.1042/BJ20090422.

(3) Camponeschi, F.; Banci, L. Metal Cofactors Trafficking and Assembly in the Cell: A Molecular View. *Pure Appl. Chem.* **2019**, *91* (2), 231–245. https://doi.org/10.1515/pac-2018-0720.

(4) Finney, L. A.; O'Halloran, T. V. Transition Metal Speciation in the Cell: Insights from the Chemistry of Metal Ion Receptors. *Science*. 2003. https://doi.org/10.1126/science.1085049.

(5) O'Halloran, T. V.; Culotta, V. C. Metallochaperones, an Intracellular Shuttle Service for Metal Ions. *Journal of Biological Chemistry*. 2000. https://doi.org/10.1074/jbc.R000006200.

(6) Ba, L. A.; Doering, M.; Burkholz, T.; Jacob, C. Metal Trafficking: From Maintaining the Metal Homeostasis to Future Drug Design. *Metallomics*. 2009. https://doi.org/10.1039/b904533c.

(7) Kuchar, J.; Hausinger, R. P. Biosynthesis of Metal Sites. *Chemical Reviews*. 2004. https://doi.org/10.1021/cr020613p.

(8) Rae, T. D.; Schmidt, P. J.; Pufahl, R. A.; Culotta, V. C.; O'Halloran, T. V. Undetectable Intracellular Free Copper: The Requirement of a Copper Chaperone for Superoxide Dismutase. *Science (80-.).* **1999**. https://doi.org/10.1126/science.284.5415.805.

(9) Letelier, M. E.; Sánchez-Jofré, S.; Peredo-Silva, L.; Cortés-Troncoso, J.; Aracena-Parks, P. Mechanisms Underlying Iron and Copper Ions Toxicity in Biological Systems: Pro-Oxidant Activity and Protein-Binding Effects. *Chem. Biol. Interact.* **2010**. https://doi.org/10.1016/j.cbi.2010.06.013.

(10) Lanz, N. D.; Pandelia, M. E.; Kakar, E. S.; Lee, K. H.; Krebs, C.; Booker, S. J. Evidence for a Catalytically and Kinetically Competent Enzyme-Substrate Cross-Linked Intermediate in Catalysis by Lipoyl Synthase. *Biochemistry* **2014**. https://doi.org/10.1021/bi500432r.

(11) Beinert, H.; Holm, R. H.; Münck, E. Iron-Sulfur Clusters: Nature's Modular, Multipurpose Structures. *Science (80-.).* **1997**. https://doi.org/10.1126/science.277.5326.653.

(12) Hentze, M. W.; Muckenthaler, M. U.; Galy, B.; Camaschella, C. Two to Tango: Regulation of Mammalian Iron Metabolism. *Cell*. 2010. https://doi.org/10.1016/j.cell.2010.06.028.

(13) Kiley, P. J.; Beinert, H. The Role of Fe-S Proteins in Sensing and Regulation in Bacteria. *Current Opinion in Microbiology*. 2003. https://doi.org/10.1016/S1369-5274(03)00039-0.

(14) Barton, J. K.; Silva, R. M. B.; O'Brien, E. Redox Chemistry in the Genome: Emergence of the [4fe4s] Cofactor in Repair and Replication. *Annu. Rev. Biochem.* **2019**. https://doi.org/10.1146/annurev-biochem-013118-110644.

(15) Tse, E. C. M.; Zwang, T. J.; Barton, J. K. The Oxidation State of [4Fe4S] Clusters Modulates the DNA-Binding Affinity of DNA Repair Proteins. *J. Am. Chem. Soc.* **2017**. https://doi.org/10.1021/jacs.7b07230.

(16) Ciofi-Baffoni, S.; Nasta, V.; Banci, L. Protein Networks in the Maturation of Human Iron-Sulfur Proteins. *Metallomics*. 2018. https://doi.org/10.1039/c7mt00269f.

(17) Andrews, N. C.; Schmidt, P. J. Iron Homeostasis. *Annual Review of Physiology*. 2007. https://doi.org/10.1146/annurev.physiol.69.031905.164337.

(18) Beinert, H. Iron-Sulfur Proteins: Ancient Structures, Still Full of Surprises. *Journal of Biological Inorganic Chemistry*. 2000. https://doi.org/10.1007/s007750050002.

(19) Hirst, J. Mitochondrial Complex I. *Annual Review of Biochemistry*. 2013. https://doi.org/10.1146/annurev-biochem-070511-103700.

(20) Rouault, T. A. The Indispensable Role of Mammalian Iron Sulfur Proteins in Function and Regulation of Multiple Diverse Metabolic Pathways. *BioMetals*. 2019. https://doi.org/10.1007/s10534-019-00191-7.

(21) Napier, I.; Ponka, P.; Richardson, D. R. Iron Trafficking in the Mitochondrion: Novel Pathways Revealed by Disease. *Blood*. 2005. https://doi.org/10.1182/blood-2004-10-3856.

(22) Andreini, C.; Banci, L.; Rosato, A. Exploiting Bacterial Operons to Illuminate Human Iron-Sulfur Proteins. *J. Proteome Res.* **2016**. https://doi.org/10.1021/acs.jproteome.6b00045.

(23) Biederbick, A.; Stehling, O.; Rösser, R.; Niggemeyer, B.; Nakai, Y.; Elsässer, H.-P.; Lill, R. Role of Human Mitochondrial Nfs1 in Cytosolic Iron-Sulfur Protein Biogenesis and Iron Regulation. *Mol. Cell. Biol.* **2006**. https://doi.org/10.1128/mcb.00112-06.

(24) Lill, R.; Stehling, O. The Role of Mitochondria in Cellular Iron – Sulfur Processes , and Diseases. *Cold Spring Harb Perspect Biol* **2013**. https://doi.org/10.1101/cshperspect.a011312.

(25) Fosset, C.; Chauveau, M. J.; Guillon, B.; Canal, F.; Drapier, J. C.; Bouton, C. RNA Silencing of Mitochondrial M-Nfs1 Reduces Fe-S Enzyme Activity Both in Mitochondria and Cytosol of Mammalian Cells. *J. Biol. Chem.* **2006**. https://doi.org/10.1074/jbc.M602979200.

(26) Martelli, A.; Wattenhofer-donzé, M.; Schmucker, S.; Bouvet, S.; Reutenauer, L.; Puccio, H. Frataxin Is Essential for Extramitochondrial Fe - S Cluster Proteins in Mammalian Tissues. *Hum. Mol. Genet.* **2007**. https://doi.org/10.1093/hmg/ddm163.

(27) Outten, C. E.; Albetel, A. N. Iron Sensing and Regulation in Saccharomyces Cerevisiae: Ironing out the Mechanistic Details. *Current Opinion in Microbiology*. 2013. https://doi.org/10.1016/j.mib.2013.07.020.

(28) Lill, R.; Hoffmann, B.; Molik, S.; Pierik, A. J.; Rietzschel, N.; Stehling, O.; Uzarska, M. A.; Webert, H.; Wilbrecht, C.; Mühlenhoff, U. The Role of Mitochondria in Cellular Iron-Sulfur Protein Biogenesis and Iron Metabolism.

Biochimica et Biophysica Acta - Molecular Cell Research. 2012. https://doi.org/10.1016/j.bbamcr.2012.05.009.

(29) Lill, R.; Lill, R.; Freibert, S. A. Mechanisms of Mitochondrial Iron-Sulfur Protein Biogenesis. *Annual Review of Biochemistry*. 2020. https://doi.org/10.1146/annurev-biochem-013118-111540.

(30) Tokumoto, U.; Kitamura, S.; Fukuyama, K.; Takahashi, Y. Interchangeability and Distinct Properties of Bacterial Fe-S Cluster Assembly Systems: Functional Replacement of the Isc and Suf Operons in Escherichia Coli with the NifSU-like Operon from Helicobacter Pylori. *J. Biochem.* **2004**. https://doi.org/10.1093/jb/mvh104.

(31) Pandey, A.; Yoon, H.; Lyver, E. R.; Dancis, A.; Pain, D. Isd11p Protein Activates the Mitochondrial Cysteine Desulfurase Nfs1p Protein. *J. Biol. Chem.* **2011**. https://doi.org/10.1074/jbc.M111.288522.

(32) Webert, H.; Freibert, S. A.; Gallo, A.; Heidenreich, T.; Linne, U.; Amlacher, S.; Hurt, E.; Mühlenhoff, U.; Banci, L.; Lill, R. Functional Reconstitution of Mitochondrial Fe/S Cluster Synthesis on Isu1 Reveals the Involvement of Ferredoxin. *Nat. Commun.* **2014**. https://doi.org/10.1038/ncomms6013.

(33) Yan, R.; Adinolfi, S.; Pastore, A. Ferredoxin, in Conjunction with NADPH and Ferredoxin-NADP Reductase, Transfers Electrons to the IscS/IscU Complex to Promote Iron-Sulfur Cluster Assembly. *Biochim. Biophys. Acta - Proteins Proteomics* **2015**. https://doi.org/10.1016/j.bbapap.2015.02.002.

(34) Foury, F.; Pastore, A.; Trincal, M. Acidic Residues of Yeast Frataxin Have an Essential Role in Fe-S Cluster Assembly. *EMBO Rep.* **2007**. https://doi.org/10.1038/sj.embor.7400881.

(35) Brancaccio, D.; Gallo, A.; Mikolajczyk, M.; Zovo, K.; Palumaa, P.; Novellino, E.; Piccioli, M.; Ciofi-Baffoni, S.; Banci, L. Formation of [4Fe-4S] Clusters in the Mitochondrial Iron-Sulfur Cluster Assembly Machinery. *J. Am. Chem. Soc.* **2014**. https://doi.org/10.1021/ja507822j.

(36) Sheftel, A. D.; Wilbrecht, C.; Stehling, O.; Niggemeyer, B.; Elsässer, H. P.; Mühlenhoff, U.; Lill, R. The Human Mitochondrial ISCA1, ISCA2, and IBA57 Proteins Are Required for [4Fe-4S] Protein Maturation. *Mol. Biol. Cell* **2012**. https://doi.org/10.1091/mbc.E11-09-0772.

(37) Rouault, T. A.; Tong, W. H. Iron-Sulfur Cluster Biogenesis and Human Disease. *Trends in Genetics*. 2008. https://doi.org/10.1016/j.tig.2008.05.008.

(38) Ye, H.; Jeong, S. Y.; Ghosh, M. C.; Kovtunovych, G.; Silvestri, L.; Ortillo, D.; Uchida, N.; Tisdale, J.; Camaschella, C.; Rouault, T. A. Glutaredoxin 5 Deficiency Causes Sideroblastic Anemia by Specifically Impairing Heme Biosynthesis and Depleting Cytosolic Iron in Human Erythroblasts. *J. Clin. Invest.* **2010**. https://doi.org/10.1172/JCI40372.

(39) Mochel, F.; Knight, M. A.; Tong, W. H.; Hernandez, D.; Ayyad, K.; Taivassalo, T.; Andersen, P. M.; Singleton, A.; Rouault, T. A.; Fischbeck, K. H.; Haller, R. G. Splice Mutation in the Iron-Sulfur Cluster Scaffold Protein ISCU Causes Myopathy with Exercise Intolerance. *Am. J. Hum. Genet.* **2008**. https://doi.org/10.1016/j.ajhg.2007.12.012.

(40) Tong, W. H.; Jameson, G. N. L.; Huynh, B. H.; Rouault, T. A. Subcellular Compartmentalization of Human Nfu, an Iron-Sulfur Cluster Scaffold Protein, and Its Ability to Assemble a [4Fe-4S] Cluster. *Proc. Natl. Acad. Sci. U. S. A.* **2003**. https://doi.org/10.1073/pnas.1732541100.

(41) Cameron, J. M.; Janer, A.; Levandovskiy, V.; MacKay, N.; Rouault, T. A.; Tong, W. H.; Ogilvie, I.; Shoubridge, E. A.; Robinson, B. H. Mutations in Iron-Sulfur Cluster Scaffold Genes NFU1 and BOLA3 Cause a Fatal Deficiency of Multiple Respiratory Chain and 2-Oxoacid Dehydrogenase Enzymes. *Am. J. Hum. Genet.* **2011**. https://doi.org/10.1016/j.ajhg.2011.08.011.

(42) Navarro-Sastre, A.; Tort, F.; Stehling, O.; Uzarska, M. A.; Arranz, J. A.; Del Toro, M.; Labayru, M. T.; Landa, J.; Font, A.; Garcia-Villoria, J.; Merinero, B.; Ugarte, M.; Gutierrez-Solana, L. G.; Campistol, J.; Garcia-Cazorla, A.; Vaquerizo, J.; Riudor, E.; Briones, P.; Elpeleg, O.; Ribes, A.; Lill, R. A Fatal Mitochondrial Disease Is Associated with Defective NFU1 Function in the Maturation of a Subset of Mitochondrial Fe-S Proteins. *Am. J. Hum. Genet.* **2011**. https://doi.org/10.1016/j.ajhg.2011.10.005.

(43) Freibert, S. A.; Weiler, B. D.; Bill, E.; Pierik, A. J.; Mühlenhoff, U.; Lill, R. Biochemical Reconstitution and Spectroscopic Analysis of Iron–Sulfur Proteins. In *Methods in Enzymology*; 2018. https://doi.org/10.1016/bs.mie.2017.11.034.

(44) Wachnowsky, C.; Wesley, N. A.; Fidai, I.; Cowan, J. A. Understanding the Molecular Basis of Multiple Mitochondrial Dysfunctions Syndrome 1 (MMDS1)—Impact of a Disease-Causing Gly208Cys Substitution on Structure and Activity of NFU1 in the Fe/S Cluster Biosynthetic Pathway. *J. Mol. Biol.* **2017**. https://doi.org/10.1016/j.jmb.2017.01.021.

(45) Melber, A.; Na, U.; Vashisht, A.; Weiler, B. D.; Lill, R.; Wohlschlegel, J. A.; Winge, D. R. Role of Nfu1 and Bol3 in Iron-Sulfur Cluster Transfer to Mitochondrial Clients. *Elife* **2016**. https://doi.org/10.7554/eLife.15991.

(46) Banci, L.; Brancaccio, D.; Ciofi-Baffoni, S.; Del Conte, R.; Gadepalli, R.; Mikolajczyk, M.; Neri, S.; Piccioli, M.; Winkelmann, J. [2Fe-2S] Cluster Transfer in Iron-Sulfur Protein Biogenesis. *Proc. Natl. Acad. Sci. U. S. A.* **2014**. https://doi.org/10.1073/pnas.1400102111.

(47) Uzarska, M. A.; Nasta, V.; Weiler, B. D.; Spantgar, F.; Ciofi-Baffoni, S.; Saviello, M. R.; Gonnelli, L.; Mühlenhoff, U.; Banci, L.; Lill, R. Mitochondrial Bol1 and Bol3 Function as Assembly Factors for Specific Iron-Sulfur Proteins. *Elife* **2016**. https://doi.org/10.7554/eLife.16673.

(48) Zhou, Y. B.; Cao, J. B.; Wan, B. B.; Wang, X. R.; Ding, G. H.; Zhu, H.; Yang, H. M.; Wang, K. S.; Zhang, X.; Han, Z. G. HBolA, Novel Non-Classical Secreted Proteins, Belonging to Different BolA Family with Functional Divergence. *Mol. Cell. Biochem.* **2008**. https://doi.org/10.1007/s11010-008-9809-2.

(49) Maio, N.; Rouault, T. A. Outlining the Complex Pathway of Mammalian Fe-S Cluster Biogenesis. *Trends Biochem. Sci.* **2020**, *45* (5), 411–426. https://doi.org/10.1016/j.tibs.2020.02.001.

(50) Nasta, V.; Giachetti, A.; Ciofi-Baffoni, S.; Banci, L. Structural Insights into the Molecular Function of Human [2Fe-2S] BOLA1-GRX5 and [2Fe-2S] BOLA3-GRX5 Complexes. *Biochim. Biophys. Acta - Gen. Subj.* **2017**. https://doi.org/10.1016/j.bbagen.2017.05.005.

(51) Stutterd, C. A.; Lake, N. J.; Peters, H.; Lockhart, P. J.; Taft, R. J.; Van Der Knaap, M. S.; Vanderver, A.; Thorburn, D. R.; Simons, C.; Leventer, R. J. Severe Leukoencephalopathy with Clinical Recovery Caused by Recessive BOLA3 Mutations. In *JIMD Reports*; 2019. https://doi.org/10.1007/8904_2018_100.

2 RESULTS

The late-acting steps of the ISC assembly machinery are responsible for [4Fe-4S] cluster assembly, trafficking and insertion into mitochondrial target Fe-S proteins[1,2]. The first studies on the mitochondrial [4Fe-4S] cluster assembly showed that two human proteins ISCA1and ISCA2 are required for this process. *In vitro* data confirmed that ISCA1 and ISCA2 form a heterodimer, which, by accepting two [2Fe-2S] clusters from the protein partner GLRX5, are able to assemble a [4Fe-4S] cluster[3,4]. The following step in the ISC assembly machinery consists on the transfer and insertion of the [4Fe-4S] cluster formed on the ISCA1-ISCA2 complex into mitochondrial target Fe-S proteins with the help of specific ISC targeting factors. Three proteins have been involved in this step. The ISC targeting factors, NFU1 and IND1, have been implicated in receiving the cluster from ISCAs complex to mature specific mitochondrial target proteins[5–7]. The third targeting factor, BOLA3, was proposed to function in a NFU1-mediated [4Fe-4S] cluster transfer to mitochondrial target proteins[8]. However, the interaction between NFU1 and BOLA3 was not clearly detected *in vivo*[9]. On the contrary, the interaction between BOLA3 and GLRX5 has been well documented by *in vivo* and *in vitro* studies[10,11].

The open question is how and whether GLRX5 performs function in the late phase of the ISC assembly machinery once complexed with BOLA3, such as [2Fe-2S] cluster trafficking and/or insertion processes. In the first work (**A pathway for assembling [4Fe-4S]$^{2+}$ clusters in mitochondrial iron-sulfur protein biogenesis**) we shed light on this question, showing that two [2Fe-2S]$^{2+}$ GLRX5-BOLA3 molecules are able to transfer their clusters to apo NFU1 by forming a [4Fe-4S]$^{2+}$ cluster on dimeric NFU1. Our data showed that the mechanism of cluster transfer and assembly from [2Fe-2S]$^{2+}$ GLRX5-BOLA3 to NFU1 brings directly to the formation of [4Fe-4S]$^{2+}$ NFU1 without the accumulation of [2Fe-2S]-bound intermediates, in agreement with a strong preference of NFU1 to bind a [4Fe-4S] cluster with respect to a [2Fe-2S] cluster. The [2Fe-2S]$^{2+}$ GLRX5-BOLA3 hetero-complex could operate specifically in the assembly of a [4Fe-4S] cluster on NFU1 and this mechanism might be alternative to the pathway involving the [4Fe-4S] cluster transfer from the ISCA1-ISCA2 complex to NFU1. Recently, proteomic studies demonstrate that human ISCA1 interact with NFU1[12], while yeast NFU1 interacts with both yeast ISCA1 and ISCA2[8]. The second work (**ISCA1 orchestrates ISCA2 and NFU1 in the maturation of mitochondrial [4Fe-4S] proteins**) provides a molecular model for the interaction between ISCA1 and NFU1. In addition, we describe the sequence of events that, acting from ISCA1-ISCA2 to NFU1, assemble the [4Fe-4S] clusters. We showed that ISCA1 is the key player

for the [4Fe-4S] protein maturation process being able indeed to interact either individually with ISCA2 or NFU1 or with both proteins in a ternary complex. In the latter case, ISCA1 works as a mediator between the two no interacting proteins ISCA2 and NFU1. The ISCA1-ISCA2 complex-bound $[4Fe\text{-}4S]^{2+}$ cluster is not donated to NFU1 and dimeric $[4Fe\text{-}4S]^{2+}$ NFU1 is not formed. On the contrary, the cluster is translocated within the ternary ISCA1-ISCA2-NFU1 complex from a bridged ISCA1-ISCA2 coordination to a bridged ISCA1-NFU1 one, thus being ISCA2 no more involved in cluster binding. In the third work (**Impact of CYS59TYR variant on the activity of BOLA3 in the Fe/S cluster biogenesis**) we studied a novel mutant of BOLA3, causing the MMDS2[5,13]. In particular, BOLA3 deficiency results in decreased functions of respiratory complexes I and II, as well as lipoic acid-dependent enzymes such as pyruvate dehydrogenase (PDH), 2-ketoglutarate dehydrogenase (KGDH), and glycine cleavage system (GCS). Here, we used solution NMR spectroscopy to investigate the structural differences underlying the functional mechanism of a novel mutation BOLA3 in which the residue implicated in the cluster binding with GLRX5, the Cys59, is substituted with a Tyrosine. Interestingly, the mutation results in a different phenotype compared to the known progression of MMDS2[14]. In the case of the Cys to Tyr mutation, the patient initially showed all the pathological symptoms, but, after the initial condition, the disease led to a milder phenotype, until the complete recovery of the pathology at the age of 8. We found that the BOLA3 Cys59Tyr structure and the binding interface with its physiological partner, GLRX5, is not markedly perturbed by the mutation.

REFERENCES

(1) Ciofi-Baffoni, S.; Nasta, V.; Banci, L. Protein Networks in the Maturation of Human Iron-Sulfur Proteins. *Metallomics*. 2018. https://doi.org/10.1039/c7mt00269f.

(2) Braymer, J. J.; Lill, R. Iron–Sulfur Cluster Biogenesis and Trafficking in Mitochondria. *Journal of Biological Chemistry*. 2017. https://doi.org/10.1074/jbc.R117.787101.

(3) Banci, L.; Brancaccio, D.; Ciofi-Baffoni, S.; Del Conte, R.; Gadepalli, R.; Mikolajczyk, M.; Neri, S.; Piccioli, M.; Winkelmann, J. [2Fe-2S] Cluster Transfer in Iron-Sulfur Protein Biogenesis. *Proc. Natl. Acad. Sci. U. S. A.* **2014**. https://doi.org/10.1073/pnas.1400102111.

(4) Brancaccio, D.; Gallo, A.; Mikolajczyk, M.; Zovo, K.; Palumaa, P.; Novellino, E.;

Piccioli, M.; Ciofi-Baffoni, S.; Banci, L. Formation of [4Fe-4S] Clusters in the Mitochondrial Iron-Sulfur Cluster Assembly Machinery. *J. Am. Chem. Soc.* **2014**. https://doi.org/10.1021/ja507822j.

(5) Cameron, J. M.; Janer, A.; Levandovskiy, V.; MacKay, N.; Rouault, T. A.; Tong, W. H.; Ogilvie, I.; Shoubridge, E. A.; Robinson, B. H. Mutations in Iron-Sulfur Cluster Scaffold Genes NFU1 and BOLA3 Cause a Fatal Deficiency of Multiple Respiratory Chain and 2-Oxoacid Dehydrogenase Enzymes. *Am. J. Hum. Genet.* **2011**. https://doi.org/10.1016/j.ajhg.2011.08.011.

(6) Navarro-Sastre, A.; Tort, F.; Stehling, O.; Uzarska, M. A.; Arranz, J. A.; Del Toro, M.; Labayru, M. T.; Landa, J.; Font, A.; Garcia-Villoria, J.; Merinero, B.; Ugarte, M.; Gutierrez-Solana, L. G.; Campistol, J.; Garcia-Cazorla, A.; Vaquerizo, J.; Riudor, E.; Briones, P.; Elpeleg, O.; Ribes, A.; Lill, R. A Fatal Mitochondrial Disease Is Associated with Defective NFU1 Function in the Maturation of a Subset of Mitochondrial Fe-S Proteins. *Am. J. Hum. Genet.* **2011**. https://doi.org/10.1016/j.ajhg.2011.10.005.

(7) Sheftel, A. D.; Stehling, O.; Pierik, A. J.; Netz, D. J. A.; Kerscher, S.; Elsässer, H.-P.; Wittig, I.; Balk, J.; Brandt, U.; Lill, R. Human Ind1, an Iron-Sulfur Cluster Assembly Factor for Respiratory Complex I. *Mol. Cell. Biol.* **2009**. https://doi.org/10.1128/mcb.00817-09.

(8) Melber, A.; Na, U.; Vashisht, A.; Weiler, B. D.; Lill, R.; Wohlschlegel, J. A.; Winge, D. R. Role of Nfu1 and Bol3 in Iron-Sulfur Cluster Transfer to Mitochondrial Clients. *Elife* **2016**. https://doi.org/10.7554/eLife.15991.

(9) Melber, A.; Winge, D. R. Steps Toward Understanding Mitochondrial Fe/S Cluster Biogenesis. In *Methods in Enzymology*; 2018. https://doi.org/10.1016/bs.mie.2017.09.004.

(10) Nasta, V.; Giachetti, A.; Ciofi-Baffoni, S.; Banci, L. Structural Insights into the Molecular Function of Human [2Fe-2S] BOLA1-GRX5 and [2Fe-2S] BOLA3-GRX5 Complexes. *Biochim. Biophys. Acta - Gen. Subj.* **2017**. https://doi.org/10.1016/j.bbagen.2017.05.005.

(11) Uzarska, M. A.; Nasta, V.; Weiler, B. D.; Spantgar, F.; Ciofi-Baffoni, S.; Saviello, M. R.; Gonnelli, L.; Mühlenhoff, U.; Banci, L.; Lill, R. Mitochondrial Bol1 and Bol3 Function as Assembly Factors for Specific Iron-Sulfur Proteins. *Elife* **2016**. https://doi.org/10.7554/eLife.16673.

(12) Beilschmidt, L. K.; De Choudens, S. O.; Fournier, M.; Sanakis, I.; Hograindleur,

M. A.; Clémancey, M.; Blondin, G.; Schmucker, S.; Eisenmann, A.; Weiss, A.; Koebel, P.; Messaddeq, N.; Puccio, H.; Martelli, A. ISCA1 Is Essential for Mitochondrial Fe4S4 Biogenesis in Vivo. *Nat. Commun.* **2017**. https://doi.org/10.1038/ncomms15124.

(13) Maio, N.; Rouault, T. A. Outlining the Complex Pathway of Mammalian Fe-S Cluster Biogenesis. *Trends Biochem. Sci.* **2020**, *45* (5), 411–426. https://doi.org/10.1016/j.tibs.2020.02.001.

(14) Stutterd, C. A.; Lake, N. J.; Peters, H.; Lockhart, P. J.; Taft, R. J.; Van Der Knaap, M. S.; Vanderver, A.; Thorburn, D. R.; Simons, C.; Leventer, R. J. Severe Leukoencephalopathy with Clinical Recovery Caused by Recessive BOLA3 Mutations. In *JIMD Reports*; 2019. https://doi.org/10.1007/8904_2018_100.

2.1 A PATHWAY FOR ASSEMBLING [4FE-4S]$^{2+}$ CLUSTERS IN MITOCHONDRIAL IRON-SULFUR PROTEIN BIOGENESIS

*[1]*Nasta V.*, *[1]***Suraci D.***, Gourdoupis S.,[1,2] Ciofi-Baffoni S., [1,2]Banci L.*

[1]Magnetic Resonance Center CERM, University of Florence, Florence, Italy;

[2]Department of Chemistry, University of Florence, Florence, Italy;

* These authors contributed equally to this work

FEBS J. 2020 Jun;287(11):2312-2327

The FEBS Journal

FEBS PRESS science publishing by scientists

A pathway for assembling $[4Fe\text{-}4S]^{2+}$ clusters in mitochondrial iron–sulfur protein biogenesis

Veronica Nasta[1,2], Dafne Suraci[1], Spyridon Gourdoupis[1], Simone Ciofi-Baffoni[1,2] and Lucia Banci[1,2]

1 Magnetic Resonance Center CERM, University of Florence, Italy
2 Department of Chemistry, University of Florence, Italy

Keywords
BOLA3; GLRX5; iron–sulfur protein; mitochondrial iron–sulfur cluster assembly machinery; NFU1

Correspondence
L. Banci, Magnetic Resonance Center CERM, University of Florence, Via Luigi Sacconi 6, 50019 Sesto Fiorentino, Florence, Italy
Tel: +39-055-4574273
E-mail: banci@cerm.unifi.it
S. Ciofi-Baffoni, Magnetic Resonance Center CERM, University of Florence, Via Luigi Sacconi 6, 50019 Sesto Fiorentino, Florence, Italy
Tel: +39-055-4574192
E-mail: ciofi@cerm.unifi.it

Veronica Nasta, Dafne Suraci, Spyridon Gourdoupis contributed equally to this work

(Received 5 August 2019, revised 8 October 2019, accepted 13 November 2019)

doi:10.1111/febs.15140

During its late steps, the mitochondrial iron–sulfur cluster (ISC) assembly machinery leads to the formation of [4Fe-4S] clusters. *In vivo* studies revealed that several proteins are implicated in the biosynthesis and trafficking of [4Fe-4S] clusters in mitochondria. However, they do not provide a clear picture into how these proteins cooperate. Here, we showed that three late-acting components of the mitochondrial ISC assembly machinery (GLRX5, BOLA3, and NFU1) are part of a ISC assembly pathway leading to the synthesis of a $[4Fe\text{-}4S]^{2+}$ cluster on NFU1. We showed that the $[2Fe\text{-}2S]^{2+}$ GLRX5-BOLA3 complex transfers its cluster to monomeric apo NFU1 to form, in the presence of a reductant, a $[4Fe\text{-}4S]^{2+}$ cluster bound to dimeric NFU1. The cluster formation on NFU1 does not occur with $[2Fe\text{-}2S]^{2+}$ GLRX5, and thus, the [4Fe-4S] cluster assembly pathway is activated only in the presence of BOLA3. These results define NFU1 as an 'assembler' of [4Fe-4S] clusters, that is, a protein able of converting two $[2Fe\text{-}2S]^{2+}$ clusters into a $[4Fe\text{-}4S]^{2+}$ cluster. Finally, we found that the $[4Fe\text{-}4S]^{2+}$ cluster bound to NFU1 has a coordination site which is easily accessible to sulfur-containing ligands, as is typically observed in metallochaperones. This finding supports a role for NFU1 in promoting rapid and controlled cluster-exchange reaction.

Introduction

Mitochondria play a key role in the maturation of iron–sulfur (Fe-S) proteins [1,2]. Within mitochondria, the biosynthesis of Fe-S clusters and their insertion into mitochondrial apo target proteins is assisted by at least 17 proteins forming the mitochondrial iron–sulfur cluster (ISC) assembly machinery [2]. In this machinery, [4Fe-4S] clusters are formed by a specific system, including ISCA1 and ISCA2 proteins, that generate a [4Fe-4S] cluster by coupling two [2Fe-2S] clusters [1,2]. The [4Fe-4S] clusters are then transferred to apo target proteins with the assistance of the so-called ISC targeting factors. One of these factors is the

Abbreviations
BMRB, biological magnetic resonance bank; Fe-S, iron–sulfur; GSH, reduced glutathione; HADDOCK, high ambiguity-driven protein–protein docking; HSQC, heteronuclear single quantum coherence; IPTG, isopropyl β-D-1-thiogalactopyranoside; ISC, iron–sulfur cluster; LB, Luria–Bertani; NOE, nuclear overhauser effect; OD, optical density; R_1, longitudinal relaxation rate; R_2, transverse relaxation rate; SAXS, small-angle X-ray scattering; SEC-MALS, size exclusion chromatography combined with multiangle light scattering; TCEP, tris (2-carboxyethyl) phosphine.

universally present NFU1 protein [3]. NFU1 was initially thought to be an alternative scaffold to ISCU [4,5], a protein *de novo* assembling Fe-S clusters [6]. Other studies supported a model that NFU1 works in a late step of the mitochondrial ISC assembly machinery transferring a [4Fe-4S] cluster to selected apo target proteins [7,8]. The current prevailing model, largely based on studies in *Saccharomyces cerevisiae* [8], proposes that NFU1 receives a [4Fe-4S] cluster assembled on the ISCAs system and then transfers it to selected apo target proteins with the assistance of BOLA3, another protein of the mitochondrial ISC assembly machinery. This model was supported by the observation of an interaction of yeast NFU1 homologue with both yeast ISCAs homologues and with [4Fe-4S] target proteins, and of an interaction of yeast BOLA3 homologue with the same target proteins of yeast NFU1 homologue [8]. However, the interaction between yeast NFU1 and BOLA3 homologues was not experimentally observed in mitochondrial lysates and not clearly identified in pull-down experiments, being proposed to be transient [8]. Thus, whether and how BOLA3 may facilitate [4Fe-4S] cluster dissociation and transfer from NFU1 to apo target proteins is still unclear. On the other hand, BOLA3 has been found to form a stable dimeric hetero-complex with GLRX5 [9,10], a monothiol glutaredoxin-related component of the mitochondrial ISC assembly machinery that operates upstream in the machinery receiving a $[2Fe\text{-}2S]^{2+}$ cluster assembled on the ISCU scaffold protein [11]. The hetero-dimeric GLRX5-BOLA3 complex is formed both as apo and having a bridged $[2Fe\text{-}2S]^{2+}$ cluster. The $[2Fe\text{-}2S]^{2+}$ GLRX5-BOLA3 hetero-dimeric complex is preferentially formed as hetero-complex with respect to homo-dimeric $[2Fe\text{-}2S]^{2+}$ GLRX5 [9,10]. The proposed functional role of the $[2Fe\text{-}2S]^{2+}$ GLRX5-BOLA3 complex is that of transferring the cluster to apo acceptor(s), although the target(s) need(s) to be identified [10].

While BOLA3 sequence analysis with sorting programs [12,13] uniquely identifies only a mitochondrial isoform, analyses of genomic DNA, transcripts, and translation products indicate that alternative splicing of a common pre-mRNA results in the synthesis of two NFU1 human isoforms with distinct subcellular localizations [5]. Isoform I of NFU1 is localized in the mitochondria and, once processed by mitochondrial processing peptidases has a mature form with a molecular mass of ~ 22 kDa (mNFU1, hereafter), whereas isoform II is present in the cytosol and the nucleus having a molecular mass of ~ 26 kDa [5]. The mitochondrial targeting sequence in mNFU1 is composed by the first 58 residues at the N terminus of the protein [14]. Human mNFU1 is required for the proper assembly of a subset of mitochondrial [4Fe-4S] proteins, which include components of respiratory complexes I and II, and lipoyl synthase [4,7,15]. A recent structural characterization of a construct of human NFU1 42-residue longer at the N terminus than mNFU1 sequence (42-NFU1 hereafter) showed that the apo protein is monomeric in solution and adopts a dumbbell-shaped structure with well-structured N- and C-domains connected by a linker [16]. It has been also shown that chemically Fe-S cluster reconstituted 42-NFU1 binds a [4Fe-4S] cluster [16]. Combined NMR and small-angle X-ray scattering (SAXS) data showed that the holo form is constituted by a trimer of dimers, each containing a [4Fe-4S] cluster [16]. Three N-domains are involved in the formation of a tripartite interface, while two conserved cysteines in the C-domain ligate a [4Fe-4S] cluster to form a dimer by bridging two C-domains.

With the aim of characterizing the molecular function of GLRX5, BOLA3, and mNFU1 in the mitochondrial ISC assembly machinery, we have here first characterized the structure of the holo form of mNFU1 and its interaction with BOLA3 and then investigated the interaction between apo mNFU1 and [2Fe-2S] GLRX5-BOLA3 or [2Fe-2S] GLRX5.

Results

Mitochondrial human NFU1 dimerizes to bind a [4Fe-4S] cluster

The mitochondrial isoform of human NFU1 has a mature state with a molecular mass of ~ 22 kDa, produced after the removal of a N-terminal mitochondrial targeting sequence of 58 residues (mNFU1, hereafter) [5,14]. mNFU1 was isolated from *Escherichia coli* cells in the apo form (see Materials and methods for details). Analytical size exclusion chromatography combined with multiangle light scattering (SEC-MALS) performed on apo mNFU1 showed the presence of a major species eluting with a molar mass of at ~ 22 kDa, corresponding to the monomeric form and of a minor species eluting with a molar mass of 47 kDa (Fig. 1A), which corresponds to a homo-dimeric form of mNFU1. The monomeric and dimeric forms are in equilibrium, whose position almost completely shifts to the monomer upon the increase of the ionic strength to 150 mM NaCl (Fig. 1B). In agreement with this, the reorientational correlation time, estimated from the average ^{15}N transverse relaxation rate (R_2)/longitudinal relaxation rate (R_1) ratios of backbone NHs (Fig. 1C), decreased from 13.5 ± 0.90 ns to 11.8 ± 0.92 ns by addition of 150 mM NaCl. The Brownian rotational

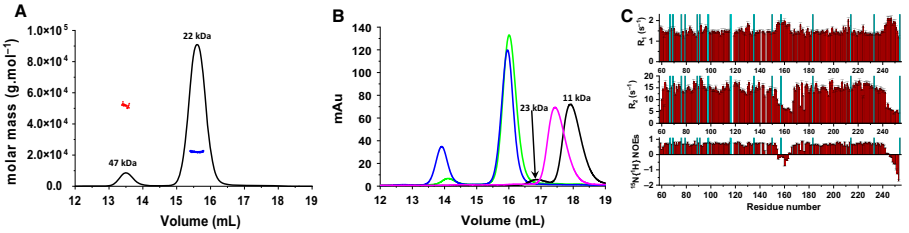

Fig. 1. Monomer-dimer equilibrium and backbone dynamics of apo mNFU1. (A) SEC-MALS profile of apo mNFU1 in phosphate buffer 50 mM pH 7.0, 5 mM DTT, 150 mM NaCl. The red and blue dots indicate the molecular masses in g·mol^{-1} of dimeric and monomeric apo mNFU1, calculated by MALS for each point of the curve. (B) Analytical gel-filtration of apo mNFU1 in phosphate buffer 50 mM pH 7.0, 5 mM DTT with (green) and without (blue) 150 mM NaCl, and of C-domain (magenta) and N-domain (black) of apo mNFU1 in phosphate buffer 50 mM pH 7.0, 150 mM NaCl, 5 mM DTT. (C) ^{15}N R_1, R_2, and heteronuclear ^{15}N{^{1}H} NOEs values (red bars) versus residue number of apo mNFU1 at 298 K in 50 mM phosphate buffer pH 7.0, 5 mM DTT, 150 mM NaCl. Error bars are represented as standard deviation. The cyan bars represent proline residues. The residues whose NHs are not detected or too broad to be analyzed are not shown. SEC-MALS and NMR relaxation experiments were repeated three times.

correlation time value of 10.11 ns calculated for a 24 kDa spherical particle surrounded by a single layer of water [17] is consistent with a globular shape for the ~ 22 kDa mNFU1 molecule, but the present data does not conclusively exclude that some flexibility between the two domains is present. Indeed, eleven backbone NHs of the residues connecting the two domains (i.e., EETPSGEAGSEE, named flexible linker hereafter) show fast backbone motions in the ns-ps time scale experiencing very low or negative heteronuclear ^{15}N [^{1}H] nuclear overhauser effect (NOEs; Fig. 1C). This behavior is typical of highly unstructured and flexible regions and suggests the possible presence of domain-domain flexibility. To investigate whether the two domains interact with each other, we have produced the single N- and C-domains. SEC-MALS data showed that the apo form of the C-domain is fully monomeric in solution, while the N-domain showed the presence of a major species eluting with a molar mass of ~ 11 kDa, corresponding to the monomer, and of a minor species eluting with a molar mass of ~ 23 kDa corresponding to the dimer (Fig. 1B). The ^{1}H-^{15}N heteronuclear single quantum coherence (HSQC) spectra of the N- and C-domains were compared with that of the full-length protein in the presence of 5 mM reduced DTT, to avoid disulfide-linked dimerization as previously observed under oxidizing conditions [16]. Chemical shifts changes were observed on the two α-helices of the C-domain and on the short α-helix, the 3_{10}-helix, and the C terminus of the N-domain (Fig. 2A,B). The flexible linker is required for determining this interaction since, by mixing at 1 : 1 ratio the two single N- and C-domains that do not contain residues 156–161 of the linker, no chemical shifts were observed. In summary, the data indicate that the two domains in the apo mNFU1 monomer, although connected by a flexible linker, are not fully independent. Docking N-domain and C-domain by high ambiguity-driven protein–protein docking (HADDOCK) [18,19] based on chemical shift perturbation data produced a top-scoring cluster of 41 structures out of 200 calculated with a RMSD, from the lowest-energy structure, of 1.1 ± 0.8 Å and a HADDOCK score of −80.0 ± 1.6 (Table 1). The obtained structural model mimics a closed conformational state of monomeric apo mNFU1, but other possible conformations describing the dynamics of the two domains of monomeric mNFU1 are likely present in solution. The best structure, shown in Fig. 2C, indicates that the two domains interact through a hydrophobic patch and a charged patch. These interactions orient the two domains so that the conserved metal-binding CXXC motif, located in the C-domain of mNFU1, is fully exposed to the solvent and can thus be involved in cluster binding (Fig. 2C).

The UV-visible absorption spectrum of the chemically Fe-S cluster reconstituted mNFU1 ([4Fe-4S]$^{2+}$ mNFU1, hereafter, Fig. 3A) showed the presence of a broadband centered at ~ 410 nm, as previously reported [5], which typically dominates the absorption spectra of biological [4Fe-4S]$^{2+}$ clusters [6]. The CD spectrum of [4Fe-4S]$^{2+}$ mNFU1 (Fig. 3B) in the UV-visible region is very weak and featureless, which is also characteristic of biological [4Fe-4S]$^{2+}$ clusters [20]. Moreover, the extinction coefficient at 410 nm of 8.3 mM^{-1}·cm^{-1}, based on the mNFU1 monomeric concentration, is consistent with one [4Fe-4S]$^{2+}$ cluster per mNFU1 dimer [21]. The C-domain of mNFU1 was also chemically Fe-S cluster reconstituted but, in

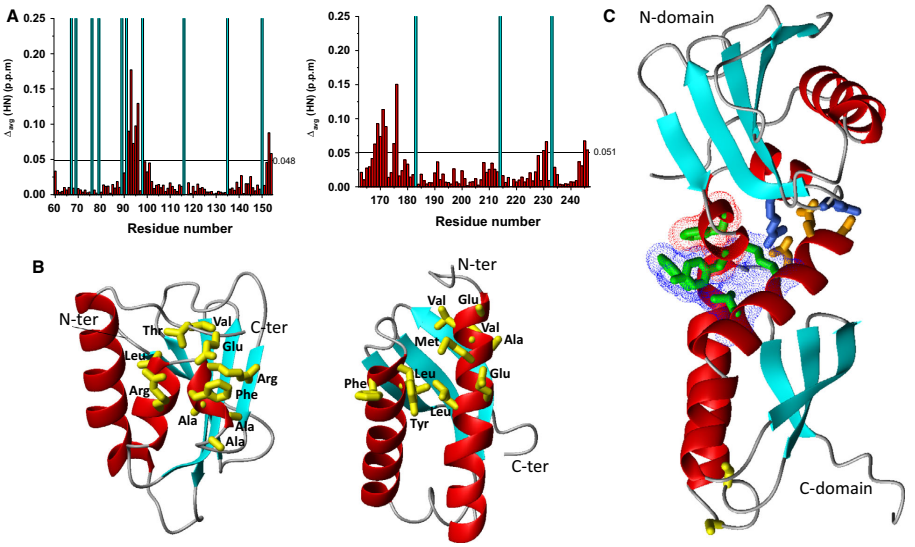

Fig. 2. Structural properties of apo mNFU1. (A) Backbone weighted average chemical shift differences Δ_{avg}(HN) (i.e., $(((\Delta H)^2 + (\Delta N/5)^2)/2)^{1/2}$) (red bars), between full-length apo mNFU1 and the N-domain (left panel) or apo C-domain (right panel) of mNFU1. The indicated threshold values (obtained by averaging Δ_{avg}(HN) values plus 1σ) were used to define meaningful chemical shift differences. The cyan bars represent proline residues. (B) The side chains of the residues experiencing meaningful chemical shift differences were mapped as yellow sticks on the solution structures of N- and apo C-domains [16]. (C) Theoretical modeling of N-domain docking to apo C-domain of mNFU1 using HADDOCK program. Hydrophobic residues on both structures are in green, and their contact surfaces are as dotted areas in red and blue on N-domain and apo C-domain, respectively. Positively charged residues, Arg and Lys, and negatively charged residues, Asp and Glu, are in blue and orange, respectively. Cysteines of the conserved CXXC motif are in yellow. NMR experiments were repeated three times. The models shown in panels B and C were rendered with MOLMOL molecular graphics program.

all tested conditions, no more than ~ 50% of $[4Fe\text{-}4S]^{2+}$ loaded mNFU1 was obtained, demonstrating that the N-domain is essential to obtain a quantitative cluster binding on the C-domain. ^{15}N heteronuclear NMR relaxation measurements on $[4Fe\text{-}4S]^{2+}$ mNFU1 (Fig. 3C) provided a reorientational correlation time of 15.1 ± 1.2 ns, increased with respect to the value of 11.8 ns estimated for apo mNFU1, in agreement with protein dimerization. The heteronuclear $^{15}N[^1H]$ NOEs of the flexible linker are still negative in $[4Fe\text{-}4S]^{2+}$ mNFU1, indicating that the linker conserves its flexibility in the holo form (Fig. 3C). The comparison of the $^1H\text{-}^{15}N$ HSQC spectrum of $[4Fe\text{-}4S]^{2+}$ mNFU1 with that of apo mNFU1 revealed that the Fe-S cluster binding led to large chemical shift perturbations and significant line broadening (Fig. 4A). Only one set of peaks for each residue was observed in the $^1H\text{-}^{15}N$ HSQC spectrum of $[4Fe\text{-}4S]^{2+}$ mNFU1, as it occurs in the $^1H\text{-}^{15}N$ HSQC spectrum of apo mNFU1 (Fig. 4A), indicating the presence of a symmetric holo dimer. Chemical shift perturbations were observed on both N- and C-domains. Specifically, while the N-domain shows only chemical shift changes, the C-domain shows also line broadening effects beyond detection for eleven backbone NHs of the region containing the conserved CXXC motif. These broadening effects are a consequence of the binding of the paramagnetic [4Fe-4S] cluster to the cysteines of the CXXC motif. The peaks of the N-domain in the $^1H\text{-}^{15}N$ HSQC spectrum of $[4Fe\text{-}4S]^{2+}$ mNFU1 do not match with those of the single N-domain of mNFU1, suggesting that the N-domain is not fully independent to move in solution in $[4Fe\text{-}4S]^{2+}$ mNFU1 (Fig. 4B). In summary, these data indicate that the cluster is bridged between two C-domains in the symmetric dimer and is coordinated by two CXXC motifs from each subunit of the dimer. On the contrary, the N-domain is not directly involved in cluster binding and the chemical shift changes observed on its residues upon cluster binding reflect a change of the intramolecular contacts between the N- and C-domains.

Table 1. Statistics of the HADDOCK docking run for the first three best-scoring clusters by docking N-domain and C-domain of mNFU1

	Cluster 1	Cluster 2	Cluster 3
HADDOCK score	−80.0 ± 1.6	−65.8 ± 5.2	−55.4 ± 2.0
Cluster size	41	18	49
RMSD from the overall lowest-energy structure	1.1 ± 0.8	5.7 ± 0.7	4.7 ± 1.3
Van der Waals energy	−26.4 ± 4.4	−21.3 ± 4.8	−16.2 ± 2.4
Electrostatic energy	−240.7 ± 49.1	−184.3 ± 30.0	−133.2 ± 25.8
Desolvation energy	−9.9 ± 6.3	−8.5 ± 5.1	13.1 ± 4.5
Restraints violation energy	44.6 ± 16.6	9.1 ± 1.88	4.5 ± 2.03
Buried surface area	911.1 ± 47.4	900.5 ± 63.2	721.6 ± 49.4
Z-score	−2.0	−0.8	0.1

The paramagnetic 1D ^{1}H NMR spectrum of [4Fe-4S]$^{2+}$ mNFU1 showed the presence of two close hyperfine-shifted signals at 20.2 and 19.5 p.p.m. and one at 12.7 p.p.m. (Fig. 4Ca), all showing an anti-Curie temperature dependence. The chemical shift values of these signals, their anti-Curie temperature dependence, and their linewidths are typical of βCH_2 signals of Cys residues bound to a [4Fe-4S]$^{2+}$ cluster with an S = 0 electronic ground state, with the paramagnetism arising from excited states of the electron spin ladder, partially populated at room temperature [22]. By adding 5 mM reduced glutathione (GSH) to [4Fe-4S]$^{2+}$ mNFU1, the 1D ^{1}H paramagnetic NMR spectrum changes showing the presence of three further hyperfine-shifted signals at 15.5, 13.5, and 11.3 p.p.m. (Fig. 4Cb), indicating that GSH modifies the coordination environment, possibly acting as a ligand with its Cys residue. Nevertheless, GSH does not fully replace the Cys protein ligand since the three signals at 20.2, 19.5, 12.7 p.p.m. are still present (Fig. 4Cb). A mixture of at least two [4Fe-4S]$^{2+}$ species is present, most likely one derived from all protein-derived Cys protein ligands and the other from a GSH ligand and three protein-derived Cys ligands. Analyzing the interaction between apo mNFU1 and GSH through ^{1}H-^{15}N HSQC experiments, it appears that the chemical shifts of the backbone NH signals of Cys 213, Ser 215, Ser 216, Ile 217, Ile 218, Leu 220, that include and surround the CXXC motif, change upon the addition of GSH (Fig. 5A). The solution NMR structure of the C-domain of mNFU1 in its apo form [16] showed that Cys 213 ligand is more solvent-exposed than the other cysteine ligand, that is, Cys 210 (Fig. 5B). Our NMR data thus indicate that GSH interacts with the region close to the solvent-exposed Cys 213, suggesting that this cysteine is the ligand preferentially displaced by GSH in [4Fe-4S]$^{2+}$ mNFU1 (Fig. 5B). Upon addition of 5 mM DTT to the 5 mM GSH/[4Fe-4S]$^{2+}$ mNFU1 mixture, the 1D ^{1}H paramagnetic NMR spectrum showed further changes. The three signals at 20.2, 19.5, 12.7 p.p.m. of the DTT- and GSH-free protein as well as the three signals of the GSH-bound form disappeared, and three new signals at 20.3, 14.5, and 13.6 p.p.m. appear, all displaying an anti-Curie temperature dependence (Fig. 4Cc). The size and the anti-Curie temperature dependence of the chemical shifts of these signals indicate that a [4Fe-4S]$^{2+}$ cluster with an S = 0 electronic ground state is still bound to mNFU1 in the presence of DTT, but the change observed in

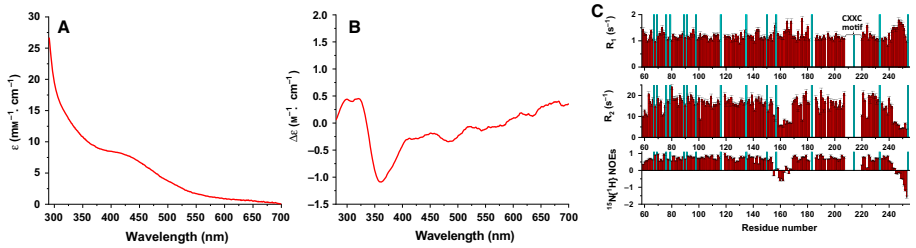

Fig. 3. UV-visible absorption spectroscopy and backbone dynamics on chemically reconstituted [4Fe-4S]$^{2+}$ mNFU1. UV-visible (A) and CD-visible (B) spectra of [4Fe-4S]$^{2+}$ mNFU1 in 50 mM phosphate buffer pH 7.0, 5 mM DTT, 150 mM NaCl. (C) ^{15}N R_1, R_2 and heteronuclear ^{15}N [^{1}H] NOEs values (red bars) versus residue number of [4Fe-4S]$^{2+}$ mNFU1 at 298 K in 50 mM phosphate buffer pH 7.0, 5 mM DTT, 150 mM NaCl. The cyan bars represent proline residues. The residues whose NHs are not detected or too broad to be analyzed are not shown. UV-vis, CD, and NMR relaxation experiments were repeated three times.

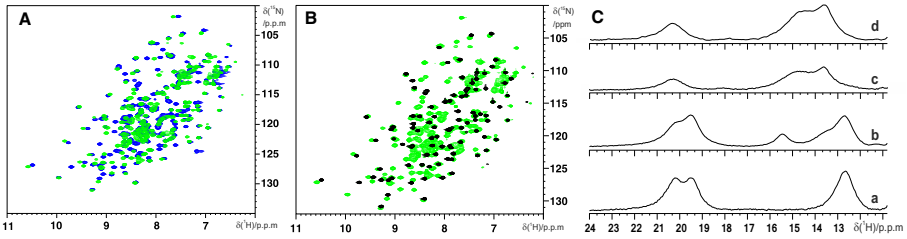

Fig. 4. NMR characterization of $[4Fe\text{-}4S]^{2+}$ mNFU1. (A) Overlay of $^{1}H\text{-}^{15}N$ HSQC spectra of apo (blue) and $[4Fe\text{-}4S]^{2+}$ (green) mNFU1, acquired at 298 K in 50 mM phosphate buffer pH 7.0, 5 mM DTT, 150 mM NaCl. (B) Overlay of $^{1}H\text{-}^{15}N$ HSQC spectra of $[4Fe\text{-}4S]^{2+}$ mNFU1 (green) and of the N-domain of mNFU1 (black), acquired at 298 K in 50 mM phosphate buffer pH 7.0, 5 mM DTT, 150 mM NaCl. (C) 1D ^{1}H NMR spectra tailored for the detection of hyperfine-shifted signals of $[4Fe\text{-}4S]^{2+}$ mNFU1 were acquired at 298 K in 50 mM phosphate buffer pH 7.0, 150 mM NaCl (a), and upon sequential additions of 5 mM GSH (b) and 5 mM DTT to the same protein sample (c), and of $[4Fe\text{-}4S]^{2+}$ mNFU1 acquired in the presence of 5 mM DTT alone. NMR experiments were repeated three times.

their pattern indicates a modified cluster coordination, where DTT acts as a cluster ligand and fully displaces GSH from coordination. In agreement with this interpretation of the NMR data, the paramagnetic 1D ^{1}H NMR spectrum of $[4Fe\text{-}4S]^{2+}$ mNFU1 acquired in the presence of 5 mM DTT alone (i.e., sample never treated with GSH) is perfectly superimposable with that acquired in the presence of 5 mM GSH and 5 mM DTT (Fig. 4Cd), confirming that DTT fully displaced GSH in the coordination sphere of the cluster.

The $^{1}H\text{-}^{15}N$ HSQC spectra acquired on $[4Fe\text{-}4S]^{2+}$ mNFU1 in the presence of DTT (or GSH) are also different from that of DTT-free (or GSH-free) $[4Fe\text{-}4S]^{2+}$ mNFU1 but the observed resonances do not have the chemical shifts of apo mNFU1 (Fig. 6A). This result agrees with the model that GSH and DTT are unable to displace a mNFU1 molecule from the holo dimer to form a monomeric $[4Fe\text{-}4S]^{2+}$ mNFU1 species where two GSH or DTT molecules bind to the cluster. In such a case, the appearance of peaks corresponding to an apo mNFU1 molecule released from the holo dimer would be indeed expected in the $^{1}H\text{-}^{15}N$ HSQC spectrum of the DTT (or GSH)/$[4Fe\text{-}4S]^{2+}$ mNFU1 mixture. Finally, 1D ^{1}H paramagnetic or $^{1}H\text{-}^{15}N$ HSQC NMR spectra (Figs 6B and 5A), acquired on $[4Fe\text{-}4S]^{2+}$ mNFU1 treated first with GSH (or DTT) or and then passed on a PD-10 desalting column, are the same as that of the GSH-free (or DTT-free) $[4Fe\text{-}4S]^{2+}$ mNFU1, indicating that the DTT and GSH molecules initially bound to the cluster are then removed from the cluster coordination, due to an equilibrium between GSH/DTT-bound holo protein and free GSH/DTT holo protein.

BOLA3 drives the [4Fe-4S] cluster assembly on mNFU1

Considering the proposed model that a mNFU1-BOLA3 complex mediates the transfer of a [4Fe-4S] cluster from ISCA complex to apo target proteins [8],

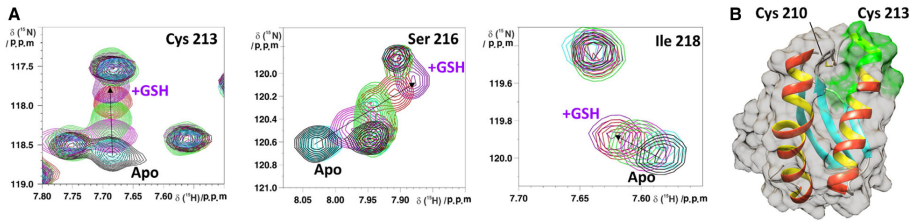

Fig. 5. Monitoring the interaction between GSH and apo mNFU1 by NMR. (A) Overlay of $^{1}H\text{-}^{15}N$ HSQC spectra of apo ^{15}N-labeled mNFU1, acquired at 298 K in 50 mM phosphate buffer pH 7.0, 150 mM NaCl, in the absence (black) and in the presence of increasing concentrations of GSH up to 7 mM (from black to violet). The final mixture was exchanged in the original buffer in the absence of GSH (cyan). (B) Mapping the chemical shift changes (shown in green) on the C-domain of mNFU1 (PDB ID 2M5O) occurring upon the interaction between apo mNFU1 and GSH. NMR experiments were repeated three times. The model shown in panel 5B was rendered with UCSF Chimera.

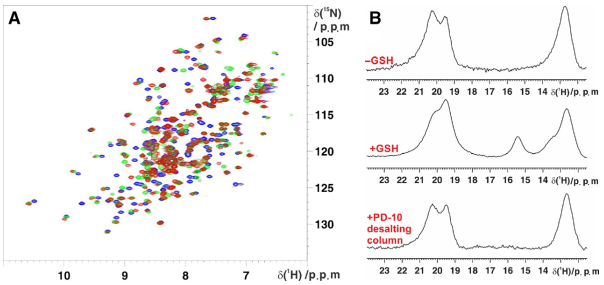

Fig. 6. DTT does not promote the formation of apo mNFU1 by its addition to $[4Fe\text{-}4S]^{2+}$ mNFU1 and GSH-binding equilibrium in $[4Fe\text{-}4S]^{2+}$ mNFU1. (A) Overlay of $^{1}H\text{-}^{15}N$ HSQC spectra of ^{15}N-labeled $[4Fe\text{-}4S]^{2+}$ mNFU1 in the presence (green) and in the absence (red) of 5 mM DTT with that of ^{15}N-labeled apo mNFU1 (blue) in the presence of 5 mM DTT, acquired at 298 K in 50 mM phosphate buffer pH 7.0, 150 mM NaCl. (B) 1D ^{1}H NMR spectra tailored for the detection of hyperfine-shifted signals of $[4Fe\text{-}4S]^{2+}$ mNFU1 in the absence of GSH (upper), in the presence of 5 mM GSH (middle) and after exchanging, through PD-10 desalting column, the latter mixture in the same buffer but not containing GSH. NMR spectra were acquired at 298 K in 50 mM phosphate buffer pH 7.0 and 150 mM NaCl. NMR experiments were repeated two times.

we have investigated, by NMR, UV-visible and CD spectroscopy, the potential interaction between BOLA3 and mNFU1. NMR titration experiments on ^{15}N-labeled samples showed that apo NFU1 does not interact with BOLA3 (Fig. 7A,B). To characterize the potential interaction between BOLA3 and mNFU1 in the presence of a Fe-S cluster, we have performed a chemical reconstitution with iron and sulfide ions on a mixture composed by apo mNFU1 and BOLA3 in various experimental conditions (see Experimental Section for details) and spectroscopically characterized it. In all cases, the UV-visible and CD spectra are essentially identical to the spectra of $[4Fe\text{-}4S]^{2+}$ mNFU1 (Fig. 8A,B), suggesting that BOLA3 does not modify the Fe-S cluster nuclearity. Consistently, the ^{1}H 1D paramagnetic NMR spectrum of the chemically reconstituted mixture is typical of that of $[4Fe\text{-}4S]^{2+}$ mNFU1 (Fig. 8C), indicating that BOLA3 does not contribute to the cluster binding. Comparison of the $^{1}H\text{-}^{15}N$ HSQC NMR spectra of the chemically reconstituted mixture with those of the isolated proteins showed that the two proteins do not interact each other since no significant chemical shift changes occurred and that only a $[4Fe\text{-}4S]^{2+}$ mNFU1 species is formed in the chemical Fe-S cluster reconstitution process (Fig. 7C,D). We also tested the potential interaction between BOLA3 and $[4Fe\text{-}4S]^{2+}$ NFU1 in the presence of GLRX5 by performing a NMR titration experiment where unlabeled $[4Fe\text{-}4S]^{2+}$ mNFU1 was added to a 1 : 1 mixture of ^{15}N-labeled BOLA3 and unlabeled apo GLRX5. The results showed that the apo protein complex formed between GLRX5 and BOLA3 [9,10] does not interact with $[4Fe\text{-}4S]^{2+}$ mNFU1 (Fig. 7E). In conclusion, we can rule out any possible interaction of BOLA3 with either apo or $[4Fe\text{-}4S]^{2+}$ mNFU1 in the absence and in the presence of GLRX5.

The latter results brought us to investigate a different pathway through which BOLA3 and mNFU1 can cooperate in assisting the formation of a [4Fe-4S] cluster on apo target proteins. Since it has been already shown that BOLA3 and GLRX5 form a heterodimeric complex able to bind a $[2Fe\text{-}2S]^{2+}$ cluster [9,10], we investigated whether this complex can interact with apo mNFU1, transfer the cluster, and form a [4Fe-4S] cluster on mNFU1. We followed these possible processes by NMR, UV-visible, and CD spectroscopy. The experiments were performed by adding either apo mNFU1 to the $[2Fe\text{-}2S]^{2+}$ GLRX5-BOLA3 hetero-complex or vice versa, and, for NMR measurements, ^{15}N-labeling one protein at a time or ^{15}N-labeling two out of the three proteins. Comparing the UV-visible spectrum of the $[2Fe\text{-}2S]^{2+}$ GLRX5-BOLA3 hetero-complex with those of two mixtures containing different ratios of $[2Fe\text{-}2S]^{2+}$ GLRX5-BOLA3 and apo mNFU1, significant changes of the absorption bands were observed (Fig. 9A). In particular, the bands characteristic of the $[2Fe\text{-}2S]^{2+}$ cluster bound to GLRX5-BOLA3 complex decrease in intensity and the final spectrum resembles to that of $[4Fe\text{-}4S]^{2+}$ mNFU1 (Fig. 9A). The same mixtures, analyzed by CD spectroscopy, showed a loss of intensity of the CD signals of the $[2Fe\text{-}2S]^{2+}$ GLRX5-BOLA3 hetero-complex, suggesting the formation of $[4Fe\text{-}4S]^{2+}$ mNFU1, whose CD signals are indeed very low in intensity (Fig. 9B) [20,23]. In the NMR titration between the $[2Fe\text{-}2S]^{2+}$

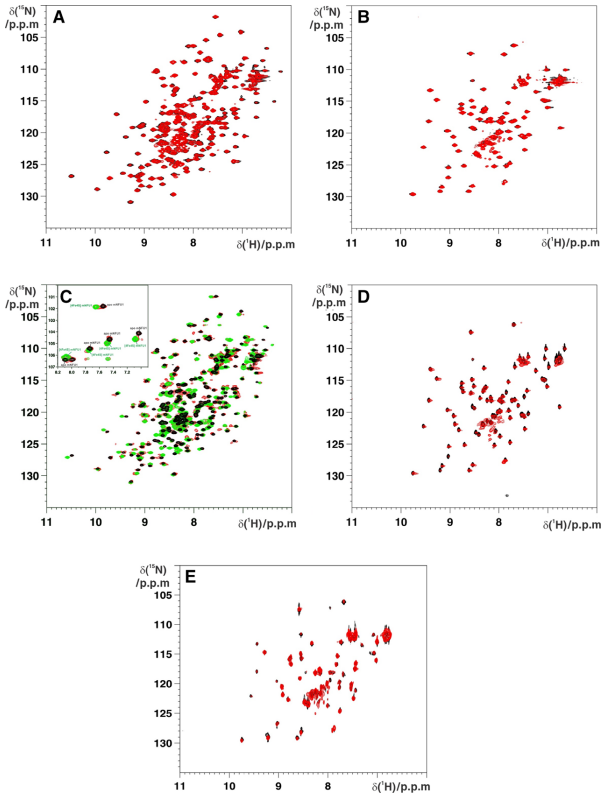

Fig. 7. BOLA3 does not interact with mNFU1. Overlay of ^{1}H-^{15}N HSQC NMR spectra of (A) ^{15}N-labeled apo mNFU1 (black) and a 1 : 1 mixture of ^{15}N-labeled apo mNFU1 and unlabeled BOLA3 (red); (B) ^{15}N-labeled BOLA3 (black) and a 1 : 1 mixture of ^{15}N-labeled BOLA3 and unlabeled apo mNFU1 (red); (C) ^{15}N-labeled apo mNFU1 (black), ^{15}N-labeled [4Fe-4S]$^{2+}$ mNFU1 (green) and a chemically Fe-S cluster reconstituted 2 : 1 mixture of unlabeled BOLA3 and ^{15}N-labeled apo mNFU1 (red); (D) ^{15}N-labeled BOLA3 (black) and a chemically Fe-S cluster reconstituted 1 : 1 mixture of ^{15}N-labeled BOLA3 and unlabeled apo mNFU1 (red); (E) apo ^{15}N-labeled BOLA3-unlabeled GLRX5 hetero-complex (black) and a 1 : 1 mixture of apo ^{15}N-labeled BOLA3-unlabeled GLRX5 hetero-complex and unlabeled [4Fe-4S]$^{2+}$ mNFU1 (red), both in the presence of 5 mM GSH. NMR spectra were acquired at 298 K in 50 mM phosphate buffer pH 7.0, 5 mM DTT and 150 mM NaCl. NMR experiments were repeated three times.

^{15}N-labeled GLRX5-unlabeled BOLA3 complex and unlabeled apo mNFU1, the resonances of the [2Fe-2S]$^{2+}$ GLRX5-BOLA3 hetero-complex disappeared and concomitantly the resonances of the apo GLRX5-BOLA3 hetero-complex appeared (Fig. 9D), indicating the cluster release from the hetero-complex. In the titration between the unlabeled [2Fe-2S]$^{2+}$ GLRX5-^{15}N-labeled BOLA3 complex and ^{15}N-labeled apo mNFU1, the changes observed for the BOLA3 resonances indicate again the occurrence of cluster release from the hetero-complex (Fig. 9E). Concomitantly, the new resonances appearing in the ^{1}H-^{15}N HSQC map of the mixture have chemical shifts matching with those of [4Fe-4S]$^{2+}$ mNFU1, indicating the formation of [4Fe-4S]$^{2+}$ mNFU1 (Fig. 9F). In agreement with the latter data, the 1D ^{1}H paramagnetic NMR spectrum acquired on the final mixture showed the presence of the typical peaks of [4Fe-4S]$^{2+}$ mNFU1 (Fig. 9C). Overall, the experimental data indicate the transfer of two [2Fe-2S]$^{2+}$ clusters from the [2Fe-2S]$^{2+}$ GLRX5-BOLA3 hetero-complex to apo mNFU1 and the concomitant formation of a [4Fe-4S]$^{2+}$ cluster. A reducing agent is absolutely required for converting ferric ions present in the [2Fe-2S]$^{2+}$ cluster into a mixture of ferric and ferrous ions in the [4Fe-4S]$^{2+}$ cluster (reductive coupling reaction) [23–25]. Considering that 5 mM DTT and 5 mM GSH were present in all protein mixtures, these two small molecules are the best candidates to act as reducing agents. To verify this hypothesis, the same experiment reported above was performed in the absence of DTT, that is, the [2Fe-2S]$^{2+}$ unlabeled GLRX5-^{15}N-labeled BOLA3 complex mixed with ^{15}N-labeled apo mNFU1. In this case, we observed that the reaction did not proceed, that is, no

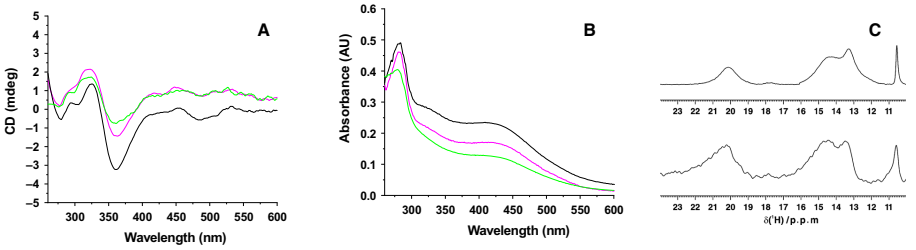

Fig. 8. BOLA3 does not modify cluster binding properties of mNFU1. UV-visible (A) and CD-visible (B) spectra of chemically reconstituted mixtures of BOLA3 and mNFU1: magenta, chemical reconstitution of BOLA3 : mNFU1 at a 1 : 1 ratio in the presence of 5 mM GSH, 5 mM DTT, and 150 mM NaCl; black, chemical reconstitution of BOLA3 : mNFU1 at a 1 : 1 ratio in the presence of 5 mM DTT and 150 mM NaCl. In green are the UV-visible and visible CD spectra of $[4Fe\text{-}4S]^{2+}$ mNFU1. (C) 1D ^{1}H NMR spectra tailored for the detection of hyperfine-shifted signals of $[4Fe\text{-}4S]^{2+}$ mNFU1 (upper) and of the chemically reconstituted 1 : 1 BOLA3:mNFU1 mixture (lower). NMR spectra were acquired at 298 K in 50 mM phosphate buffer pH 7.0, 5 mM DTT, and 150 mM NaCl. UV-vis, CD, and NMR experiments were repeated three times.

$[2Fe\text{-}2S]^{2+}$ cluster transfer occurred nor $[4Fe\text{-}4S]^{2+}$ cluster was formed. Indeed, the $^{1}H\text{-}^{15}N$ HSQC spectrum of the mixture is superimposable with those of the individual proteins and no peaks of the $[4Fe\text{-}4S]^{2+}$ mNFU1 product are formed (Fig. 10). DTT is therefore the reducing agent *in vitro* required for the reductive coupling reaction to occur. DTT is, however, not an efficient reducing system. Indeed, DTT is not able to quantitatively form the $[4Fe\text{-}4S]^{2+}$ mNFU1 product in the 1 : 1 $[2Fe\text{-}2S]^{2+}$ GLRX5-BOLA3/apo mNFU1 mixture, being the amount of $[4Fe\text{-}4S]^{2+}$ mNFU1 65% (estimated from $^{1}H\text{-}^{15}N$ HSQC NMR data, see Fig. 8F). Even when an excess of two equivalents of $[2Fe\text{-}2S]^{2+}$ GLRX5-BOLA3 was added to apo mNFU1, the resonances associated with apo mNFU1 do not disappear completely. Moreover, the formation of $[4Fe\text{-}4S]^{2+}$ mNFU1 occurs slowly upon time in the presence of 5 mM DTT, that is, it reaches the equilibrium only after 1 day. Overall, from these data we can gather that a physiological electron donor is required to efficiently promote $[4Fe\text{-}4S]^{2+}$ cluster formation on mNFU1. The best candidate physiological electron donor might be a ferredoxin, a versatile protein family typically involved in electron transfer in mitochondria [26]. Human mitochondria possess two mitochondrial ferredoxins, which are both present in the matrix of mitochondria and have been shown to be versatile electron mediators involved in multiple physiological processes such as Fe-S cluster biogenesis, steroidogenesis, vitamin D metabolism, and heme A biosynthesis [26–28].

We have finally observed by NMR and UV-visible spectroscopy that, when apo or $[2Fe\text{-}2S]^{2+}$ GLRX5 was mixed with apo mNFU1 using DTT as electron source, no protein–protein interaction, no cluster transfer from GLRX5 to mNFU1, and no formation of a $[4Fe\text{-}4S]^{2+}$ cluster on mNFU1 occurred (Fig. 11). This indicates that both cluster transfer and reductive coupling reactions encompassing mNFU1 require BOLA3 to occur. Thus, BOLA3 acts as a trigger factor activating cluster transfer and assembly on mNFU1.

Discussion

The late stages of the mitochondrial ISC assembly machinery are responsible of [4Fe-4S] cluster assembly, trafficking, and insertion into mitochondrial target Fe-S proteins [1,2]. The first studies on the mitochondrial [4Fe-4S] cluster assembly step showed that three human proteins ISCA1, ISCA2, and IBA57 are required for this process [29]. This functional association has been revisited in a recent work [30], which showed that ISCA2 and IBA57 are not required under standard physiological conditions for the maturation of mitochondrial [4Fe-4S] proteins. Therefore, the so far available *in vivo* data do not provide a clear picture on how the three proteins operate in the cell for assembling a [4Fe-4S] cluster. *In vitro* experiments helped to shed some light on this issue showing that (a) ISCA1 and ISCA2 form a hetero-dimer, which, by accepting two $[2Fe\text{-}2S]^{2+}$ clusters from the protein partner GLRX5 (component of the mitochondrial ISC assembly machinery receiving the $[2Fe\text{-}2S]^{2+}$ cluster from ISCU), is able to assemble a $[4Fe\text{-}4S]^{2+}$ cluster, without any need of IBA57 [25,31]; (b) ISCA2, but not ISCA1, after having received a $[2Fe\text{-}2S]^{2+}$ cluster from GLRX5, forms a $[2Fe\text{-}2S]^{2+}$-bridged hetero-dimeric

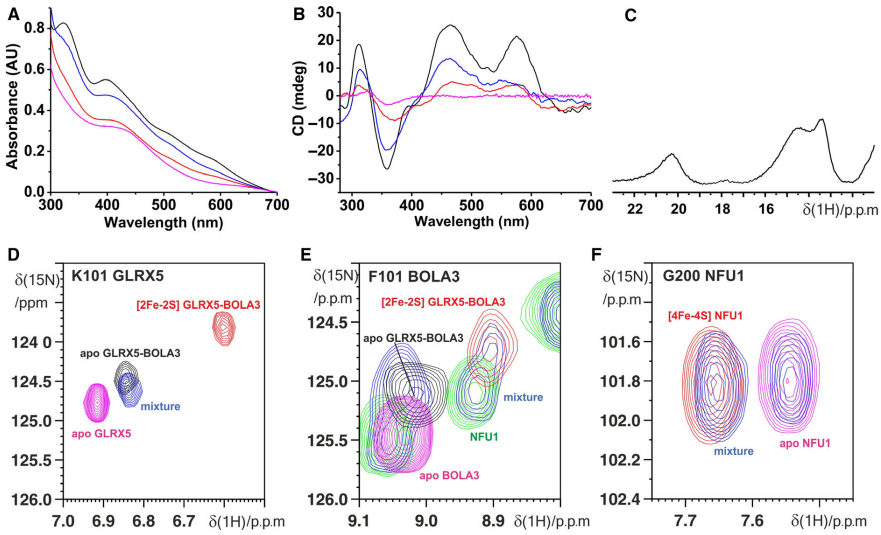

Fig. 9. $[2Fe\text{-}2S]^{2+}$ GLRX5-BOLA3 assembles a $[4Fe\text{-}4S]^{2+}$ cluster on mNFU1. UV-visible (A) and CD (B) spectra of 0.5 : 1 (blue) and 1 : 1 (red) mixtures of $[2Fe\text{-}2S]^{2+}$ GLRX5-BOLA3 hetero-complex and apo mNFU1, compared with spectra of $[2Fe\text{-}2S]^{2+}$ GLRX5-BOLA3 (black) and $[4Fe\text{-}4S]^{2+}$ mNFU1 (magenta). (C) 1D ^{1}H NMR spectra of the hyperfine-shifted signals of the 1 : 1 mixture of $[2Fe\text{-}2S]^{2+}$ GLRX5-BOLA3 hetero-complex and apo mNFU1. Overlay of ^{1}H-^{15}N HSQC NMR spectra of (D) the 1 : 1 mixture of $[2Fe\text{-}2S]^{2+}$ ^{15}N-labeled GLRX5-unlabeled BOLA3 hetero-complex and unlabeled apo mNFU1 (blue), $[2Fe\text{-}2S]^{2+}$ ^{15}N-labeled GLRX5-unlabeled BOLA3 (red), apo ^{15}N-labeled GLRX5-unlabeled BOLA3 (black) and apo ^{15}N-labeled GLRX5 (fuchsia); (E) the 1 : 1 mixture of $[2Fe\text{-}2S]^{2+}$ unlabeled GLRX5-^{15}N-labeled BOLA3 hetero-complex and apo ^{15}N-labeled mNFU1 (blue), $[2Fe\text{-}2S]^{2+}$ unlabeled GLRX5-^{15}N-labeled BOLA3 (red), apo unlabeled GLRX5-^{15}N-labeled BOLA3 (black), apo ^{15}N-labeled BOLA3 (fuchsia), and $[4Fe\text{-}4S]^{2+}$/apo ^{15}N-labeled mNFU1 (green); (F) the 1 : 1 mixture of $[2Fe\text{-}2S]^{2+}$ unlabeled GLRX5-unlabeled BOLA3 hetero-complex and apo ^{15}N-labeled mNFU1 (blue), $[4Fe\text{-}4S]^{2+}$ ^{15}N-labeled mNFU1 (red) and apo ^{15}N-labeled mNFU1 (fuchsia). All spectra were acquired at 298 K in 50 mM phosphate buffer pH 7.0, 5 mM GSH, 5 mM DTT, 150 mM NaCl. UV-vis, CD, and NMR experiments were repeated three times.

complex with IBA57, which results resistant to highly oxidative environments and capable of reactivating apo aconitase [32]. In conclusion, the *in vitro* studies suggested a model of $[4Fe\text{-}4S]^{2+}$ cluster assembly on the ISCA1-ISCA2 complex, while IBA57 might be involved with GLRX5 and ISCA2 in a specific pathway maturing Fe-S proteins under oxidative metabolism. The proposed following step of the mitochondrial ISC assembly machinery consists of the transfer and insertion of the $[4Fe\text{-}4S]^{2+}$ cluster assembled on the ISCA1-ISCA2 complex into mitochondrial target Fe-S proteins with the help of specific ISC targeting factors [1,2]. Two proteins, that is, BOLA3 and NFU1, have been proposed to be involved in this step. NFU1 was implicated in receiving the cluster from the ISCA1-ISCA2 complex [4,7], and BOLA3 was proposed to mediate the transfer of the $[4Fe\text{-}4S]^{2+}$ cluster bound to NFU1 into specific mitochondrial target proteins [8]. However, the interaction between NFU1 and BOLA3 was not clearly detected *in vivo* and it was proposed to be transient [8]. On the contrary, the interaction between BOLA3 and GLRX5 has been well documented by *in vivo* studies [33], and *in vitro* studies recently showed that BOLA3 strongly binds GLRX5, while the binding of BOLA3 to NFU1 is weak [34]. As mentioned above, GLRX5 acts in the early-acting steps of the mitochondrial ISC assembly machinery donating its $[2Fe\text{-}2S]^{2+}$ cluster to the ISCA1-ISCA2 complex [11,25]. Therefore, the raising question is whether GLRX5 has a further role as $[2Fe\text{-}2S]^{2+}$ cluster trafficking protein in the late stages of the mitochondrial ISC assembly machinery once complexed with BOLA3. Our work sheds light on this question, showing that two $[2Fe\text{-}2S]^{2+}$ GLRX5-BOLA3 complexes are able to transfer their clusters to apo NFU1 to form a $[4Fe\text{-}4S]^{2+}$ cluster on dimeric

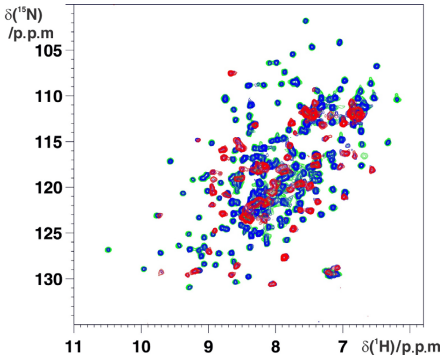

Fig. 10. A reductant is required to assemble a $[4Fe\text{-}4S]^{2+}$ cluster on mNFU1 upon the interaction with the cluster donor $[2Fe\text{-}2S]^{2+}$ GLRX5-BOLA3. Overlay of ^{1}H-^{15}N HSQC NMR spectra of $[2Fe\text{-}2S]^{2+}$ unlabeled GLRX5-^{15}N-labeled BOLA3 (red), apo ^{15}N-labeled mNFU1 (green), and a 1 : 1 mixture of $[2Fe\text{-}2S]^{2+}$ unlabeled GLRX5-^{15}N-labeled BOLA3 and apo ^{15}N-labeled mNFU1 (blue), acquired at 298 K in 50 mM phosphate buffer pH 7.0, 5 mM GSH, and 150 mM NaCl. NMR experiments were repeated three times.

NFU1 (Fig. 12). Our data showed that the mechanism for cluster transfer and assembly from $[2Fe\text{-}2S]^{2+}$ GLRX5-BOLA3 to NFU1 leads directly to the formation of $[4Fe\text{-}4S]^{2+}$ NFU1 without the accumulation of [2Fe-2S]-bound intermediates, in support of a strong preference of NFU1 to bind a [4Fe-4S] cluster with respect to a [2Fe-2S] cluster. The cluster formation on NFU1 does not occur with $[2Fe\text{-}2S]^{2+}$ GLRX5 alone, thus this pathway being activated only upon the formation of the $[2Fe\text{-}2S]^{2+}$ GLRX5-BOLA3 hetero-complex (Fig. 12). Therefore, homo-dimeric $[2Fe\text{-}2S]^{2+}$ GLRX5 only operates in the early-acting steps of the mitochondrial ISC assembly machinery donating its $[2Fe\text{-}2S]^{2+}$ cluster to the ISCA1-ISCA2 complex, while the $[2Fe\text{-}2S]^{2+}$ GLRX5-BOLA3 hetero-complex operates downstream specifically in the assembly of a [4Fe-4S] cluster on NFU1. This pathway might be alternative to the pathway involving the [4Fe-4S] cluster transfer from the ISCA1-ISCA2 complex to NFU1. Considering that the *S. cerevisiae* homologue of NFU1 plays a crucial role for the function of mitochondrial [4Fe-4S] enzymes under oxidative metabolism as opposed to anoxic metabolism [8], the here-characterized pathway might be activated under oxidative cellular conditions only. In conclusion, we establish a role of NFU1 as an 'assembler' of [4Fe-4S] clusters alternative to the ISCA1-ISCA2 complex, possibly being operative for a subset of mitochondrial Fe-S target proteins, which are highly susceptible to be damaged in oxidatively growing cells, that is, enzymes with a labile [4Fe-4S] cluster such as aconitase and lipoyl synthase [35]. Moreover, the model shown in Fig. 12 can help to rationalize the complexity observed in human/*S. cerevisiae* NFU1 and BOLA3 phenotypes [4,7–9]. In particular, it was shown that *S. cerevisiae* BolA3 requires *S. cerevisiae* Nfu1 for its function and that Nfu1 and BolA3 cannot mutually substitute each other's biochemical function, even upon overproduction [9]. Thus, these data suggest that BolA3 and Nfu1 perform individual, nonoverlapping functions during the late stages of the mitochondrial ISC machinery, and the here-characterized pathway shows how this cooperative role can be achieved.

We also reported a structural characterization of NFU1 showing that (a) apo NFU1 is present in a monomer-dimer equilibrium, in which the dimer formation is mediated by the N-domain, (b) the two domains in monomeric apo NFU1, although connected by a flexible linker, are not fully independent, (c) that $[4Fe\text{-}4S]^{2+}$ cluster binding to NFU1 causes the quantitative formation of a dimer, (d) that the two NFU1 subunits of the dimer bridge a $[4Fe\text{-}4S]^{2+}$ cluster that is coordinated by two cysteines of each CXXC motif of two C-domains, and (e) the presence of an equilibrium between a $[4Fe\text{-}4S]^{2+}$ NFU1 dimer where the cluster is coordinated by the Cys residues of two CXXC motifs and a $[4Fe\text{-}4S]^{2+}$ NFU1 dimer where a Cys ligand of the CXXC motif is replaced by a S-donor small molecule ligand, such as GSH or DTT. These results are consistent with *in vivo* data reported on *S. cerevisiae* Nfu1 [8]. Indeed, it has been shown that (a) apo Nfu1 in *S. cerevisiae* cells is present as a mixture of a predominant monomer and a minor dimeric species, whose formation is due by the presence of the N-domain of Nfu1; (b) in mitochondrial lysates the bulk of *S. cerevisiae* Nfu1 is a homo-dimeric species, whose abundance is unaffected with DTT but affected by cluster binding. In conclusion, the structural characterization of dimeric $[4Fe\text{-}4S]^{2+}$ NFU1 showed that the cluster has a coordination site accessible to sulfur-containing ligands. This site might be optimal for being invaded by the S-donor ligand of the metal-receiving partner (i.e., the mitochondrial target protein in the presence or not of other possibly required accessory proteins) in order to promote a rapid and controlled cluster-exchange reaction (Fig. 12), following a mechanism typically observed for proteins involved in metal transfer, that is, metallochaperones [36–39].

The recent structural characterization of a construct of human NFU1 42-residue longer at the N terminus

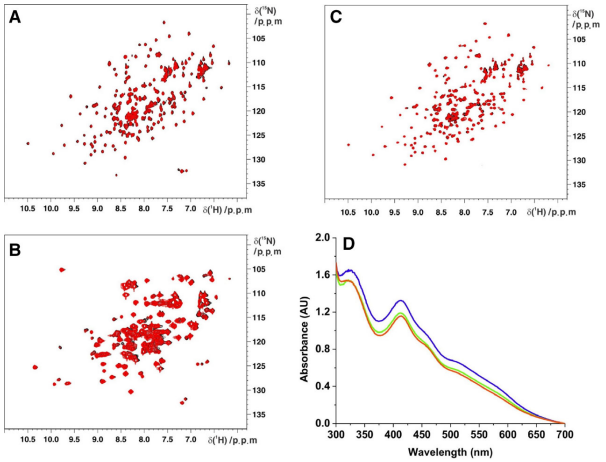

Fig. 11. Both apo and $[2Fe\text{-}2S]^{2+}$ GLRX5 do not interact with mNFU1 and $[2Fe\text{-}2S]^{2+}$ GLRX5 does not assemble a $[4Fe\text{-}4S]^{2+}$ cluster on mNFU1. Overlay of $^{1}H\text{-}^{15}N$ HSQC NMR spectra of: (A) ^{15}N-labeled apo mNFU1 (black) and a 1 : 2 mixture of ^{15}N-labeled apo mNFU1 and unlabeled apo GLRX5 (red); (B) a 60 : 40 mixture of ^{15}N-labeled $[2Fe\text{-}2S]^{2+}$ and apo GLRX5 (black) before and after the addition of two equivalents of apo mNFU1 (red); (C) ^{15}N-labeled apo mNFU1 (black) and a 1 : 2 mixture of ^{15}N-labeled apo mNFU1 and unlabeled $[2Fe\text{-}2S]^{2+}$ GLRX5 (red). NMR spectra were acquired at 298 K in 50 mM phosphate buffer pH 7.0, 5 mM GSH, 5 mM DTT and 150 mM NaCl; (D) UV-visible spectra of $[2Fe\text{-}2S]^{2+}$ GLRX5 (blue), and of a 1 : 2 mixture of mNFU1: $[2Fe\text{-}2S]^{2+}$ GLRX5 (green) and the same mixture after 1 day (red). The UV-vis spectra were acquired at 298 K in 50 mM phosphate buffer pH 7.0, 5 mM GSH, 5 mM DTT, and 150 mM NaCl. UV-vis and NMR experiments were repeated three times.

than mNFU1 sequence showed that the apo protein is monomeric in solution and adopts a dumbbell-shaped structure with well-structured N- and C-domains connected by a flexible linker [16]. It has been also observed that chemically Fe-S cluster reconstituted 42-NFU1 binds a [4Fe-4S] cluster [16]. Combined NMR and SAXS data showed that the holo form of 42-NFU1 is constituted by a trimer of dimers, each containing a [4Fe-4S] cluster [16]. Three N-domains are involved in the formation of a tripartite interface, while two conserved cysteines in the C-domain ligate a [4Fe-4S] cluster to form a dimer by bridging two C-domains. Our NMR data indicate the presence of a single species for $[4Fe\text{-}4S]^{2+}$ NFU1 having a reorientational correlation time of 15.1 ± 1.2 ns, which fully excludes the presence of the trimer of dimers as previously observed for $[4Fe\text{-}4S]^{2+}$ 42-NFU1 [16], while it supports the occurrence of protein dimerization upon cluster binding. Moreover, in the $^{1}H\text{-}^{15}N$ HSQC spectrum of the $[4Fe\text{-}4S]^{2+}$ 42-NFU1, a few residues of the N-domain exhibited two sets of peaks with equal peak volume [16]. They were, respectively, assigned to the free N-domains and to the N-domains that form the tripartite interface in the trimer of dimers of $[4Fe\text{-}4S]^{2+}$ 42-NFU1 [16]. This behavior differs from what we have observed in the $^{1}H\text{-}^{15}N$ HSQC spectrum of our construct for $[4Fe\text{-}4S]^{2+}$ NFU1, which shows indeed only one set of peaks. The different quaternary structure of [4Fe-4S] mNFU1 with respect to that of $[4Fe\text{-}4S]^{2+}$ 42-NFU1 can be rationalized considering that the two NFU1 constructs used in the two studies are different. Indeed, the mitochondrial isoform of NFU1, used in our studies, consists of 59–254 residues [5], while 42-NFU1, previously studied by NMR and SAXS [16], consists of residues 16–254. It might be that the longer N-terminal tail of $[4Fe\text{-}4S]^{2+}$ 42-NFU1 drives the formation of the trimer of dimers binding three [4Fe-4S] clusters. In the structural model of $[4Fe\text{-}4S]^{2+}$ 42-NFU1, the N-domain is, indeed, involved in the formation of the tripartite interface of the trimer [16].

Materials and methods

Protein production

The pETG20A plasmid containing N-terminal tagged mNFU1 (UniProt: Q9UMS0, residues 59–254 with

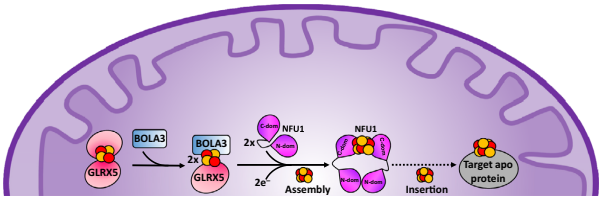

Fig. 12. Model of BOLA3/NFU1-dependent [4Fe-4S] cluster assembly pathway. Two molecules of $[2Fe\text{-}2S]^{2+}$ GLRX5-BOLA3 transfer the cluster to apo NFU1 that assembles a $[4Fe\text{-}4S]^{2+}$ cluster by receiving two electrons. The assembled $[4Fe\text{-}4S]^{2+}$ cluster is then inserted to mitochondrial target apo proteins with or without the requirement of other accessory proteins (dotted arrow).

N-terminal TRX-6His-tag) was used to transform in *E. coli* BL21-Gold(DE3) (Agilent, Santa Clara, CA, USA) competent cells. Cells were cultivated at 37 °C in 1 L of Luria–Bertani (LB) media adding ampicillin (100 $\mu g \cdot mL^{-1}$), until the OD_{600} reached 3–5. The cells were spun down (1693 ***g*** for 20 min) and resuspended in 1 L of fresh LB or minimal media [with 1 g $(^{15}NH_4)_2SO_4$ and 3 g glucose] containing ampicillin (100 $\mu g \cdot mL^{-1}$). The culture was left at 37 °C, 160 r.p.m. for approximately 1 h, and then, protein expression was induced by adding 1 mM of isopropyl β-D-1-thio-galactopyranoside (IPTG), shaking overnight at 30 °C, 160 r.p.m. The cell paste was dissolved in the binding buffer (20 mM phosphate buffer, 500 mM NaCl, 30 mM imidazole, pH 7.8), and the cells were lysated using the CelLytic Express (C1990; Sigma-Aldrich, St. Louis, MO, USA). All the following purification steps were performed aerobically. The N-terminal TRX-6His-tag mNFU1 protein was purified from *E. coli* using a HisTrap HP column (GE Healthcare, Chicago, IL, USA). The TRX-6His-tag was cleaved by tobacco etch virus protease overnight at room temperature in 20 mM phosphate buffer, 500 mM NaCl, 500 mM imidazole, pH 7.8 (UniProt: Q9UMS0, residues 59–254 with N-terminal GSFT residues). The buffer was exchanged to binding buffer, and a second His-trap chromatography column was performed to separate the digested mNFU1 from TRX-6His-tag mNFU1 and TRX-6His-tag. Recovered mNFU1 was pure enough to be used for spectroscopic and biochemical studies. The final yield of apo mNFU1 was ~ 60 mg per liter of LB culture. 2.5 mM tris (2-carboxyethyl) phosphine (TCEP) was added in all the purification steps to avoid disulfide bond formation.

The pETG20A plasmid containing N-domain of mNFU1 (UniProt: Q9UMS0, residues 59–155 with N-terminal TRX-6His-tag; after tag cleavage the N-domain sequence contains N-terminal GSFT residues similarly to the full-length protein) was obtained by a site-directed mutagenesis with a prokaryotic codon stop. The protein expression was performed likewise mNFU1, in BL21-GOLD(DE3) cells. Cells were cultivated at 37 °C in 1 L of LB or minimal media adding ampicillin (100 $\mu g \cdot mL^{-1}$), until the OD_{600} reached 0.6–0.8, and then, protein expression was induced by adding 1 mM of IPTG, shaking overnight at 20 °C, 160 r.p.m. Protein purification steps were performed following the protocol of mNFU1, except that, during TEV protease cleavage, a dialysis step in the binding buffer (20 mM phosphate buffer, 500 mM NaCl, 30 mM imidazole, pH 7.8) was performed. The C-domain of mNFU1 (UniProt: Q9UMS0, residues 162–247 with N-terminal GIDPFTM residues) was cloned by a TOPO cloning reaction (Invitrogen, Carlsbad, CA, USA). The gene was inserted in the pET151/D-TOPO (Invitrogen) vector that present a polyhistidine (6x His) region, a TEV recognition site and a TOPO cloning site. Protein expression and purification steps do not differ from the previously described for the N-domain, and the apo form of C-domain was purified. The final yields of N- and C-domain of mNFU1 were ~ 60 $mg \cdot L^{-1}$ of LB culture. 2.5 mM TCEP was added in all the purification steps to avoid disulfide bond formation.

$[4Fe\text{-}4S]^{2+}$ mNFU1 and $[4Fe\text{-}4S]^{2+}$ C-domain were chemically Fe-S cluster reconstituted in anaerobic conditions in 50 mM Tris(hydroxymethyl)aminomethane hydrochloride, 100 mM NaCl, 5 mM DTT buffer at pH 8.0 with eightfold $FeCl_3$ and Na_2S for 16 h at room temperature. Chemical Fe-S cluster reconstitution was performed with protein concentrations of ~ 40–80 μM. Anaerobic conditions were obtained by degassing all buffers and performing the chemical reconstitution in glove-box with less than 5 p.p.m. of oxygen.

The expression and purification of human BOLA3 and GLRX5 in their apo monomeric forms and in their homo-dimeric (for GLRX5) and hetero-dimeric (for GLRX5-BOLA3) $[2Fe\text{-}2S]^{2+}$ cluster-bound forms were obtained as previously reported [9,10,40].

NMR spectroscopy

1D ^1H paramagnetic-tailored NMR experiments were performed at 400 MHz with a ^1H optimized 5 mm probe at temperatures ranging from 280 and 307 K. Water signal was suppressed via fast repetition experiments and water selective irradiation. Experiments were typically performed using an acquisition time of 50 ms and an overall recycle delay of 90 ms. The protein concentration was 0.5–1 mM, and the spectra were acquired in different buffer conditions

as detailed in the Results section. Squared cosine and exponential multiplications were applied prior to Fourier transformation. Manual baseline correction was performed, using polynomial functions.

^{15}N heteronuclear relaxation experiments on ^{15}N-labeled samples of apo and $[4Fe\text{-}4S]^{2+}$ mNFU1 were recorded on Bruker AVANCE 500 MHz spectrometer at 298 K to measure ^{15}N backbone R_1 and R_2, as well as the heteronuclear $^{15}N[^1H]$ NOEs. Spectra were processed using TopSpin (Bruker BioSpin, Billerica, MA, USA) and analyzed with CARA software (CARA is a free software that can be downloaded fromcara.nmr.ch). The rotational correlation time value was estimated from the R_2/R_1 ratio using the program QUADRATIC_DIFFUSION. The relaxation data for those NHs having an exchange contribution to the R_2 value or exhibiting large-amplitude fast internal motions were excluded from the analysis [41]. NMR relaxation experiments were acquired at 298 K in 50 mM phosphate buffer pH 7.0, 5 mM DTT, and 150 mM NaCl.

SEC-MALS, UV-visible, CD, and NMR spectroscopy for protein–protein interaction studies

SEC-MALS data were aerobically acquired on the apo proteins by attaching a SuperdexTM 200 Increase 10/300 GL column to a DAWN HELEOS system with a continuous flow rate of 0.6 mL·min^{-1} using a filtered degassed buffer (50 mM phosphate buffer, 150 mM NaCl, 5 mM DTT, pH 7.0).

The ^{1}H-^{15}N HSQC NMR spectrum of apo mNFU1 was compared, using CARA software [42], with those of the N- and apo C-domains or with that of $[4Fe\text{-}4S]^{2+}$ mNFU1. The observed chemical shift changes were plotted calculating the backbone weighted average chemical shift differences (Δ_{avg}(HN) (i.e., $(((\Delta H)^2 + (\Delta N/5)^2)/2)^{1/2}$, where ΔH and ΔN are chemical shift differences for backbone amide ^{1}H and ^{15}N nuclei, respectively). Backbone chemical shift assignments of full-length NFU1 and of N- and C-domains of NFU1 in their apo forms were already available in the literature [16]. The ^{1}H-^{15}N HSQC NMR spectra were acquired at 298 K in 50 mM phosphate buffer pH 7.0, 5 mM DTT and 150 mM NaCl.

Protein–protein (or protein–GSH or protein-DTT) interaction, cluster transfer, and assembly experiments were followed performing UV-visible and CD spectra and 2D diamagnetic-tailored ^{1}H-^{15}N HSQC and 1D paramagnetic-tailored ^{1}H NMR experiments in anaerobic conditions. Anaerobic conditions were obtained by degassing all buffers and performing the experiments in glove-box with less than 5 p.p.m. of oxygen. The samples were then sealed in a gas-tight NMR tube or a UV-vis cuvette for the spectroscopic analysis. Each experiment was successfully repeated three times. UV-visible and CD spectra were acquired anaerobically at 298 K in 50 mM phosphate buffer, 5 mM DTT, 150 mM NaCl, pH 7.0 on a Cary 50 Eclipse spectrophotometer (Varian-Agilent Technologies, Palo Alto, CA, USA) and JASCO J-810 spectropolarimeter (JASCO, Easton, MD, USA), respectively. NMR experiments were performed on Bruker AVANCE 400, 700, 900, and 950 MHz spectrometers at 298 K on 0.3–1 mM protein samples. Backbone chemical shift assignments of BOLA3, of BOLA3 in the apo and $[2Fe\text{-}2S]^{2+}$ hetero-complex with GLRX5, of apo GLRX5, and of $[2Fe\text{-}2S]^{2+}$ GLRX5 were already available [10,40]. Chemical shift assignment of the individual N- and C-domains of NFU1 and full-length NFU1 are available in the Biological Magnetic Resonance Bank (under accession codes BMRB: 18489 [NFU1 N-domain], BMRB: 19068 [NFU1 C-domain], and BMRB: 26801 [full-length NFU1]) [16].

The potential interaction between apo mNFU1 and BOLA3 was followed, in 50 mM phosphate buffer, 150 mM NaCl, 5 mM DTT pH 7.0, titrating ^{15}N-labeled (or unlabeled) apo mNFU1 with unlabeled (or ^{15}N-labeled) BOLA3. The potential interaction between $[4Fe\text{-}4S]^{2+}$ mNFU1 and BOLA3 was investigated in anaerobic conditions by (a) chemically reconstituting, in the presence of iron and sulfide ions, equimolar or 1 : 2 mixtures of unlabeled (or ^{15}N-labeled) apo mNFU1 and ^{15}N-labeled (or unlabeled) BOLA3 in 5 mM GSH, 5 mM DTT, 150 mM NaCl, 50 mM Tris base pH 8, or in 5 mM DTT, 150 mM NaCl, 50 mM Tris base pH 8, and spectroscopically investigating the final mixture after having exchanged it in 50 mM phosphate buffer, 150 mM NaCl, 5 mM DTT pH 7.0; (b) titrating a 1 : 1 mixture of ^{15}N-labeled BOLA3 and unlabeled apo GLRX5 with 1 equivalent of $[4Fe\text{-}4S]^{2+}$ mNFU1 in 50 mM phosphate buffer, 150 mM NaCl, 5 mM DTT pH 7.0.

The cluster transfer and assembly observed upon mixing $[2Fe\text{-}2S]^{2+}$ GLRX5-BOLA3 and apo mNFU1 in 50 mM phosphate buffer, 150 mM NaCl, 5 mM GSH, 5 mM DTT pH 7.0 was followed in anaerobic conditions titrating ^{15}N-labeled (or unlabeled) mNFU1 with $[2Fe\text{-}2S]^{2+}$ GLRX5-BOLA3 (unlabeled or ^{15}N-labeled GLRX5 or ^{15}N-labeled BOLA3). The same experiment was also performed in 50 mM phosphate buffer pH 7.0, 5 mM GSH, and 150 mM NaCl.

The potential interaction, cluster transfer, and assembly between GLRX5 and mNFU1 were followed in anaerobic conditions in 50 mM phosphate buffer pH 7.0, 5 mM GSH, 5 mM DTT, and 150 mM NaCl by (a) titrating ^{15}N-labeled apo mNFU1 with unlabeled apo GLRX5; (b) titrating a 60 : 40 mixture of ^{15}N-labeled (or unlabeled) $[2Fe\text{-}2S]^{2+}$ and apo GLRX5 with unlabeled (or ^{15}N-labeled) apo mNFU1.

Molecular docking

The structural model of monomeric apo mNFU1 was calculated using the protein–protein docking program HADDOCK2.2 by following the standard HADDOCK procedure [18,19]. The structures of the individual N- and C-domains (PDB entries 2LTM and 2M5O, respectively)

[16], to which the N- and C-flexible termini have been removed, have been used as input data. The meaningful NMR chemical shift differences, shown in Fig. 2A,B, were used to define ambiguous interaction restraints for the residues at the protein–protein interface. The 'active' residues were defined as those having a chemical shift perturbation upon complex formation larger than the average of Δ_{avg}(HN) plus 1σ and with a solvent accessibility higher than 45%; the 'passive' residues were defined as those being surface neighbors to the active residues and with a solvent accessibility higher than 45%. Following the standard HADDOCK algorithm, HADDOCK clustered 152 structures in eight clusters, which represents 76.0% of the water-refined models HADDOCK generated. The clusters were ranked based on the averaged HADDOCK score of their top four members. The best-scoring HADDOCK cluster resulted in 41 structures, whose statistics are reported in Table 1.

Acknowledgements

The authors acknowledge the support and the use of resources of Instruct-ERIC, a Landmark ESFRI project, and specifically the CERM/CIRMMP Italy Centre. This article is based upon work from COST Action CA15133, supported by COST (European Cooperation in Science and Technology).

Conflict of interest

The authors declare no conflict of interest.

Author contributions

LB and SC-B designed the research; VN, SG, and DS performed research; VN, DS, SC-B, and LB analyzed data; and LB and SC-B wrote the paper.

References

1 Braymer JJ & Lill R (2017) Iron-sulfur cluster biogenesis and trafficking in mitochondria. *J Biol Chem* **292**, 12754–12763.
2 Ciofi-Baffoni S, Nasta V & Banci L (2018) Protein networks in the maturation of human iron-sulfur proteins. *Metallomics* **10**, 49–72.
3 Andreini C, Banci L & Rosato A (2016) Exploiting bacterial operons to illuminate human iron-sulfur proteins. *J Proteome Res*. **15**, 1308–1322.
4 Cameron JM, Janer A, Levandovskiy V, MacKay N, Rouault TA, Tong WH, Ogilvie I, Shoubridge EA & Robinson BH (2011) Mutations in iron-sulfur cluster scaffold genes NFU1 and BOLA3 cause a fatal deficiency of multiple respiratory chain and 2-oxoacid dehydrogenase enzymes. *Am J Hum Genet* **89**, 486–495.
5 Tong WH, Jameson GN, Huynh BH & Rouault TA (2003) Subcellular compartmentalization of human Nfu, an iron-sulfur cluster scaffold protein, and its ability to assemble a [4Fe-4S] cluster. *Proc Natl Acad Sci USA* **100**, 9762–9767.
6 Agar JN, Krebs C, Frazzon J, Huynh BH, Dean DR & Johnson MK (2000) IscU as a scaffold for iron-sulfur cluster biosynthesis: sequential assembly of [2Fe-2S] and [4Fe-4S] clusters in IscU. *Biochemistry* **39**, 7856–7862.
7 Navarro-Sastre A, Tort F, Stehling O, Uzarska MA, Arranz JA, Del TM, Labayru MT, Landa J, Font A, Garcia-Villoria J *et al.* (2011) A fatal mitochondrial disease is associated with defective NFU1 function in the maturation of a subset of mitochondrial Fe-S proteins. *Am J Hum Genet* **89**, 656–667.
8 Melber A, Na U, Vashisht A, Weiler BD, Lill R, Wohlschlegel JA & Winge DR (2016) Role of Nfu1 and Bol3 in iron-sulfur cluster transfer to mitochondrial clients. *Elife*. **5**, e15991.
9 Uzarska MA, Nasta V, Weiler BD, Spantgar F, Ciofi-Baffoni S, Saviello M, Gonnelli L, Muhlenhoff U, Banci L & Lill R (2016) Mitochondrial Bol1 and Bol3 function as assembly factors for specific iron-sulfur proteins. *Elife* **5**, e16673.
10 Nasta V, Giachetti A, Ciofi-Baffoni S & Banci L (2017) Structural insights into the molecular function of human (2Fe-2S) BOLA1-GRX5 and (2Fe-2S) BOLA3-GRX5 complexes. *Biochim Biophys Acta* **1861**, 2119–2131.
11 Uzarska MA, Dutkiewicz R, Freibert SA, Lill R & Muhlenhoff U (2013) The mitochondrial Hsp70 chaperone Ssq1 facilitates Fe/S cluster transfer from Isu1 to Grx5 by complex formation. *Mol Biol Cell* **24**, 1830–1841.
12 Nakai K & Horton P (1999) PSORT: a program for detecting sorting signals in proteins and predicting their subcellular localization. *Trends Biochem Sci* **24**, 34–36.
13 Emanuelsson O (2002) Predicting protein subcellular localisation from amino acid sequence information. *Brief Bioinform* **3**, 361–376.
14 Liu Y & Cowan JA (2007) Iron sulfur cluster biosynthesis. Human NFU mediates sulfide delivery to ISU in the final step of [2Fe-2S] cluster assembly. *Chem Commun (Cambridge)* **30**, 3192–3194.
15 Lebigot E, Gaignard P, Dorboz I, Slama A, Rio M, de Lonlay P, Heron B, Sabourdy F, Boespflug-Tanguy O, Cardoso A *et al.* (2017) Impact of mutations within the [Fe-S] cluster or the lipoic acid biosynthesis pathways on mitochondrial protein expression profiles in fibroblasts from patients. *Mol Genet Metab* **122**, 85–94.
16 Cai K, Liu G, Frederick RO, Xiao R, Montelione GT & Markley JL (2016) Structural/functional properties of human NFU1, an intermediate [4Fe-4S] carrier in

human mitochondrial iron-sulfur cluster biogenesis. *Structure* **24**, 2080–2091.
17 Shapiro YE, Sinev MA, Sineva EV, Tugarinov V & Meirovitch E (2000) Backbone dynamics of *Escherichia coli* adenylate kinase at the extreme stages of the catalytic cycle studied by (15)N NMR relaxation. *Biochemistry* **39**, 6634–6644.
18 Dominguez C, Boelens R & Bonvin AM (2003) HADDOCK: a protein-protein docking approach based on biochemical or biophysical information. *J Am Chem Soc* **125**, 1731–1737.
19 van Zundert GC, Rodrigues JP, Trellet M, Schmitz C, Kastritis PL, Karaca E, Melquiond AS, van Dijk M, de Vries SJ & Bonvin AM (2016) The HADDOCK2.2 web server: user-friendly integrative modeling of biomolecular complexes. *J Mol Biol* **428**, 720–725.
20 Freibert SA, Weiler BD, Bill E, Pierik AJ, Muhlenhoff U & Lill R (2018) Biochemical reconstitution and spectroscopic analysis of iron-sulfur proteins. *Methods Enzymol* **599**, 197–226.
21 Bandyopadhyay S, Naik SG, O'Carroll IP, Huynh BH, Dean DR, Johnson MK & Dos Santos PC (2008) A proposed role for the *Azotobacter vinelandii* NfuA protein as an intermediate iron-sulfur cluster carrier. *J Biol Chem* **283**, 14092–14099.
22 Banci L, Camponeschi F, Ciofi-Baffoni S & Piccioli M (2018) The NMR contribution to protein-protein networking in Fe-S protein maturation. *J Biol Inorg Chem* **23**, 665–685.
23 Mapolelo DT, Zhang B, Naik SG, Huynh BH & Johnson MK (2012) Spectroscopic and functional characterization of iron-sulfur cluster-bound forms of *Azotobacter vinelandii* (Nif)IscA. *Biochemistry* **51**, 8071–8084.
24 Chandramouli K, Unciuleac MC, Naik S, Dean DR, Huynh BH & Johnson MK (2007) Formation and properties of [4Fe-4S] clusters on the IscU scaffold protein. *Biochemistry* **46**, 6804–6811.
25 Brancaccio D, Gallo A, Mikolajczyk M, Zovo K, Palumaa P, Novellino E, Piccioli M, Ciofi-Baffoni S & Banci L (2014) Formation of [4Fe-4S] clusters in the mitochondrial iron-sulfur cluster assembly machinery. *J Am Chem Soc* **136**, 16240–16250.
26 Ewen KM, Ringle M & Bernhardt R (2012) Adrenodoxin–a versatile ferredoxin. *IUBMB Life* **64**, 506–512.
27 Sheftel AD, Stehling O, Pierik AJ, Elsasser HP, Muhlenhoff U, Webert H, Hobler A, Hannemann F, Bernhardt R & Lill R (2010) Humans possess two mitochondrial ferredoxins, Fdx1 and Fdx2, with distinct roles in steroidogenesis, heme, and Fe/S cluster biosynthesis. *Proc Natl Acad Sci USA* **107**, 11775–11780.
28 Shi Y, Ghosh M, Kovtunovych G, Crooks DR & Rouault TA (2012) Both human ferredoxins 1 and 2 and ferredoxin reductase are important for iron-sulfur cluster biogenesis. *Biochim Biophys Acta* **1823**, 484–492.
29 Sheftel AD, Wilbrecht C, Stehling O, Niggemeyer B, Elsasser HP, Muhlenhoff U & Lill R (2012) The human mitochondrial ISCA1, ISCA2, and IBA57 proteins are required for [4Fe-4S] protein maturation. *Mol Biol Cell* **23**, 1157–1166.
30 Beilschmidt LK, Ollagnier de Choudens S, Fournier M, Sanakis I, Hograindleur MA, Clemancey M, Blondin G, Schmucker S, Eisenmann A, Weiss A *et al.* (2017) ISCA1 is essential for mitochondrial Fe4S4 biogenesis *in vivo*. *Nat Commun* **8**, 15124.
31 Brancaccio D, Gallo A, Piccioli M, Novellino E, Ciofi-Baffoni S & Banci L (2017) [4Fe-4S] cluster assembly in mitochondria and its impairment by copper. *J Am Chem Soc* **139**, 719–730.
32 Gourdoupis S, Nasta V, Calderone V, Ciofi-Baffoni S & Banci L (2018) IBA57 recruits ISCA2 to form a [2Fe-2S] cluster-mediated complex. *J Am Chem Soc* **140**, 14401–14412.
33 Floyd BJ, Wilkerson EM, Veling MT, Minogue CE, Xia C, Beebe ET, Wrobel RL, Cho H, Kremer LS, Alston CL *et al.* (2016) Mitochondrial protein interaction mapping identifies regulators of respiratory chain function. *Mol Cell* **63**, 621–632.
34 Sen S, Rao B, Wachnowsky C & Cowan JA (2018) Cluster exchange reactivity of [2Fe-2S] cluster-bridged complexes of BOLA3 with monothiol glutaredoxins. *Metallomics* **10**, 1282–1290.
35 McCarthy EL & Booker SJ (2017) Destruction and reformation of an iron-sulfur cluster during catalysis by lipoyl synthase. *Science* **358**, 373–377.
36 Robinson NJ & Winge DR (2010) Copper metallochaperones. *Annu Rev Biochem* **79**, 537–562.
37 Banci L, Bertini I, Cantini F & Ciofi-Baffoni S (2010) Cellular copper distribution: a mechanistic systems biology approach. *Cell Mol Life Sci* **67**, 2563–2589.
38 O'Halloran TV & Culotta VC (2000) Metallochaperones: an intracellular shuttle service for metal ions. *J Biol Chem* **275**, 25057–25060.
39 Boal AK & Rosenzweig AC (2009) Structural biology of copper trafficking. *Chem Rev* **109**, 4760–4779.
40 Banci L, Brancaccio D, Ciofi-Baffoni S, Del Conte R, Gadepalli R, Mikolajczyk M, Neri S, Piccioli M & Winkelmann J (2014) [2Fe-2S] cluster transfer in iron-sulfur protein biogenesis. *Proc Natl Acad Sci USA* **111**, 6203–6208.
41 Banci L, Bertini I, Cantini F, Ciofi-Baffoni S, Cavet JS, Dennison C, Graham AI, Harvie DR & Robinson NJ (2007) NMR structural analysis of cadmium-sensing by winged helix repressor CMTR. *J Biol Chem* **282**, 30181–30188.
42 Keller R (2004) The Computer Aided Resonance Assignment Tutorial. CANTINA Verlag, Goldau.

2.2 ISCA1 ORCHESTRATES ISCA2 AND NFU1 IN THE MATURATION OF MITOCHONDRIAL [4FE-4S] PROTEINS

Dafne Suraci[1,2,*], *Giovanni Saudino*[1,2,*], *Veronica Nasta*[1,2], *Simone Ciofi-Baffoni*[1,2] , *Lucia Banci*[1,2]

[1] Magnetic Resonance Center CERM, University of Florence, Via Luigi Sacconi 6, 50019, Sesto Fiorentino, Florence, Italy.

[2]Department of Chemistry, University of Florence, Via della Lastruccia 3, 50019 Sesto Fiorentino, Florence, Italy.

*These authors contributed equally to this work.

Under submission

Abstract

The last steps of the pathway responsible of the maturation of mitochondrial [4Fe-4S] proteins are still elusive. Three proteins ISCA1, ISCA2 and NFU1 have been shown to be implicated in the assembly of [4Fe-4S] clusters and their transfer into the mitochondrial apo client proteins, i.e. aconitase, respiratory complexes I and II and lipoyl synthase. The available genetic and proteomic data did not provide a clear and definitive picture on which of the three proteins are essential for this process and how they operate. In order to shed light on this, we here present a NMR-based study on how ISCA1, ISCA2 and NFU1 proteins act. Our data defines a detailed molecular model of the succession of events performed in a coordinated manner by ISCA1, ISCA2 and NFU1 to make [4Fe-4S] clusters available to mitochondrial apo client proteins. We showed that ISCA1 is the key player of the [4Fe-4S] protein maturation process, working as a mediator between the two no interacting proteins ISCA2 and NFU1 to form a ternary complex. The ternary complex allows the cluster to be safely moved from the cluster binding site where it is assembled, i.e. in the ISCA1-ISCA2 complex, to a cluster binding site formed by ISCA1 and NFU1 proteins, making the cluster available for mitochondrial apo client proteins with no risk of being lost in solution where it might damage the cellular environment.

Introduction

In eukaryotes, mitochondria are the primary site for the biosynthesis of iron-sulfur (Fe-S) clusters.[1-2] Within the mitochondrial matrix, the biosynthesis of Fe-S clusters and their insertion into apo proteins is assisted by several accessory proteins that are highly conserved from bacteria to mammals.[3-4] Among these proteins, three of them, i.e. ISCA1, ISCA2 and NFU1, have been shown to be implicated in the assembly and transfer of [4Fe-4S] clusters to be inserted into mitochondrial apo client proteins.[5-12] ISCA1 and ISCA2 are two highly homologous members of the A-type evolutionarily conserved protein family, which is characterized by three highly conserved cysteine residues organized in a C-X_n-C-G-C sequence motif (n is usually 63-65, but is increased by a 21-residue insert in some eukaryotic proteins).[13] This motif has been shown to be involved in both [2Fe-2S] and [4Fe-4S] cluster binding.[14-19] In humans, a ISCA1-ISCA2 complex was identified *in vivo*[20] and in its heterodimeric state was shown to act *in vitro* as a platform to assemble a [4Fe-4S] cluster from two [2Fe-2S] clusters received by GLRX5, the [2Fe-2S] metallochaperone of the mitochondrial matrix.[16, 21] This pathway was proposed to act *in vivo* to assemble [4Fe-4S] clusters in mitochondria. On the other hand, *in vivo* data also provided evidence that only human ISCA1 is essential for mitochondrial [4Fe-4S] proteins in skeletal muscle or primary neuronal cells under defined physiological conditions, while ISCA2 is dispensable.[20] These data contrast with what was found in HeLa cells in which similar phenotypes were observed for ISCA1 and ISCA2 knockdowns, i.e. the two proteins seem to function together in the biosynthesis of mitochondrial [4Fe-4S] clusters.[6] Collectively, the results available in the literature suggest that a still elusive, dynamic network of interactions of ISCA proteins probably exists *in vivo* and that the biogenesis of mitochondrial [4Fe-4S] client proteins is a complex and dynamic system that may have tissue and temporal specificity.

The other player of the ISCA1-ISCA2 pathway is NFU1, a universally present protein composed by well-structured N- and C-domains connected by a flexible linker.[22-24] Human NFU1 contains a conserved CXXC-motif located in the C-domain, shown to be involved in [4Fe-4S] cluster binding.[12, 23, 25] NFU1 was proposed to act downstream the ISCA1-ISCA2 complex.[2] The current prevailing model was largely based on studies in *Saccharomyces cerevisiae*[26] which suggested that NFU1 receives the [4Fe-4S] cluster assembled on the ISCAs complex and then transfers it to selected apo client proteins. As support to this model, it was found that yeast Nfu1 specifically interacts *in vivo* with the

yeast homologues of both human ISCA1 and ISCA2.[26] On the other hand, human ISCA1 and ISCA2 have found to have distinct interacting partners. Indeed, while a specific interaction was found *in vivo* between ISCA1 and NFU1 by immunoprecipitation experiments, NFU1 did not co-immunoprecipitate with ISCA2.[20] In addition, it has been recently proposed that the ISCA1-ISCA2-NFU1-dependent pathway might be not unique, being other alternative pathways also operative. In a recent study we showed that [2Fe-2S] GLRX5-BOLA3, a candidate physiologically relevant complex operating upstream of the ISCAs complex[27-28], is able to promote the assembly of a [4Fe-4S] cluster on NFU1 with no requirement of the ISCA1-ISCA2 complex.[25] This alternative pathway was proposed to be required in specific cellular conditions. Indeed, it was demonstrated that yeast NFU1 has a heightened importance in cells undergoing oxidative metabolism as opposed to anoxic metabolism,[26] and thus this specific pathway may be activated under oxidative stress. Similarly, it has been recently shown by *in vitro* experiments that a [4Fe-4S]-bound form of ISCU1, operating upstream of the ISCA1-ISCA2 complex, transfers its cluster to apo NFU1, leading to the formation of [4Fe-4S] NFU1, and thus *de facto* also this pathway bypasses the ISCA1-ISCA2 complex.[29] The latter pathway, however, contrasts with studies indicating that [4Fe-4S] ISCU1 is not a physiologically relevant species.[30-31] Collectively, all the data available up to now in the literature cannot depict a molecular view on how the three ISCA1, ISCA2 and NFU1 proteins cooperate in the maturation of mitochondrial [4Fe-4S] proteins. In order to shed light on this matter, we here report a NMR-based study on the ISCA1, ISCA2 and NFU1 patterns of interactions and functional processes. Our data allowed to define a detailed molecular model of the succession of events performed in a coordinated manner by ISCA1, ISCA2 and NFU1 to assemble and make available [4Fe-4S] clusters for mitochondrial apo client proteins.

Experimental section

Protein expression and purification

pDONR221 plasmid containing full-length ISCA1 gene (UniProt: Q9BUE6) was purchased by Genescript. Gateway cloning technology (Invitrogen) was then applied to clone full-length ISCA1 gene into pDEST-HisMBP plasmid to express N-terminal Histag-MBP tagged ISCA1. The latter plasmid was transformed in *Escherichia coli* BL21-Gold(DE3) (Agilent) competent cells. Cells were cultivated at 37°C in Luria-Bertani (LB) media adding ampicillin (100 µg/mL), 4 mL of Solution Q and 250 µM of $FeCl_3$ per liter of sterile LB until OD_{600} reached 0.8-1. Protein expression was induced with 0.2 mM isopropyl ◘-D-1-thiogalactopyranoside (IPTG) at 18°C for 16 hours. The cells were harvested by centrifugation at 5000 rpm for 20 min (JA-10, Beckman Coulter) and then resuspended in binding buffer (50 mM Tris-HCl, 500 mM NaCl, 15 mM Imidazole, pH 8.0). The cells were lysed by sonication (40 minutes, 2'' ON and 9.9'' OFF) at 4 °C. The N-terminal 6Histag-MBP-ISCA1 protein was purified from the lysate using a HisTrap HP column (GE Healthcare) and then the MBP-6His-tag was cleaved by tobacco etch virus protease treatment over-night at room temperature in binding buffer. His-trap column followed by amylose resin column were performed to separate the digested ISCA1 from MBP-6His-tag and from undigested MBP-6His-tag ISCA1. The final yield of ISCA1 was ~15 mg/L of LB culture. Apo ISCA1 was obtained performing all the purification steps under aerobic conditions, while a mixture of apo and $[2Fe\text{-}2S]^{2+}$ ISCA1 was purified under anaerobic conditions (anaerobically purified ISCA1). The anaerobically purified ISCA1 protein was characterized by UV- and CD-visible absorption and 1D ^1H paramagnetic NMR spectroscopies, analytical size exclusion chromatography (**Figure S1**), and iron and acid-labile sulfide content. Protein quantification was carried out with the Bradford protein assay, using BSA as a standard. Nonheme iron and acid-labile sulfide content was determined as described previously.[32] In the UV-visible absorption spectrum of anaerobically purified ISCA1, the extinction coefficients at 325 and 420 nm (ranging from 4200 to 5700 and from 2100 to 3900 M^{-1} cm^{-1} depending on protein preparation, respectively) are far from the lower end of the range of values that are considered typical for [2Fe-2S] clusters (11000 and 8000 M^{-1} cm^{-1}, respectively[33]), indicating a partial [2Fe-2S] cluster occupancy in the homodimer. Iron and acid-labile sulfide analyses of anaerobically purified ISCA1 samples indicate ~0.3 $[2Fe\text{-}2S]^{2+}$ cluster per homodimer.

Moreover, after chemically reconstituting anaerobically purified ISCA1, we observed in the UV-visible absorption spectrum an increase of the molar extinction coefficients of the [2Fe-2S] cluster absorption bands (**Figure S1**). However, no formation of a [4Fe-4S] cluster-bound species was observed as shown by the 1D ^{1}H paramagnetic NMR spectrum, which has indeed the same signals of anaerobically purified $[2Fe\text{-}2S]^{2+}$ ISCA1 species (**Figure S1**). This behavior differs from what observed for the anaerobically purified ISCA2, which, indeed, upon chemical reconstitution, produced a [4Fe-4S] bound dimeric species.[16]

The production of human ISCA2 and full-length and C-domain NFU1 in their apo and Fe-S cluster-bound forms were obtained as previously described in literature.[15, 25] As previously reported,[16] the purification under anaerobic conditions of ISCA2 resulted in a dimer, which is composed by a mixture of apo and $[2Fe\text{-}2S]^{2+}$ cluster-bound species with a $[2Fe\text{-}2S]^{2+}$ cluster occupancy of 0.1-0.2 cluster per homodimer.

Production of Fe-S cluster-bound species

A 1:1 mixture of ISCA1 and ISCA2 was produced by stepwise titrating anaerobically purified ^{15}N ISCA2 with anaerobically purified ISCA1 and monitoring changes in the ^{1}H-^{15}N HSQC NMR maps. Chemical shift changes occur in a slow exchange regime on the NMR time scale, which were completed once the 1:1 protein ratio was reached, indicating that an ISCA1-ISCA2 hetero-complex is fully formed at this stoichiometric ratio. The ISCA1-ISCA2 complex was then chemically reconstituted to obtain the $[4Fe\text{-}4S]^{2+}$ cluster-bound hetero-complex. Chemical reconstitution was anaerobically performed in 50 mM Tris-HCl, 100 mM NaCl and 5 mM DTT buffer at pH 8.0 adding eight equivalents of $FeCl_3$ and Na_2S to a protein solution of ~40-80 μM. The reaction was incubated for 16 h at room temperature. Anaerobic conditions were obtained performing the chemical reconstitution in glove-box (MBraun Labstar 130) with less than 2 ppm of oxygen and by using all buffers degassed. Anaerobically purified ISCA1 and a 1:1 mixture of anaerobically purified ISCA1 and apo NFU1 were chemically reconstituted following the same procedure. This led to dimeric $[2Fe\text{-}2S]^{2+}$ and hetero-dimeric $[4Fe\text{-}4S]^{2+}$ cluster-bound species, respectively. Dimeric $[4Fe\text{-}4S]^{2+}$ NFU1 was produced following the protocol previously reported.[25]

Analytical size exclusion chromatography and SEC-MALS

For analytical size exclusion chromatography analysis, purified samples were loaded on a Superdex^{TM} 200 Increase 10/300 GL column attached to an AKTA pure chromatography unit with a continuous flow rate of 0.65 mL/min. The column was calibrated with gel filtration marker calibration kit, 6500–66000 Da (Sigma-Aldrich), to obtain the apparent

molecular masses of the detected species. The column was equilibrated with degassed phosphate buffer 50 mM, 150 mM NaCl, 5 mM DTT and pH 7.0. SEC-MALS data were acquired by attaching a Superdex^{TM} 200 Increase 10/300 GL column to a DAWN HELEOS system with a continuous flow rate of 0.6 mL/min using a filtered buffer (50 mM, 150 mM NaCl, 5 mM DTT and pH 7.0). Each experiment was successfully repeated at least three times.

UV- and CD-visible spectroscopy

UV- and CD-visible spectra were performed to characterize the cluster bound to anaerobically purified and chemically reconstituted ISCA1. The experiments were performed under anaerobic conditions, working in glove-box with less than 5 p.p.m. of oxygen, by degassing the buffer and using a gas-tight cuvette. UV- and CD-visible spectra were purchased at room temperature (25 °C) in 50 mM phosphate buffer, 150 mM NaCl, 5 mM DTT and pH 7.0 on a Cary 50 Eclipse spectrophotometer and JASCO J-810 spectropolarimeter, respectively. Each experiment was successfully repeated three times.

NMR spectroscopy

^{1}H-^{15}N HSQC spectra were acquired at 298 K in 50 mM phosphate, 150 mM NaCl, 5 mM DTT pH 7.0 buffer, 10% (v/v) D_2O. All NMR spectra were recorded on Bruker AVANCE 700, 900 and 950 MHz, processed using the standard Bruker software (Topspin) and analyzed with CARA program. To monitor the possible interaction among ISCA1, ISCA2 and NFU1 in their apo and Fe-S cluster-bound states, ^{15}N labeled protein(s) were stepwise titrated in anaerobic conditions with increasing amounts of unlabeled or ^{15}N-labelled protein(s). Chemical shifts of the backbone NHs observed in the ^{1}H ^{15}N HSQC spectra along the additions of the unlabeled or ^{15}N-labelled protein(s) were compared with chemical shifts of ^{15}N-labelled protein(s) in the initial state. The observed chemical shift changes were reported as backbone weighted average chemical shift differences $\Delta\delta_{avg}$(HN), i.e. $(((\Delta H)^2 + (\Delta N/5)^2)/2)^{1/2}$, where ΔH and ΔN are chemical shift differences for backbone amide ^{1}H and ^{15}N nuclei, respectively. Chemical shift assignment of full-length NFU1 and of the C-domain of NFU1 were available in the Biological Magnetic Resonance Bank (under accession codes BMRB: 26801 [full-length NFU1] and BMRB: 19068 [NFU1 C-domain] [23]. Chemical shift assignment of apo ISCA2 was already available.[16] Each titration was successfully repeated three times.

1D ^{1}H paramagnetic NMR experiments were acquired at 400 MHz with a ^{1}H optimized 5 mm probe at temperatures ranging from 283 K and 298 K, with protein samples in 50 mM

phosphate, 150 mM NaCl, 5 mM DTT pH 7.0 buffer, 99% (v/v) D_2O. The protein concentration was 0.5-0.8 mM. Water signal was suppressed via fast repetition experiments and water selective irradiation. Experiments were typically performed using an overall recycle delay of 90 ms. Squared cosine and exponential multiplications were applied prior to Fourier transformation. Manual baseline correction was performed, using polynomial functions. Each experiment was successfully repeated three times.

Results

Interaction network among ISCA1, ISCA2 and NFU1 in their apo forms

Protein-protein interaction studies were performed by titrating two or three proteins in their apo forms (i.e. ISCA1, ISCA2 and NFU1) with different mixing sequences and then analyzed by NMR spectroscopy and analytical size exclusion chromatography. In these experiments, the protein constructs used were: i) the mitochondrial isoform of human NFU1 having, in the mature state, a molecular mass of ~22 kDa, as obtained upon removal of the N-terminal mitochondrial targeting sequence of 58 residues;[12] ii) human ISCA2 lacking the predicted N-terminal mitochondrial targeting sequence of 43 residues and thus resulting in a molecular mass of ~12 kDa;[15] iii) human ISCA1 in the full-length form (molecular mass of ~14 kDa) as its mitochondrial presequence is not removed upon its mitochondrial import.[34]

First, we investigated protein-protein interactions occurring between couples of proteins. When apo ^{15}N ISCA2 was stepwise titrated with apo ^{15}N NFU1 up to a 1:1 protein ratio (estimated considering monomeric protein concentrations), no chemical shift changes were observed along the ^{1}H-^{15}N HSQC NMR experiments and the ^{1}H-^{15}N HSQC map of the final 1:1 mixture is the sum of the ^{1}H-^{15}N HSQC maps of the two isolated proteins (**Figure 1A**). The resulting picture coming from these experiments is that the two proteins do not interact each other. Analytical size exclusion chromatography data confirm this result showing that no peaks with an apparent molar mass higher than those of the two isolated ISCA2 and NFU1 proteins (running, respectively, as a homodimer and a monomer with a low percentage of homodimer[16, 25]) were observed in the final 1:1 mixture (**Figure 1B**).

When apo ^{15}N ISCA2 was stepwise titrated with apo ISCA1 up to a 1:1 protein ratio (estimated considering monomeric protein concentrations), chemical shift changes were observed in the ^{1}H-^{15}N HSQC maps of apo ^{15}N ISCA2 in a slow exchange regime on the NMR time scale, i.e. signals of apo ISCA2 decreased in intensity and those of a new species, assigned to the apo ISCA1-ISCA2 complex, appeared and increased in intensity along the titration (**Figure 1C**). Once the 1:1 ISCA1-ISCA2 ratio was reached, the signals of apo ISCA2 completely disappeared and the signals of the apo ISCA1-ISCA2 complex reached their maximal intensity, indicating that the complex is fully formed at the 1:1 stoichiometric ratio. Analytical size exclusion chromatography of the final 1:1 mixture showed: i) a single peak with an apparent molar mass of ~24 kDa, which is close to the

molecular weight calculated from a dimeric apo ISCA1-ISCA2 complex (26 kDa), ii) that monomeric apo ISCA1 is no longer present in the mixture (**Figure 1D**). Overall, the NMR and analytical size exclusion chromatography data indicate the formation of a heterodimeric apo ISCA1-ISCA2 complex. The meaningful (1σ $\Delta\delta_{avg}$(HN) > 0.05 ppm) ^{1}H and ^{15}N chemical shift changes between apo ISCA2 alone and in the 1:1 protein mixture (**Figure S2**) are localized in a well-defined region of the protein. This region matches with the subunit-subunit interface stabilizing the dimeric state of apo ISCA2,[16] thus supporting that apo ISCA1 and apo ISCA2 are interacting each other by forming a dimeric structure similar to that formed by homodimeric ISCA2 (**Figure S2**). The same results were previously found using a shorter ISCA1 construct obtained deleting its predicted mitochondrial presequence of 1-23 amino acids,[16] thus indicating that the latter stretch does not affect complex formation and does not take part as active contributor to complex formation.

Apo ISCA1 forms a heterocomplex also with apo NFU1. Indeed, when apo ^{15}N NFU1 was stepwise titrated with apo ISCA1 up to a 1:1 protein ratio (estimated considering monomeric protein concentrations), chemical shift changes were observed on the ^{1}H-^{15}N HSQC maps of apo NFU1 in an intermediate exchange regime on the NMR time scale (**Figure 2A**). Several resonances of the C-domain of NFU1 broaden beyond detection upon addition of apo ISCA1 (**Figure 2A** and **Figure S3**). Analytical size exclusion chromatography equipped with multiangle light scattering (SEC-MALS) of the final 1:1 apo NFU1-apo ISCA1 mixture showed a single peak with a molar mass of 29.2 ± 0.5 kDa (**Figure S3**). This value is intermediate between those of the isolated proteins (apo ISCA1: 14 kDa, and apo NFU1: 22 kDa) and that expected from a heterodimeric apo NFU1-ISCA1 complex (36 kDa), while the peaks of monomeric apo ISCA1 and dimeric apo NFU1 are not present in the final mixture (**Figure 2B**), supporting that the two proteins are complexed in a heterodimer. Overall, both NMR and SEC-MALS data showed that a heterodimeric ISCA1-NFU1 complex is formed once the 1:1 protein ratio is reached and that it is formed via the interaction of the C-domain of NFU1 with ISCA1. However, a few resonances of the N-domain of NFU1 are also affected by apo ISCA1 additions (residues 54-58, **Figure S3**). These residues are located at the interacting interface between the N- and C-domains of apo NFU1 when takes a closed conformation.[25] This closed conformation of the two interacting domains is in equilibria with an open conformation where the N- and C-domains freely move in solution.[23, 25] Considering this structural feature and the effect of ISCA1 addition on the NH signals of residues 54-58, we can propose a model where ISCA1-NFU1

complex formation induces structural rearrangements at the interaction interface between the N- and C-domains of NFU1, possibly affecting the open-closed conformational equilibrium. This exchange among different conformations might also explain the lower than expected molar mass of the ISCA1-NFU1 complex, as derived by SEC-MALS analysis. Mapping the meaningful chemical shift changes (both broadening beyond detection effects and chemical shift changes with 1σ $\Delta\delta_{avg}(HN) > 0.03$ ppm) on the closed conformation of apo NFU1, it results that the two helices of the C-domain are largely affected by the protein-protein interaction, while the β-sheet of the C-domain is essentially unaffected (**Figure 2C**). The two helices encase the cluster binding CXXC motif of NFU1, indicating that ISCA1 in the complex is positioned close to the cluster binding region, although the CXXC motif is not largely involved in protein-protein recognition.

The apo complexes, ISCA1-^{15}N NFU1 and ISCA1-^{15}N ISCA2, were then titrated with apo ISCA2 and apo ^{15}N NFU1, respectively, and the resulting mixtures were again analyzed by NMR. In the first titration, the comparison of the ^{1}H-^{15}N HSQC map of the final mixture, with 1:1 ratio of the apo ^{15}N NFU1-ISCA1 complex and apo ISCA2, with the maps of apo ^{15}N NFU1 and of the ISCA1-^{15}N NFU1 apo complex, indicated that NFU1 remains complexed with ISCA1, thus ISCA2 not being able to extract ISCA1 from the ISCA1-NFU1 complex to form an isolated ISCA1-ISCA2 complex. Indeed, the chemical shifts of NFU1 complexed with ISCA1 were not affected by the addition of apo ISCA2 and the chemical shifts of isolated apo NFU1 were not detected, thus indicating that free apo NFU1 was not released in solution, as it would have expected in the case of the formation of an isolated ISCA1-ISCA2 complex (**Figure 3A**). In the second titration, when the ISCA1-^{15}N ISCA2 apo complex is titrated with apo ^{15}N NFU1 up to a 1:1 ratio, ISCA2 remains complexed with ISCA1, thus NFU1 not being able to extract ISCA1 from the ISCA1-ISCA2 complex to form an isolated ISCA1-NFU1 complex. Indeed, the chemical shifts of ISCA2 complexed with ISCA1 were not significantly affected by the addition of apo NFU1 and the chemical shifts of isolated apo ISCA2 were not detected (**Figure 3B**), thus indicating that free apo ISCA2 was not released in solution, as it would have expected in the case of the formation of an isolated ISCA1-NFU1 complex. On the contrary, the backbone NH chemical shifts of NFU1 changed upon its addition to the ISCA1-ISCA2 complex. Specifically, the backbone NH signals of NFU1 in the ^{1}H-^{15}N HSQC map of the final apo ISCA1- apo ^{15}N ISCA2- apo ^{15}N NFU1 mixture well overlaps with that of the ISCA1-^{15}N NFU1 apo complex, while does not with that of apo ^{15}N NFU1 alone (**Figure 3C**). Overall, we can conclude that: i) apo NFU1 interacts with the ISCA1-ISCA2 apo

complex via the C-domain of NFU1 similarly to what happens in the NFU1-ISCA1 apo complex; ii) apo ISCA1 is the protein mediating the interaction with both apo NFU1 and apo ISCA2, being the latter two, on the contrary, not interacting each other, in agreement with the lack of interactions when just the two of them are mixed (as described above). Thus, these data indicated that ISCA1, interacting with both ISCA2 and NFU1, mediates the formation of a ternary complex.

To further corroborate this model, apo ISCA1 was stepwise added to a 1:1 mixture containing the two not-interacting apo ^{15}N ISCA2 and apo ^{15}N NFU1 proteins. The ^{1}H-^{15}N HSQC maps showed the occurrence of the interaction of apo ISCA1 with both apo ISCA2 and apo NFU1. In the final mixture, the NH signals of apo NFU1 overlap with those of apo NFU1 complexed with apo ISCA1, and not with those of isolated apo NFU1 (**Figure S4**), and the NH signals of apo ISCA2 overlap with those of apo ISCA2 complexed with apo ISCA1, and not with those of isolated apo ISCA2 (**Figure S4**). The observed chemical shift changes are concurrent on both proteins along the titration and the chemical shift changes on both ^{15}N ISCA2/NFU1 apo proteins are complete once one equivalent of apo ISCA1 was added to the 1:1 ISCA2/NFU1 apo mixture, i.e. indeed, the addition of two equivalents of apo ISCA1 to the mixture did not significantly affect the ^{1}H-^{15}N HSQC map. These results conclusively indicated that apo ISCA1 interacts in tandem with both apo ISCA2 and apo NFU1, by promoting the formation of a ternary complex. Thus, ISCA1 mediates the interaction between the two not interacting proteins apo ISCA2 and apo NFU1. On the other hand, analytical size exclusion chromatography of the final mixture did not show the presence of a peak with an elution volume smaller than those of the two isolated ISCA1-ISCA2 and ISCA1-NFU1 apo complexes, as it would be expected for the presence of a ternary complex. This indicates that the latter can be readily released at the lower protein concentrations used in the analytical size exclusion chromatography with respect to those used in the NMR experiments.

Protein-protein interaction studies between [4Fe-4S] ISCA1-ISCA2 and apo NFU1

Anaerobical purification of ISCA1 and ISCA2 led to a mixture of apo and $[2Fe\text{-}2S]^{2+}$ cluster-bound forms (see Materials and Methods for details). While chemical reconstitution of anaerobically purified ISCA2 led to the formation of a $[4Fe\text{-}4S]^{2+}$ cluster-bound dimeric form,[16] chemical reconstitution of anaerobically purified ISCA1 led only to an increase of the $[2Fe\text{-}2S]^{2+}$ cluster-bound form. On the other hand, chemical reconstitution of the 1:1 ISCA1-ISCA2 heterodimer (see Materials and Methods for details) led to the formation of

a [4Fe-4S]$^{2+}$-bound, dimeric species ([4Fe-4S] ISCA1-ISCA2, hereafter). The 1D ^{1}H paramagnetic NMR spectrum is similar to that of homodimeric [4Fe-4S] ISCA2 as previously shown,[16] with down-field shifted signals having an anti-Curie temperature dependence, which originate from βCH_2 of the Cys ligands, and differs from that of [2Fe-2S]$^{2+}$ cluster-bound species of both ISCA1 and ISCA2 (**Figure 4A**, **Figure S1**, and [16]). Analytical size exclusion chromatography showed the presence of a single peak eluting at a volume very similar to that of the dimeric ISCA2 with no presence of monomeric ISCA1, consistent with the complete formation of a dimeric hetero-complex (**Figure 4B**). The ^{1}H-^{15}N HSQC spectra of the 1:1 ISCA1-^{15}N ISCA2 mixture before (i.e. anaerobically purified) and after chemical reconstitution showed that chemical shifts of most of the backbone NH signals did not vary, consistent with ISCA2 being still complexed with ISCA1. Only residues of ISCA2 surrounding the cluster binding cysteines (Cys 79, Cys 144 and Cys 146), i.e. Gly 76, Gly 77, Gly 78, Gly 81, Gly 143 and Gly 147, (**Figure 4C** compare red with blue), broaden beyond detection in the ^{1}H-^{15}N HSQC spectrum of the chemically reconstituted ISCA1-ISCA2 complex, due to the binding of the paramagnetic [4Fe-4S]$^{2+}$ cluster, indicating that the C-X_{64}-C-G-C conserved sequence motif is involved in [4Fe-4S]$^{2+}$ cluster binding in the ISCA1-ISCA2 complex.

When the [4Fe-4S] ISCA1-^{15}N ISCA2 complex was stepwise titrated with apo ^{15}N NFU1 up to a 1:1 ratio, the backbone NH signals of ISCA2 did not show any significant chemical shift changes, with the exception of the Gly residues close to the Cys cluster ligands, whose backbone NH signals, at the end of the titration, became detectable again in the ^{1}H-^{15}N HSQC map at the chemical shift values of the apo ISCA1-ISCA2 complex (**Figure 4C** compare green with blue and red). On the contrary, many spectral shift changes (mostly line broadening effects) were observed for the backbone NH signals of the C-domain of NFU1. The affected residues are located on the same interacting region mapped in the ISCA1-NFU1 and ISCA1-ISCA2-NFU1 apo complexes. Overall, these NMR data allowed to propose that: i) NFU1 interacts with the [4Fe-4S] ISCA1-ISCA2 complex via its C-domain similarly to what found in the apo ternary complex, i.e. ISCA1 complexed with ISCA2 mediates the interaction with NFU1; iii) the [4Fe-4S] cluster is no longer bound to the ISCA2 protein, likely being shared by ISCA1 and NFU1 in the ternary ISCA1-ISCA2-NFU1 complex.

To further support this model, [4Fe-4S] ISCA1-^{15}N ISCA2 complex was titrated with a ^{15}N labelled construct of apo NFU1 comprising only the C-domain, up to the 1:1 ratio. The spectral patterns on the ^{1}H-^{15}N HSQC NMR maps (**Figure S5**) were the same as those

observed in the titration with full-length NFU1, both on ISCA2 (no spectral changes) and NFU1 where the changes map on the same region of C-domain identified in the apo ISCA1-NFU1 interaction (compare inset of **Figure S5** with **Figure 2C**), indicating that the C-domain of NFU1 interacts with ISCA1 complexed with ISCA2. These data corroborate the proposed model that ISCA1 mediates the protein-protein interaction between NFU1 and the [4Fe-4S] ISCA1-ISCA2 complex, being ISCA1, and not ISCA2, the protein interacting with NFU1.

The final question is now to define which kind of cluster and cluster coordination is present in the ISCA1-ISCA2-NFU1 complex. The paramagnetic 1D ^{1}H NMR spectrum of the 1:1 mixture of $[4Fe\text{-}4S]^{2+}$ ISCA1-ISCA2 and apo NFU1 showed the presence of two hyperfine-shifted signals at 19.3 and 12.9 ppm and two close signals at around 10.5 ppm (**Figure 5A**), all having an anti-Curie temperature dependence. The chemical shift values of these signals, their anti-Curie temperature dependence, and their linewidths are typical of βCH_2 signals of Cys residues bound to a $[4Fe\text{-}4S]^{2+}$ cluster with an S=0 electronic ground state, with the paramagnetism arising from excited states of the electron spin ladder, partially populated at room temperature.[35-36] The paramagnetic 1D ^{1}H NMR spectrum of the 1:1 $[4Fe\text{-}4S]^{2+}$ ISCA1-ISCA2/apo NFU1 mixture is completely different with respect to that of the $[4Fe\text{-}4S]^{2+}$ ISCA1-ISCA2 complex while it is closer, although not superimposable, to that of dimeric $[4Fe\text{-}4S]^{2+}$ NFU1 (compare **Figure 5A** with **Figures 5B** and **4A**). The same hyperfine-shifted signals were also obtained by mixing, at 1:1 ratio, dimeric $[4Fe\text{-}4S]^{2+}$ NFU1 and apo ISCA1-ISCA2 complex (**Figure 5C**). Therefore, the 1D ^{1}H paramagnetic NMR data indicated that a $[4Fe\text{-}4S]^{2+}$ cluster is bound to the ternary ISCA1-ISCA2-NFU1 complex. Since the ^{1}H-^{15}N HSQC NMR data described above showed that ISCA2 is not involved in cluster binding, we can envisage that the $[4Fe\text{-}4S]^{2+}$ cluster is bridged between NFU1 and ISCA1 in the ternary complex. In order to validate this model, the heterodimeric ISCA1-NFU1 complex, obtained by mixing anaerobically purified ISCA1 and apo ^{15}N NFU1, was chemically reconstituted. Its paramagnetic 1D ^{1}H NMR spectrum (**Figure 5D**) showed the presence of the same anti-Curie, hyperfine-shifted signals observed when the $[4Fe\text{-}4S]^{2+}$ cluster is bound to the ternary ISCA1-ISCA2-NFU1 complex. This data provides the conclusive evidence that the $[4Fe\text{-}4S]^{2+}$ cluster is shared by ISCA1 and NFU1 in the ternary complex. In addition, the latter data showed that the ISCA1-NFU1 complex binds a $[4Fe\text{-}4S]^{2+}$ cluster, independently of the presence of ISCA2. To investigate whether the $[4Fe\text{-}4S]^{2+}$ cluster-bound ISCA1-NFU1 complex can also be formed upon mixing dimeric $[4Fe\text{-}4S]^{2+}$ NFU1 and apo ISCA1, ^{1}H-^{15}N HSQC and 1D ^{1}H paramagnetic NMR

data were acquired on dimeric [4Fe-4S]$^{2+}$ ^{15}N NFU1 titrated with apo ISCA1. Once the 1:1 [4Fe-4S]$^{2+}$ NFU1-apo ISCA1 ratio was reached, the 1D ^{1}H paramagnetic NMR spectrum indicated the complete formation of a heterodimeric [4Fe-4S]$^{2+}$ NFU1-ISCA1 complex (**Figure 5E**).

Discussion

The late steps of the maturation of mitochondrial [4Fe-4S] proteins, comprising the assembly and transfer of [4Fe-4S] clusters into mitochondrial apo client proteins, are not yet fully understood. The available genetic and proteomic data did not provide indeed a clear picture on which are the proteins essential for the assembly and transfer of the [4Fe-4S] clusters into the final client proteins and how they operate. Depending on the type of human cells or of the eukaryotic organisms, the genetic data pointed out at different mechanisms where either ISCA1 only [20], or both ISCA1 and ISCA2, [5-6, 37] are essential for the mitochondrial [4Fe-4S] biogenesis *in vivo*. There is also a significant discrepancy about the proteomic data, as human ISCA1 was found to interact with NFU1 only,[20] while yeast NFU1 interacts with both yeast ISCA1 and ISCA2.[26] The here presented NMR-based study provides a molecular model for the succession of events orchestrated by ISCA1, ISCA2 and NFU1 to assemble [4Fe-4S] clusters and make them available for mitochondrial apo client proteins, reconciling all the genetic and proteomic studies. We have showed that ISCA1 is the key player of the [4Fe-4S] protein maturation process being able indeed to interact either individually with ISCA2 or NFU1 or with both proteins in a ternary complex. In the latter case, ISCA1 works as a mediator between the two no interacting proteins ISCA2 and NFU1. The ISCA1-ISCA2 complex-bound [4Fe-4S]$^{2+}$ cluster is not donated to NFU1 and dimeric [4Fe-4S]$^{2+}$ NFU1[12, 23, 25] is not formed. On the contrary, the cluster is translocated within the ternary ISCA1-ISCA2-NFU1 complex from a bridged ISCA1-ISCA2 coordination to a bridged ISCA1-NFU1 one, thus being ISCA2 no more involved in cluster binding. The pathway of the maturation of mitochondrial [4Fe-4S] proteins (ISCAs-dependent maturation pathway, hereafter, **Figure 6**) can thus be outlined as it follows: i) the [4Fe-4S]$^{2+}$ cluster is assembled on the ISCA1-ISCA2 heterodimer by reductively coupling two [2Fe-2S]$^{2+}$ clusters donated by GLRX5;[16, 21] ii) [4Fe-4S]$^{2+}$ ISCA1-ISCA2 complex can transfer the cluster to client proteins that do not require NFU1 for their maturation, i.e. aconitase;[8-9] iii) ISCA1, through its specific recognition with the C-domain of NFU1, mediates the [4Fe-4S]$^{2+}$ cluster translocation from ISCA1-ISCA2 to ISCA1-

NFU1 within a formed ternary ISCA1-ISCA2-NFU1 complex; iv) the ISCA1-ISCA2-NFU1 complex to which the $[4Fe\text{-}4S]^{2+}$ cluster is coordinated by ISCA1 and NFU1 specifically can direct the $[4Fe\text{-}4S]^{2+}$ cluster to mitochondrial client proteins that require NFU1 for their maturation, i.e. respiratory complexes I and II and the radical SAM protein lipoyl synthase.[8-9, 38-40] In this mechanism, the cluster can be safely moved from where it is assembled, i.e. the ISCA1-ISCA2 complex, to the final client protein in a specific manner, with no risk of being lost in solution where it might damage the cellular environment. This pathway is in agreement with the *in vivo* results showing that ISCA2 cannot compensate for the loss of ISCA1 function and that ISCA1 and ISCA2 are not functionally redundant.[20] We also found that the interaction between ISCA1 and NFU1 specifically involves the C-domain of NFU1, being the N-domain of NFU1 essentially not part of the protein-protein recognition. The two helices of NFU1 encasing the cluster binding CXXC motif are involved in the interaction with ISCA1. The same two helices of NFU1 were recently shown to be involved in a specific interaction with ISCU.[29] This interaction was proposed to be physiologically relevant to drive the cluster transfer observed when a [4Fe-4S] ISCU form was mixed with apo NFU1 leading to the formation of [4Fe-4S] NFU1, which in turn was shown to be able to mature mitochondrial aconitase.[23, 29] Although the physiological relevance of the [4Fe-4S] ISCU form is still debated,[30-31, 41] the finding that the same interacting region of NFU1 is found with both ISCA1 and ISCU suggests the occurrence of a mitochondrial [4Fe-4S] protein maturation pathway dependent on the formation of a dimeric [4Fe-4S] NFU1 species ([4Fe-4S] NFU1-dependent maturation pathway, hereafter, **Figure 6**). At support of this pathway, a dimeric Fe-S cluster bridged NFU1 was showed to form in yeast mitochondria,[26] and double deletion of yeast NFU1 and ISU1 is associated with more severe defects in aconitase and in mitochondrial respiratory complexes with respect to single NFU1 deletion which is associated only with weak defects in mitochondrial [4Fe-4S] proteins.[7] This pathway was also already suggested based on the functional impairment of the Gly194Cys pathogenic mutant of NFU1, whose cluster synthesis in yeast depends on Isu1, Grx5 and Ssq1.[9] We recently showed that dimeric [4Fe-4S] NFU1 can also be formed by the $[2Fe\text{-}2S]^{2+}$ GLRX5-BOLA3 complex.[25] Indeed, the latter transfers its cluster to monomeric apo NFU1 to form, in the presence of a reductant, a $[4Fe\text{-}4S]^{2+}$ cluster-bound to dimeric NFU1. In this case, NFU1 works, not as a $[4Fe\text{-}4S]^{2+}$ cluster acceptor, as it occurs upon interaction with [4Fe-4S] ISCU,[29] but as an 'assembler' of $[4Fe\text{-}4S]^{2+}$ clusters converting two $[2Fe\text{-}2S]^{2+}$ clusters into a $[4Fe\text{-}4S]^{2+}$ cluster.[25] Overall, the [4Fe-4S] NFU1-dependent maturation pathway can thus be a physiological pathway

alternative to the ISCAs-dependent maturation pathway. We now observed that dimeric $[4Fe\text{-}4S]^{2+}$ NFU1 when mixed with apo ISCA1 or with the apo ISCA1-ISCA2 complex forms, respectively, the $[4Fe\text{-}4S]^{2+}$ NFU1-ISCA1 adduct or the ternary $[4Fe\text{-}4S]^{2+}$ ISCA1-ISCA2-NFU1 complex where the $[4Fe\text{-}4S]^{2+}$ cluster is shared by NFU1 and ISCA1. Thus, the ISCAs-dependent and [4Fe-4S] NFU1-dependent mitochondrial [4Fe-4S] protein maturation pathways resulted strictly connected (**Figure 6**, dashed arrow). In conclusion, dimeric $[4Fe\text{-}4S]^{2+}$ NFU1, formed by $[4Fe\text{-}4S]^{2+}$ ISCU or $[2Fe\text{-}2S]^{2+}$ GLRX5-BOLA3 complex, can activate alternative pathways to mature mitochondrial [4Fe-4S] client proteins thanks to the two connections, shown as dashed arrows in **Figure 6**, that we identified between the ISCAs-dependent and [4Fe-4S] NFU1-dependent pathways.

The proposed molecular pathways orchestrated by ISCA1, ISCA2 and NFU1 to assemble and make available [4Fe-4S] clusters for mitochondrial apo client proteins fully rationalizes the *in vivo* data previously reported for these components. Indeed, from our molecular model it resulted that ISCA1 is the crucial protein activating all [4Fe-4S] protein maturation pathways, i.e. ISCAs-dependent and [4Fe-4S] NFU1-dependent ones, in agreement with knockdown experiments in mouse skeletal muscle and in primary cultures of neurons that suggested that ISCA1, but not ISCA2, is required for mitochondrial [4Fe-4S] proteins biogenesis.[20] On the other hand, similar phenotypes were observed in HeLa cells for ISCA1 and ISCA2 knockdowns, resulting both proteins crucial for the mitochondrial [4Fe-4S] protein biogenesis.[6] Our molecular model showed that ISCA2 plays a crucial role in assembling [4Fe-4S] clusters once complexed with ISCA1 in the ISCAs-dependent pathway, and the latter seems to be primarily required in HeLa cells, with respect to the [4Fe-4S] NFU1-dependent pathway. On the contrary, in mouse skeletal muscle and in primary cultures of neurons once ISCA2 was knockdown, the [4Fe-4S] NFU1-dependent pathway is efficiently activated for maturing all [4Fe-4S] mitochondrial proteins, so, basically, substituting the ISCAs-dependent pathway. Specifically, aconitase might be directly matured by dimeric $[4Fe\text{-}4S]^{2+}$ NFU1, as observed by Cai et al.,[23] while respiratory complexes I and II and the radical SAM protein lipoyl synthase by the $[4Fe\text{-}4S]^{2+}$ NFU1-ISCA1 adduct (**Figure 6**, dashed arrow). The existence of the [4Fe-4S] NFU1-dependent route is supported by previous findings indicating that the binding of ^{55}Fe to the pathogenic Nfu1 Gly194Cys mutant in yeast cells was dependent on both the major scaffold protein Isu1 and factors releasing the Fe-S cluster from Isu1 (Ssq1, Grx5), but not on the late-acting Isa1-2 proteins.[9] In conclusion, our data provide a molecular model for the maturation of mitochondrial [4Fe-4S] proteins that is able to fully interpret the available *in vivo* data.

ACKNOWLEDGEMENTS

The authors acknowledge funding from timb3, grant number 810856, funded by the Horizon 2020 programme of the European Commission. Work at CERM is supported by the Italian Ministry for University and Research (FOE funding) to the Italian Center (CERM, University of Florence) of Instruct-ERIC, a European Research Infrastructure, ESFRI Landmark. This article is based upon work from COST Action CA15133, supported by COST (European Cooperation in Science and Technology).

SUPPORTING INFORMATION

Supporting information contains a file reporting Figures S1-S5 (PDF).

COMPETING INTERESTS STATEMENT

The authors declare no competing financial interests.

References

1. Maio, N.; Rouault, T. A., Outlining the Complex Pathway of Mammalian Fe-S Cluster Biogenesis. *Trends Biochem Sci* **2020,** *45* (5), 411-426.

2. Lill, R.; Freibert, S. A., Mechanisms of Mitochondrial Iron-Sulfur Protein Biogenesis. *Annu Rev Biochem* **2020,** *89*, 471-499.

3. Ciofi-Baffoni, S.; Nasta, V.; Banci, L., Protein networks in the maturation of human iron-sulfur proteins. *Metallomics* **2018,** *10*, 49-72.

4. Andreini, C.; Banci, L.; Rosato, A., Exploiting bacterial operons to illuminate human iron-sulfur proteins. *J. Proteome Res* **2016,** *15*, 1308-1322.

5. Muhlenhoff, U.; Richter, N.; Pines, O.; Pierik, A. J.; Lill, R., Specialized function of yeast Isa1 and Isa2 proteins in the maturation of mitochondrial [4Fe-4S] proteins. *J. Biol. Chem* **2011,** *286* (48), 41205-41216.

6. Sheftel, A. D.; Wilbrecht, C.; Stehling, O.; Niggemeyer, B.; Elsasser, H. P.; Muhlenhoff, U.; Lill, R., The human mitochondrial ISCA1, ISCA2, and IBA57 proteins are required for [4Fe-4S] protein maturation. *Mol. Biol. Cell* **2012,** *23* (7), 1157-1166.

7. Schilke, B.; Voisine, C.; Beinert, H.; Craig, E., Evidence for a conserved system for iron metabolism in the mitochondria of Saccharomyces cerevisiae. *Proc Natl Acad Sci U S A* **1999,** *96* (18), 10206-11.

8. Cameron, J. M.; Janer, A.; Levandovskiy, V.; MacKay, N.; Rouault, T. A.; Tong, W. H.; Ogilvie, I.; Shoubridge, E. A.; Robinson, B. H., Mutations in iron-sulfur cluster scaffold genes NFU1 and BOLA3 cause a fatal deficiency of multiple respiratory chain and 2-oxoacid dehydrogenase enzymes. *Am. J. Hum. Genet* **2011,** *89* (4), 486-495.

9. Navarro-Sastre, A.; Tort, F.; Stehling, O.; Uzarska, M. A.; Arranz, J. A.; Del, T. M.; Labayru, M. T.; Landa, J.; Font, A.; Garcia-Villoria, J.; Merinero, B.; Ugarte, M.; Gutierrez-Solana, L. G.; Campistol, J.; Garcia-Cazorla, A.; Vaquerizo, J.; Riudor, E.; Briones, P.; Elpeleg, O.; Ribes, A.; Lill, R., A fatal mitochondrial disease is associated with defective NFU1 function in the maturation of a subset of mitochondrial Fe-S proteins. *Am. J. Hum. Genet* **2011,** *89* (5), 656-667.

10. Kaut, A.; Lange, H.; Diekert, K.; Kispal, G.; Lill, R., Isa1p is a component of the mitochondrial machinery for maturation of cellular iron-sulfur proteins and requires conserved cysteine residues for function. *J. Biol. Chem* **2000,** *275* (21), 15955-15961.

11. Pelzer, W.; Muhlenhoff, U.; Diekert, K.; Siegmund, K.; Kispal, G.; Lill, R., Mitochondrial Isa2p plays a crucial role in the maturation of cellular iron-sulfur proteins. *FEBS Lett* **2000,** *476* (3), 134-139.

12. Tong, W. H.; Jameson, G. N.; Huynh, B. H.; Rouault, T. A., Subcellular compartmentalization of human Nfu, an iron-sulfur cluster scaffold protein, and its ability to assemble a [4Fe-4S] cluster. *Proc. Natl. Acad. Sci. USA* **2003,** *100* (17), 9762-9767.

13. Vinella, D.; Brochier-Armanet, C.; Loiseau, L.; Talla, E.; Barras, F., Iron-sulfur (Fe/S) protein biogenesis: phylogenomic and genetic studies of A-type carriers. *PLoS Genet* **2009,** *5* (5), e1000497.

14. Mapolelo, D. T.; Zhang, B.; Naik, S. G.; Huynh, B. H.; Johnson, M. K., Spectroscopic and functional characterization of iron-sulfur cluster-bound forms of Azotobacter vinelandii (Nif)IscA. *Biochemistry* **2012,** *51* (41), 8071-8084.

15. Banci, L.; Brancaccio, D.; Ciofi-Baffoni, S.; Del Conte, R.; Gadepalli, R.; Mikolajczyk, M.; Neri, S.; Piccioli, M.; Winkelmann, J., [2Fe-2S] cluster transfer in iron-sulfur protein biogenesis. *Proc. Natl. Acad. Sci. USA* **2014,** *111* (17), 6203-6208.

16. Brancaccio, D.; Gallo, A.; Mikolajczyk, M.; Zovo, K.; Palumaa, P.; Novellino, E.; Piccioli, M.; Ciofi-Baffoni, S.; Banci, L., Formation of [4Fe-4S] clusters in the mitochondrial iron-sulfur cluster assembly machinery. *J. Am. Chem Soc* **2014,** *136* (46), 16240-16250.

17. Wu, G.; Mansy, S. S.; Hemann, C.; Hille, R.; Surerus, K. K.; Cowan, J. A., Iron-sulfur cluster biosynthesis: characterization of Schizosaccharomyces pombe Isa1. *J. Biol. Inorg. Chem* **2002,** *7* (4-5), 526-532.

18. Krebs, C.; Agar, J. N.; Smith, A. D.; Frazzon, J.; Dean, D. R.; Huynh, B. H.; Johnson, M. K., IscA, an alternate scaffold for Fe-S cluster biosynthesis. *Biochemistry* **2001,** *40* (46), 14069-14080.

19. Ollagnier-de-Choudens, S.; Mattioli, T.; Takahashi, Y.; Fontecave, M., Iron-sulfur cluster assembly: characterization of IscA and evidence for a specific and functional complex with ferredoxin. *J. Biol. Chem* **2001,** *276* (25), 22604-22607.

20. Beilschmidt, L. K.; Ollagnier de Choudens, S.; Fournier, M.; Sanakis, I.; Hograindleur, M. A.; Clemancey, M.; Blondin, G.; Schmucker, S.; Eisenmann, A.; Weiss, A.; Koebel, P.; Messaddeq, N.; Puccio, H.; Martelli, A., ISCA1 is essential for mitochondrial Fe4S4 biogenesis in vivo. *Nature communications* **2017,** *8*, 15124.

21. Brancaccio, D.; Gallo, A.; Piccioli, M.; Novellino, E.; Ciofi-Baffoni, S.; Banci, L., [4Fe-4S] Cluster Assembly in Mitochondria and Its Impairment by Copper. *J. Am. Chem. Soc* **2017,** *139*, 719-730.

22. Py, B.; Gerez, C.; Angelini, S.; Planel, R.; Vinella, D.; Loiseau, L.; Talla, E.; Brochier-Armanet, C.; Garcia, S. R.; Latour, J. M.; Ollagnier-de, C. S.; Fontecave, M.; Barras, F., Molecular organization, biochemical function, cellular role and evolution of NfuA, an atypical Fe-S carrier. *Mol. Microbiol* **2012,** *86* (1), 155-171.

23. Cai, K.; Liu, G.; Frederick, R. O.; Xiao, R.; Montelione, G. T.; Markley, J. L., Structural/Functional Properties of Human NFU1, an Intermediate [4Fe-4S] Carrier in Human Mitochondrial Iron-Sulfur Cluster Biogenesis. *Structure* **2016,** *24* (12), 2080-2091.

24. Li, J.; Ding, S.; Cowan, J. A., Thermodynamic and structural analysis of human NFU conformational chemistry. *Biochemistry* **2013,** *52* (29), 4904-13.

25. Nasta, V.; Suraci, D.; Gourdoupis, S.; Ciofi-Baffoni, S.; Banci, L., A pathway for assembling [4Fe-4S](2+) clusters in mitochondrial iron-sulfur protein biogenesis. *Febs j* **2020,** *287* (11), 2312-2327.

26. Melber, A.; Na, U.; Vashisht, A.; Weiler, B. D.; Lill, R.; Wohlschlegel, J. A.; Winge, D. R., Role of Nfu1 and Bol3 in iron-sulfur cluster transfer to mitochondrial clients. *Elife* **2016,** *5*, e15991.

27. Sen, S.; Rao, B.; Wachnowsky, C.; Cowan, J. A., Cluster exchange reactivity of [2Fe-2S] cluster-bridged complexes of BOLA3 with monothiol glutaredoxins. *Metallomics* **2018,** *10* (9), 1282-1290.

28. Nasta, V.; Giachetti, A.; Ciofi-Baffoni, S.; Banci, L., Structural insights into the molecular function of human (2Fe-2S) BOLA1-GRX5 and (2Fe-2S) BOLA3-GRX5 complexes. *Biochim Biophys Acta* **2017,** *1861*, 2119-2131.

29. Cai, K.; Frederick, R. O.; Markley, J. L., ISCU interacts with NFU1, and ISCU[4Fe-4S] transfers its Fe-S cluster to NFU1 leading to the production of holo-NFU1. *J Struct Biol* **2020,** *210* (2), 107491.

30. Fox, N. G.; Chakrabarti, M.; McCormick, S. P.; Lindahl, P. A.; Barondeau, D. P., The Human Iron-Sulfur Assembly Complex Catalyzes the Synthesis of [2Fe-2S] Clusters on ISCU2 That Can Be Transferred to Acceptor Molecules. *Biochemistry* **2015,** *54* (25), 3871-9.

31. Webert, H.; Freibert, S. A.; Gallo, A.; Heidenreich, T.; Linne, U.; Amlacher, S.; Hurt, E.; Muhlenhoff, U.; Banci, L.; Lill, R., Functional reconstitution of *de novo* mitochondrial Fe/S cluster synthesis reveals an essential role of ferredoxin. *Nat. Commun* **2014,** *5*, 5013-5025.

32. Banci, L.; Bertini, I.; Ciofi-Baffoni, S.; Boscaro, F.; Chatzi, A.; Mikolajczyk, M.; Tokatlidis, K.; Winkelmann, J., Anamorsin is a 2Fe2S cluster-containing substrate of the Mia40-dependent mitochondrial protein trapping machinery. *Chem. Biol* **2011,** *18* (6), 794-804.

33. Dailey, H. A.; Finnegan, M. G.; Johnson, M. K., Human ferrochelatase is an iron-sulfur protein. *Biochemistry* **1994,** *33* (2), 403-407.

34. Torraco, A.; Stehling, O.; Stümpfig, C.; Rösser, R.; De Rasmo, D.; Fiermonte, G.; Verrigni, D.; Rizza, T.; Vozza, A.; Di Nottia, M.; Diodato, D.; Martinelli, D.; Piemonte, F.; Dionisi-Vici, C.; Bertini, E.; Lill, R.; Carrozzo, R., ISCA1 mutation in a patient with infantile-onset leukodystrophy causes defects in mitochondrial [4Fe-4S] proteins. *Hum Mol Genet* **2018,** *27* (15), 2739-2754.

35. Bertini, I.; Capozzi, F.; Luchinat, C.; Piccioli, M., ^{1}H NMR investigation of oxidized and reduced HiPIP from *R. globiformis*. *Eur. J. Biochem* **1993,** *212*, 69-78.

36. Banci, L.; Camponeschi, F.; Ciofi-Baffoni, S.; Piccioli, M., The NMR contribution to protein-protein networking in Fe-S protein maturation. *Journal of Biological Inorganic Chemistry* **2018,** *23* (4), 687-687.

37. Muhlenhoff, U.; Gerl, M. J.; Flauger, B.; Pirner, H. M.; Balser, S.; Richhardt, N.; Lill, R.; Stolz, J., The ISC proteins Isa1 and Isa2 are required for the function but not for the de novo synthesis of the Fe/S clusters of biotin synthase in Saccharomyces cerevisiae. *Eucaryotic Cell* **2007,** *6*, 495-504.

38. Lebigot, E.; Gaignard, P.; Dorboz, I.; Slama, A.; Rio, M.; de Lonlay, P.; Heron, B.; Sabourdy, F.; Boespflug-Tanguy, O.; Cardoso, A.; Habarou, F.; Ottolenghi, C.; Therond, P.; Bouton, C.; Golinelli-Cohen, M. P.; Boutron, A., Impact of mutations within the [Fe-S] cluster or the lipoic acid biosynthesis pathways on mitochondrial protein expression profiles in fibroblasts from patients. *Mol Genet Metab* **2017,** *122* (3), 85-94.

39. Ahting, U.; Mayr, J. A.; Vanlander, A. V.; Hardy, S. A.; Santra, S.; Makowski, C.; Alston, C. L.; Zimmermann, F. A.; Abela, L.; Plecko, B.; Rohrbach, M.; Spranger, S.; Seneca, S.; Rolinski, B.; Hagendorff, A.; Hempel, M.; Sperl, W.; Meitinger, T.; Smet, J.; Taylor, R. W.; Van, C. R.; Freisinger, P.; Prokisch, H.; Haack, T. B., Clinical, biochemical, and genetic spectrum of seven patients with NFU1 deficiency. *Front Genet* **2015,** *6*, 123.

40. Culley, M. K.; Perk, D.; Chan, S. Y., NFU1, Iron-Sulfur Biogenesis, and Pulmonary Arterial Hypertension: A (Metabolic) Shift in Our Thinking. *Am J Respir Cell Mol Biol* **2020,** *62* (2), 136-138.

41. Colin, F.; Martelli, A.; Clemancey, M.; Latour, J. M.; Gambarelli, S.; Zeppieri, L.; Birck, C.; Page, A.; Puccio, H.; Ollagnier de, C. S., Mammalian frataxin controls sulfur production and iron entry during de novo Fe4S4 cluster assembly. *J. Am. Chem Soc* **2013,** *135* (2), 733-740.

42. Lill, R., From the discovery to molecular understanding of cellular iron-sulfur protein biogenesis. *Biol Chem* **2020,** *401* (6-7), 855-876.

Figure 1. Apo ISCA2 interacts with apo ISCA1 and not with apo NFU1. (**A**) Overlay of the ^{1}H-^{15}N HSQC spectrum of a 1:1 mixture of apo ^{15}N ISCA2 and apo ^{15}N NFU1 (red) with those of apo ^{15}N ISCA2 (cyano) and apo ^{15}N NFU1 (black). (**B**) Analytical size exclusion chromatography of apo ISCA2 (blue), apo NFU1 (green) and a 1:1 mixture of apo ISCA2 and apo NFU1 (black). (**C**) Overlay of the ^{1}H-^{15}N HSQC spectrum of a 1:1 mixture of apo ^{15}N ISCA2 and apo ISCA1 (red) with that of apo ^{15}N ISCA2 (black). In the insets, overlay of regions of ^{1}H-^{15}N HSQC spectra of apo ^{15}N ISCA2 (black) and of 1:1 (red) and 1:0.5 (blue) mixtures of apo ^{15}N ISCA2 and apo ISCA1. (**D**) Analytical size exclusion chromatography of apo ISCA2 (blue), apo ISCA1 (cyano) and a 1:1 mixture of apo ISCA2 and apo ISCA1 (black).

Figure 2. Apo ISCA1 interacts with the C-domain of apo NFU1. (**A**) Overlay of the ^{1}H-^{15}N HSQC spectrum of a 1:1 mixture of apo ^{15}N NFU1 and apo ISCA1 (red) with that of apo ^{15}N NFU1 (black). In the inset, overlay of a region of the ^{1}H-^{15}N HSQC spectra of mixtures of apo ^{15}N NFU1 with apo ISCA1 at increasing concentration. (**B**) Analytical size exclusion chromatography of apo ISCA1 (red), apo NFU1 (black) and a 1:1 mixture of apo NFU1 and apo ISCA1 (blue). (**C**) Meaningful chemical shift changes for the backbone NHs of apo ^{15}N NFU1 upon the addition of 1 equivalent of apo ISCA1 are mapped on a structural model of monomeric apo NFU1 in a closed conformation [25]. In orange are the sidechains of the solvent exposed (> 50%) residues showing chemical shift changes (line broadening beyond detection effects and/or meaningful chemical shift changes). The protein stretches in blue represent residues showing meaningful chemical shift changes but not solvent exposed. The sidechains of the proline residues are shown in gray.

Figure 3. Apo ISCA1-ISCA2 heterodimeric complex interacts with the C-domain of apo NFU1. Overlay of the ^{1}H-^{15}N HSQC spectrum of (**A**) a 1:1:1 mixture of apo ^{15}N NFU1-apo ISCA1- apo ISCA2 (green) with those of apo ^{15}N NFU1 (black) and of a 1:1 mixture of apo ^{15}N NFU1 and apo ISCA1 (red); (**B**) a 1:1:1 mixture of apo ^{15}N NFU1-apo ISCA1-apo ISCA2 (black) with that of a 1:1 mixture of apo ^{15}N ISCA2 and apo ISCA1 (red); (**C**) a 1:1:1 mixture of apo ^{15}N NFU1-apo ISCA1-apo ISCA2 (black) with those of apo ^{15}N NFU1 (red) and of a 1:1 mixture of apo ^{15}N NFU1 and apo ISCA1 (green).

Figure 4. The ISCA1-ISCA2 heterodimer binds a [4Fe-4S]$^{2+}$ cluster. (**A**) 1D ^{1}H paramagnetic NMR spectrum at 283 K of [4Fe-4S]$^{2+}$ ISCA1-ISCA2, obtained by chemically reconstituting a 1:1 mixture of anaerobically purified ISCA1 and ISCA2. (**B**) Analytical size exclusion chromatography of [4Fe-4S]$^{2+}$ ISCA1-ISCA2 (red), apo ISCA2 (green) and apo ISCA1 (black). (**C**) Overlay of the ^{1}H-^{15}N HSQC spectra of apo ^{15}N ISCA2 (black), ^{15}N ISCA2-ISCA1 apo complex (red), [4Fe-4S] ^{15}N ISCA2-ISCA1 complex (blue), of a 1:1 mixture of [4Fe-4S] ^{15}N ISCA2-ISCA1 complex and apo ^{15}N NFU1 (green). The marked signals indicate the backbone NHs of ISCA2 residues, and the N-domain, the linker and the C-domain of NFU1, labelled as N-, L- and C-NFU1, respectively.

Figure 5. A [4Fe-4S]$^{2+}$ cluster is bound to the ternary ISCA1-ISCA2-NFU1 complex. 1D ^{1}H paramagnetic NMR spectra of (**A**) a 1:1 mixture of [4Fe-4S]$^{2+}$ ISCA1-ISCA2 and apo NFU1, (**B**) dimeric [4Fe-4S]$^{2+}$ NFU1, (**C**) a 1:1 mixture of apo ISCA1-ISCA2 and dimeric [4Fe-4S]$^{2+}$ NFU1, (**D**) a chemically reconstituted 1:1 mixture of anaerobically purified ISCA1 and apo NFU1, (**E**) a 1:1 mixture of dimeric [4Fe-4S]$^{2+}$ NFU1 and apo ISCA1. The spectra were acquired at 298 K in 50 mM phosphate buffer pH 7.0, 150 mM NaCl, 5 mM DTT.

Figure 6. Iron-sulfur cluster assembly pathways for the maturation of mitochondrial [4Fe-4S] proteins. The ISCAs-dependent pathway requires ISCA1 and ISCA2 to mature [4Fe-4S]$^{2+}$ mitochondrial proteins: 1) the ISCA1-ISCA2 complex receives two [2Fe-2S]$^{2+}$ clusters from GLRX5[16] and two electrons from ferredoxin FDX2[42] to assemble a [4Fe-4S]$^{2+}$ cluster; 2) the [4Fe-4S]$^{2+}$ ISCA1-ISCA2 complex can transfer the cluster to aconitase maturing it or can specifically interact with the C-domain of apo NFU1 forming a ternary [4Fe-4S]$^{2+}$ NFU1-ISCA1-ISCA2 complex; 3) the [4Fe-4S]$^{2+}$ cluster is moved within the ternary complex from a bridged ISCA1-ISCA2 coordination to a bridged ISCA1-NFU1 coordination; 4) [4Fe-4S]$^{2+}$ ISCA1-ISCA2-NFU1 complex transfers the cluster to mature respiratory complexes I and II and LIAS, with the help of other accessory proteins when required (not shown in Figure). The [4Fe-4S] NFU1-dependent pathway is activated upon the formation of dimeric [4Fe-4S]$^{2+}$ NFU1. The latter might be formed following two different pathways described in the literature dependent on [2Fe-2S]$^{2+}$ GLRX3-BOLA3 complex[25] or [4Fe-4S]$^{2+}$ ISCU.[29] We showed here that dimeric [4Fe-4S]$^{2+}$ NFU1 by interacting with apo ISCA1 or with the apo ISCA1-ISCA2 complex can form the [4Fe-4S]$^{2+}$ ISCA1-NFU1 complex and the ternary [4Fe-4S]$^{2+}$ ISCA1-NFU1-ISCA2 complex,

respectively. These connections are indicated with dashed arrow. Thus, the two ISCAs-dependent and [4Fe-4S] NFU1-dependent pathways are strictly connected.

Figure 1

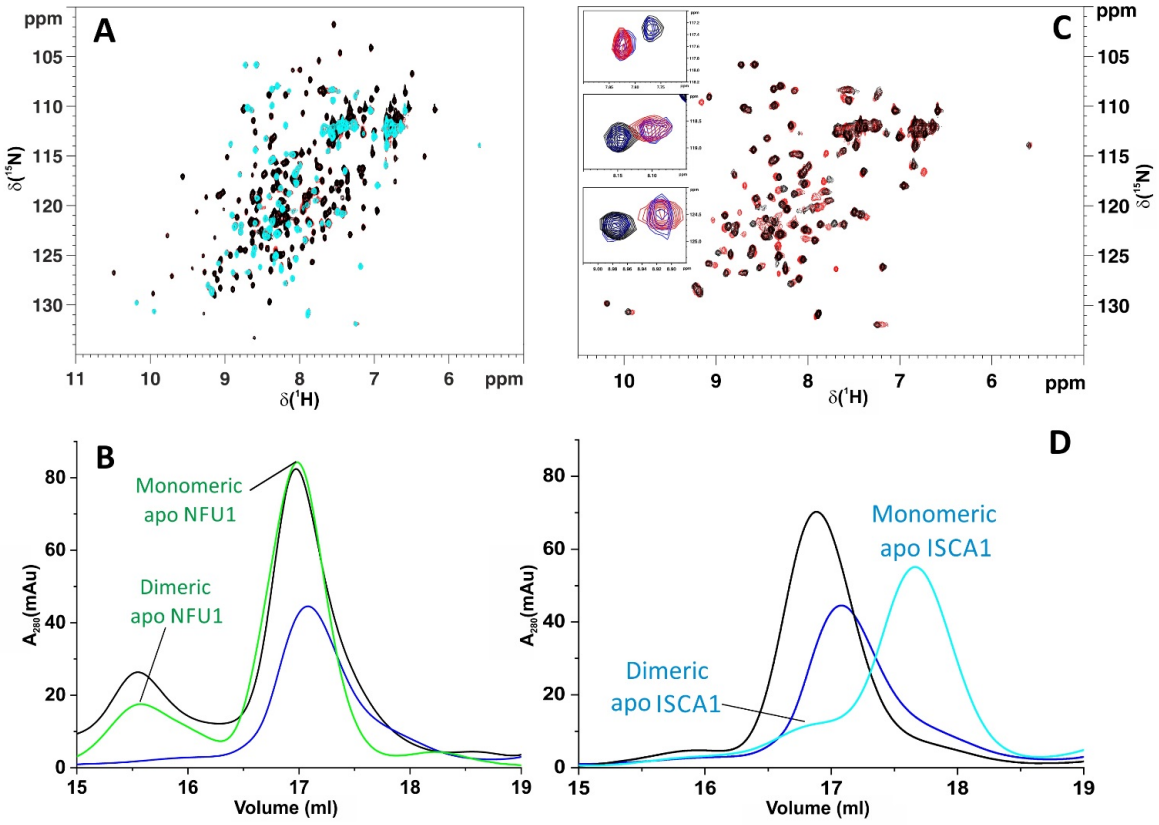

Figure 2

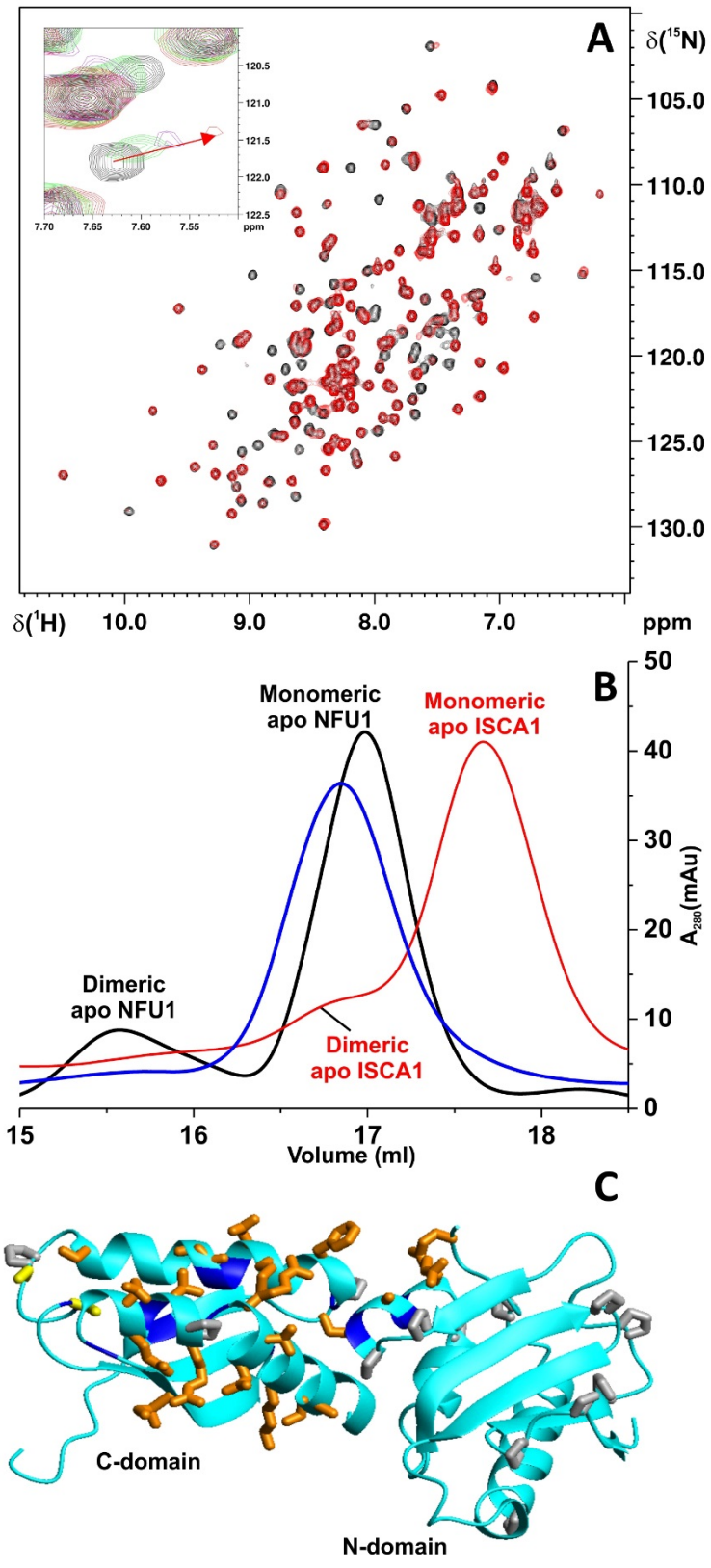
A
δ(15N)
105.0
110.0
115.0
120.0
125.0
130.0
δ(1H)
10.0
9.0
8.0
7.0
ppm
120.5
121.0
121.5
122.0
122.5
7.70
7.65
7.60
7.55
ppm
B
Monomeric apo NFU1
Monomeric apo ISCA1
Dimeric apo NFU1
Dimeric apo ISCA1
50
40
30
20
10
0
A280(mAu)
15
16
17
18
Volume (ml)
C
C-domain
N-domain

Figure 3

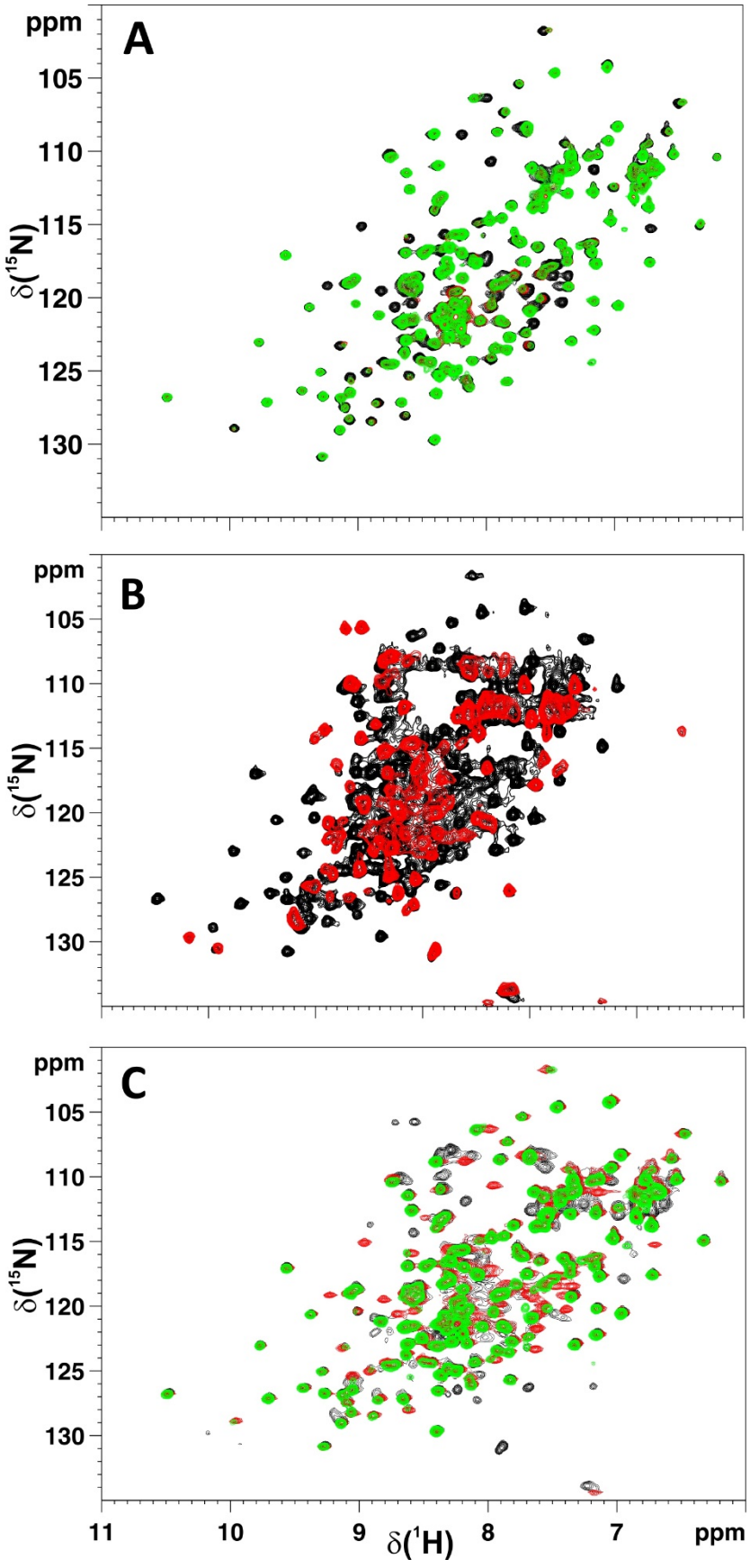

Figure 4

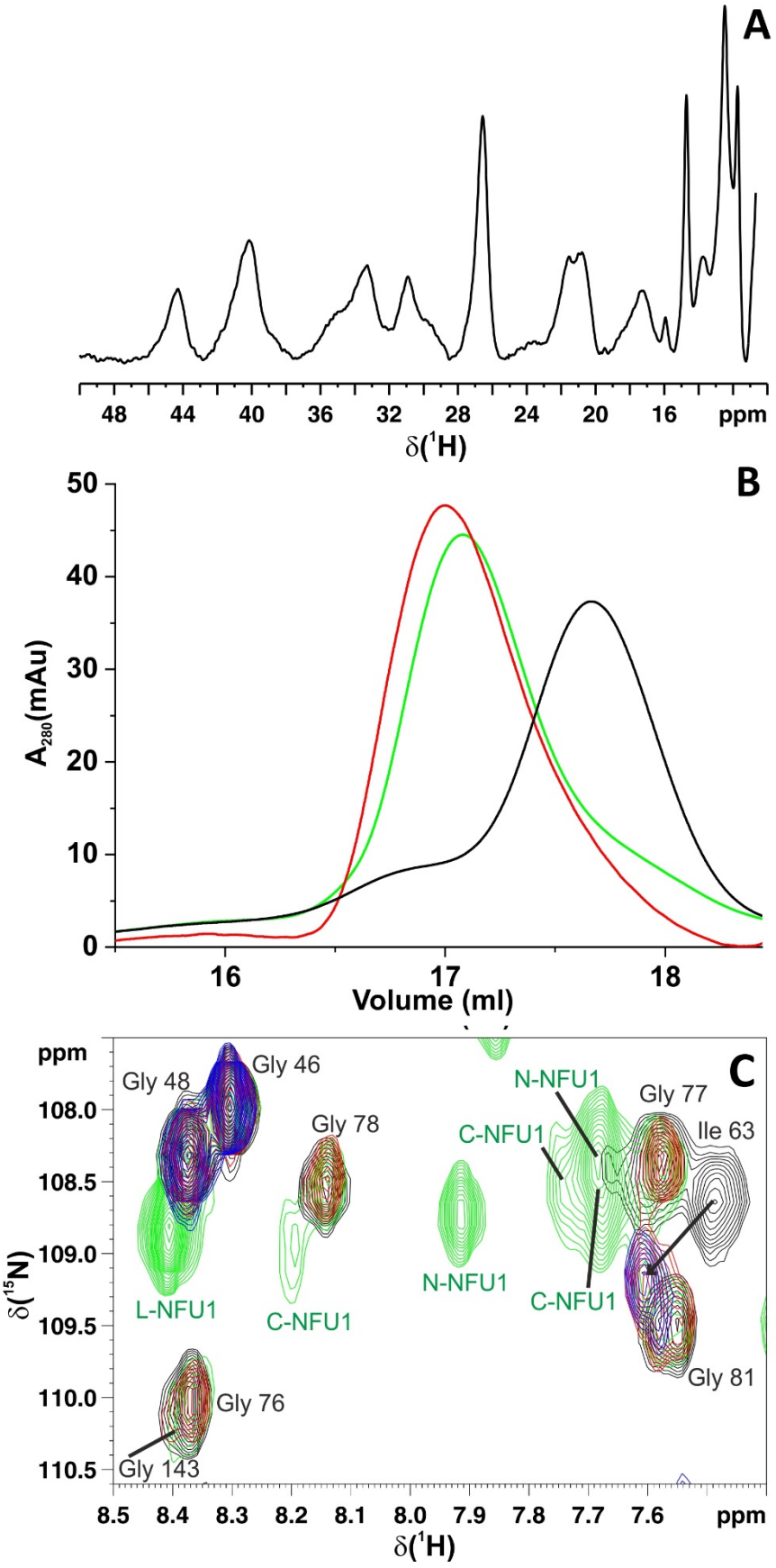
A
48
44
40
36
32
28
24
20
16
ppm
δ(¹H)
B
50
40
30
20
10
0
A280(mAu)
16
17
18
Volume (ml)
C
ppm
108.0
108.5
109.0
109.5
110.0
110.5
δ(¹⁵N)
Gly 48
Gly 46
Gly 78
L-NFU1
C-NFU1
N-NFU1
Gly 77
C-NFU1
Ile 63
N-NFU1
C-NFU1
Gly 81
Gly 76
Gly 143
8.5
8.4
8.3
8.2
8.1
8.0
7.9
7.8
7.7
7.6
ppm
δ(¹H)

Figure 5

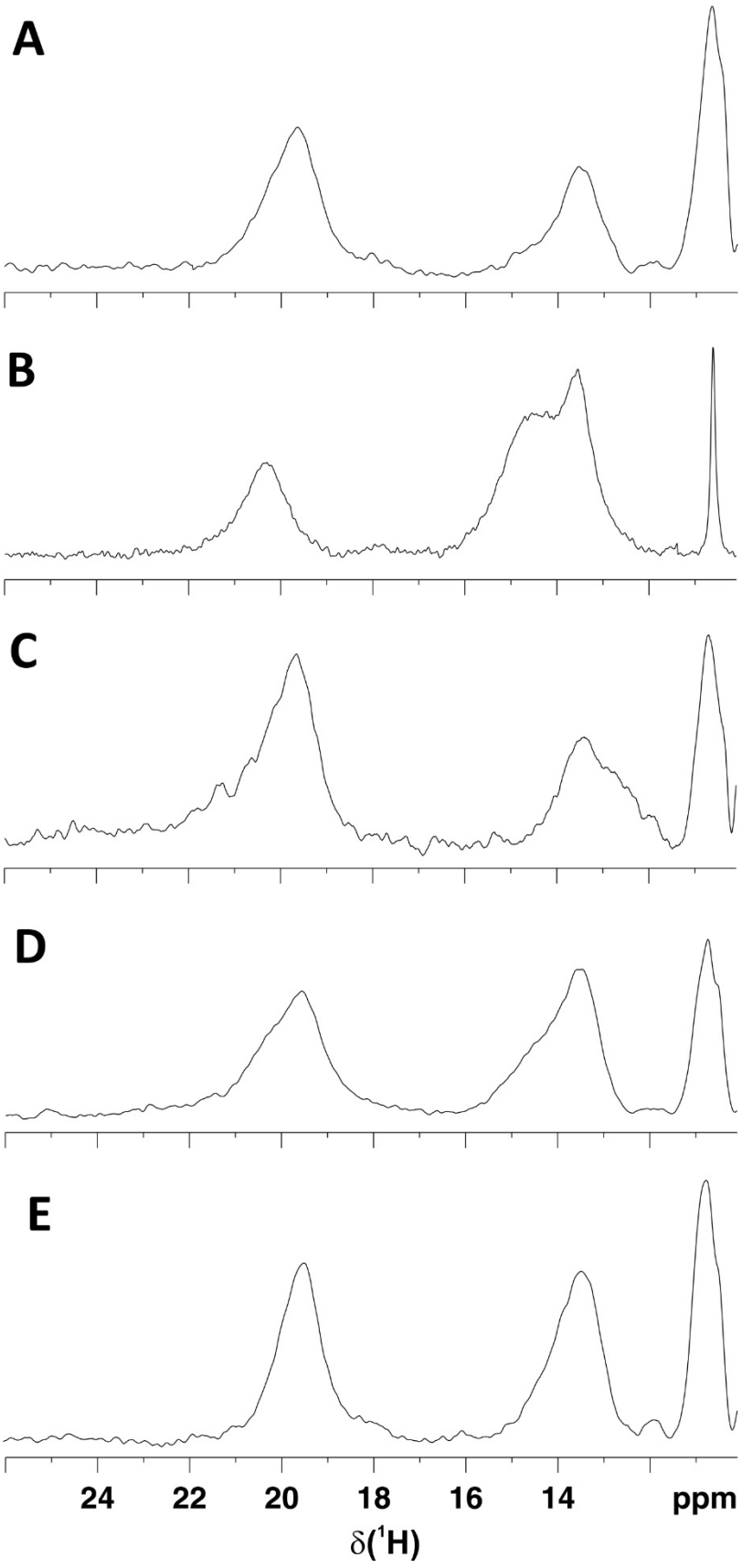

Figure 6

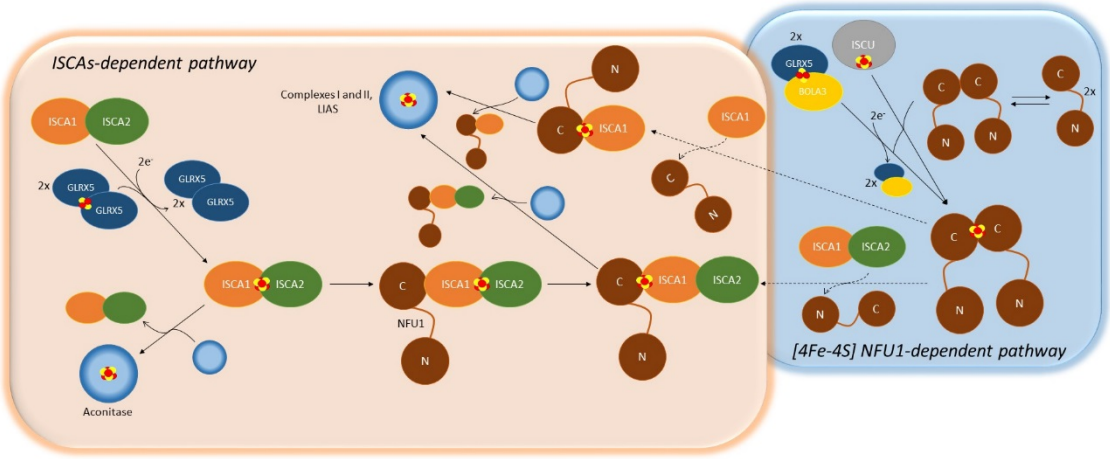

TABLE OF CONTENTS GRAPHICS

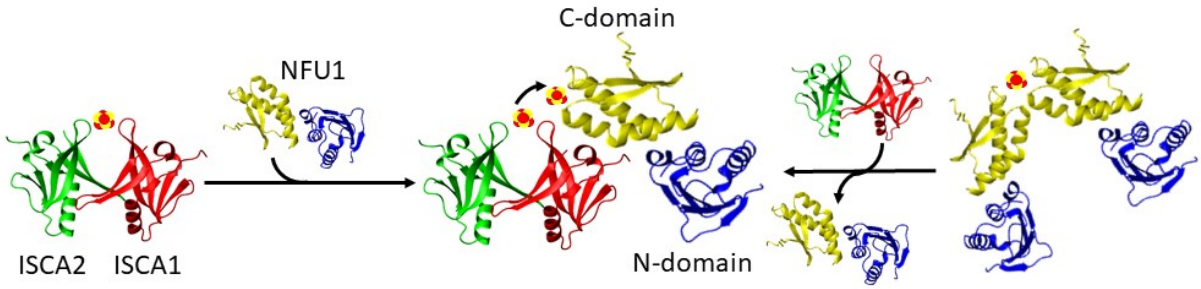

SUPPORTING INFORMATION

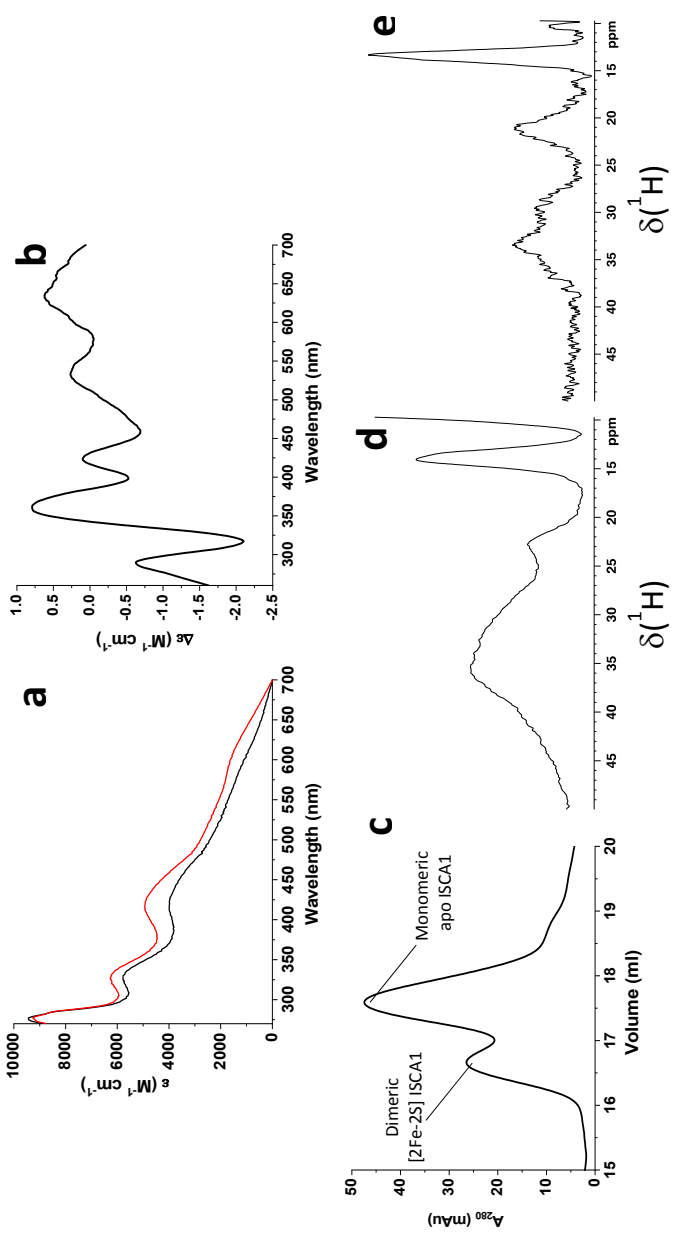

Figure S1. ISCA1 binds [2Fe-2S]$^{2+}$ cluster. UV-visible (**a**) and CD-visible (**b**) absorption spectra of anaerobically purified (black) and chemically reconstituted (red) ISCA1. (**c**) Analytical gel filtration of anaerobically purified ISCA1. Paramagnetic 1D ^{1}H NMR spectrum of anaerobically purified (**d**) and chemically reconstituted (**e**) ISCA1 at 298 K, respectively. The signal-to-noise ratio of the NMR spectrum is worse in (**e**) than in (**d**) because the protein largely precipitates during the acquisition time of the (**e**) NMR experiment. All data were collected in 50 mM phosphate buffer pH 7.0, 150 mM NaCl, 5 mM DTT.

Figure S2. Apo ISCA1 and apo ISCA2 form a heterodimeric complex. (**a**) Weighted-average chemical shift differences $\Delta\delta_{avg}$ (that is, $([(\delta_{HN})^2 + (\delta_N/5)^2]/2)^{1/2}$, where δ_{HN} and δ_N are chemical shift differences for ^{1}HN and ^{15}N, respectively) between apo ^{15}N ISCA2 alone and in a 1:1 mixture with apo ISCA1. The cyano bars represent proline residues. The blue bars represent residues whose NHs are not detected or too broad to be analyzed. The dotted horizontal line indicates the threshold to consider chemical shift changes as meaningful ($1\sigma\ \Delta\delta_{avg} > 0.04$ ppm). (**b**) Meaningful chemical shift changes for the backbone NHs of apo ^{15}N ISCA2 upon the addition of 1 equivalent of apo ISCA1 are mapped on a structural model of apo ISCA1 (ivory)-ISCA2 (gray) heterodimer, based on the available structure of homodimeric ISCA2. In red are the sidechains of the residues showing meaningful chemical shift changes. The protein stretches in blue and cyano represent residues whose NHs are not detected or too broad to be analyzed and proline residues, respectively.

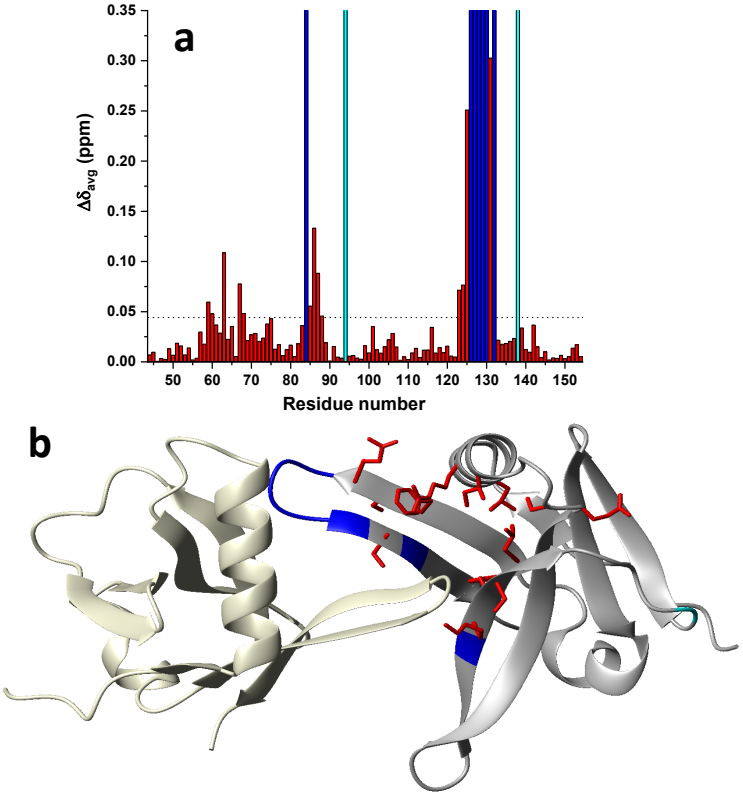

3

Figure S3. Apo ISCA1 interacts with the C-domain of apo NFU1 forming a heterodimeric complex. (**a**) Weighted-average chemical shift differences $\Delta\delta_{avg}$ (that is, $([(\delta_{HN})^2 + (\delta_N/5)^2]/2)^{1/2}$, where δ_{HN} and δ_N are chemical shift differences for ^{1}HN and ^{15}N, respectively) between apo ^{15}N NFU1 alone and in a 1:1 mixture with apo ISCA1. The cyano bars represent proline residues. The yellow bars represent residues whose NHs broaden beyond detection or are very broad upon additions of apo ISCA1. The dotted horizontal line indicates the threshold to consider chemical shift changes as meaningful (1σ $\Delta\delta_{avg}$ > 0.03 ppm). (**b**) Analytical gel filtration equipped with multiangle light scattering (SEC-MALS) of the 1:1 apo NFU1-apo ISCA1 mixture.

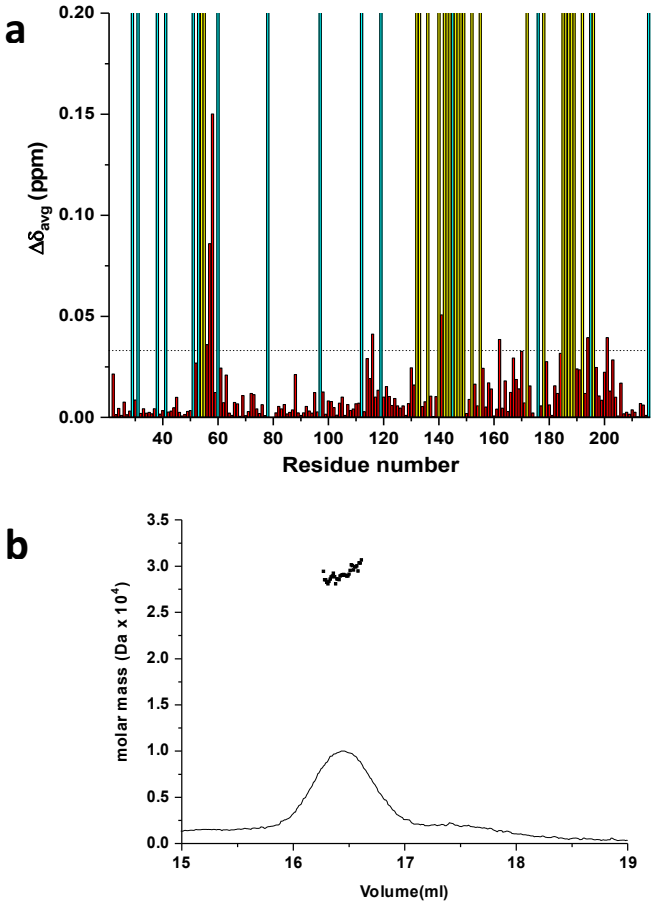

4

Figure S4. Apo ISCA1 promotes the formation of a ternary complex between apo ISCA2 and apo NFU1. (**a**) Overlay of the ^{1}H-^{15}N HSQC spectrum of a 1:1:1 mixture of ^{15}N apo ISCA2-apo ^{15}N NFU1-apo ISCA1 (black) with those of apo ^{15}N NFU1 (red) and of a 1:1 mixture of apo ^{15}N NFU1 and apo ISCA1 (green). (**b**) Overlay of the ^{1}H-^{15}N HSQC spectrum of a 1:1:1 mixture of apo ^{15}N ISCA2- apo ^{15}N NFU1-apo ISCA1 (black) with those of apo ^{15}N ISCA2 (cyano) and of a 1:1 mixture of apo ^{15}N ISCA2 and apo ISCA1 (red). In the inset, an overlay of a region of the previous ^{1}H-^{15}N HSQC spectra is shown. The arrow indicates a specific backbone NH signal of ISCA2 that monitors the formation of ISCA2 fully complexed with ISCA1 at the final 1:1:1 mixture. In green is the ^{1}H-^{15}N HSQC spectrum of the 1:1 mixture of apo ^{15}N NFU1 and apo ISCA1 to identify in the inset the NH signals of NFU1 complexed with ISCA1.

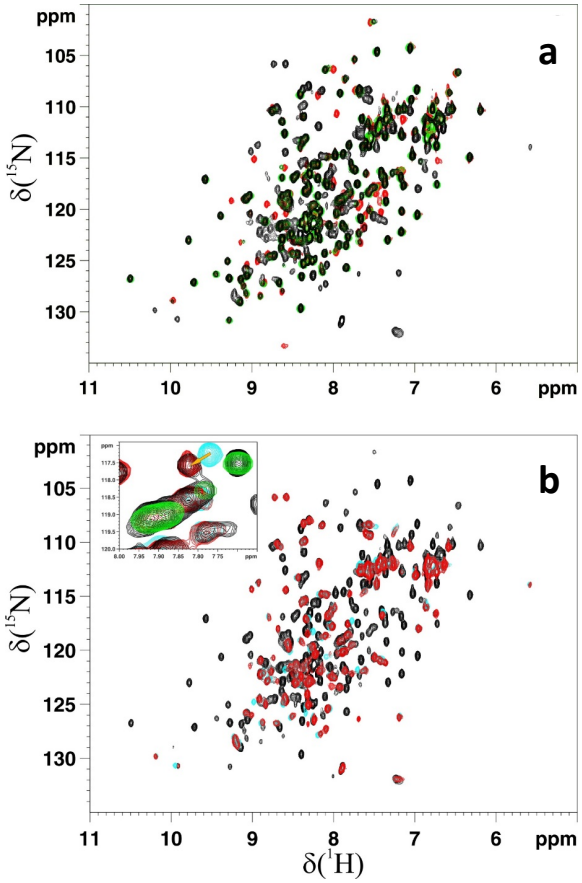

Figure S5. $[4Fe\text{-}4S]^{2+}$ ISCA1-ISCA2 interacts with apo NFU1 via its C-domain. (**a**) Overlay of the ^{1}H-^{15}N HSQC spectra of ^{15}N ISCA2-ISCA1 apo complex (red) and of a 1:1 mixture of $[4Fe\text{-}4S]^{2+}$ ^{15}N ISCA2-ISCA1 complex and C-domain of apo ^{15}N NFU1 (black). (**b**) Overlay of the ^{1}H-^{15}N HSQC spectra of C-domain of apo ^{15}N NFU1 (red) and a 1:1 mixture of $[4Fe\text{-}4S]^{2+}$ ^{15}N ISCA2-ISCA1 complex and C-domain of apo ^{15}N NFU1 (black). The residues of the C-domain of NFU1 whose backbone NH chemical shifts were affected (i.e. in terms of line broadening beyond detection effects and/or meaningful chemical shift changes) in the final mixture when compared to those of apo NFU1 are indicated in the ^{1}H-^{15}N HSQC spectrum and are shown in the inset on the structure of the C-domain of NFU1 (PDB ID 2M5O) with orange sidechains. The sidechains of proline residues are shown in gray.

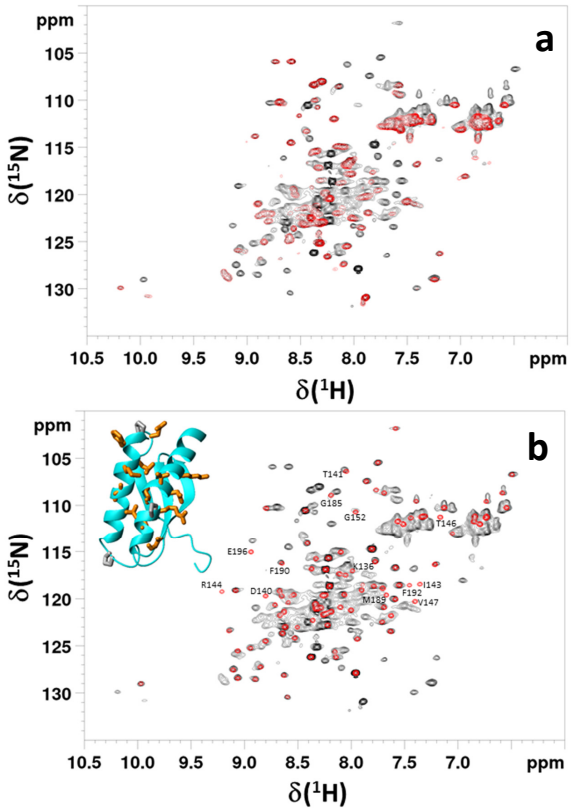

2.3 IMPACT OF CYS59TYR VARIANT ON THE ACTIVITY OF BOLA3 IN THE FE/S CLUSTER BIOGENESIS

Giovanni Saudino[1,2,], **Dafne Suraci**[1,2,*], Veronica Nasta[1,2], Simone Ciofi-Baffoni[1,2] , Lucia Banci[1,2]*

[1] Magnetic Resonance Center CERM, University of Florence, Via Luigi Sacconi 6, 50019, Sesto Fiorentino, Florence, Italy.

[2]Department of Chemistry, University of Florence, Via della Lastruccia 3, 50019 Sesto Fiorentino, Florence, Italy.

*These authors contributed equally to this work.

In progress

Introduction

Iron sulfur clusters (ISC) are essential cofactors found in all kingdoms of life, with highly conserved functional roles throughout evolution[1]. ISC biogenesis is an essential process for all living organisms, which developed complex and tightly controlled pathways for the cluster synthesis, transfer and insertion into the final targets[2–5]. The most ancient and common process for eukaryotic organisms occurs in mitochondria, which involves the de novo synthesis of a [2Fe-2S] cluster[6]. In human cells this process involves at least 17 proteins, constituting the mitochondrial ISC assembly machinery[2,7,8]. Alterations and mutations in any step of this ISC machinery determine pathological conditions, such as Multiple mitochondrial dysfunction syndromes (MMDS) that comprise a group of severe autosomal recessive diseases characterized by impaired respiration and lipoic acid metabolism[9–14]. Four different MMDS have been attributed to point mutations in proteins involved in iron-sulfur (Fe/S) biosynthesis; in particular, bi-allelic homozygous mutations in BOLA3 are associated with MMDS2[15–17]. This is a sever disorder of mitochondrial energy metabolism, characterized by hyperglycinaemia, encephalopathy, lactic acidosis, leukodystrophy and death in early childhood[18,19].

Recently Stutterd et. al. (2019), have reported a novel phenotype for MMDS2 associated with complete clinical recovery, due to the recessive Cys59Tyr BOLA3 mutation (C59Y hereafter)[20]. This mutation is present in heterozygosis and has a much milder phenotype patients with respect to other mutations previously reported [15,18,19,21]. The essential discrepancy is the different life span: while the phenotype at 18 months is comparable with that of other MMDs cases, the grown patient (after 8 years old) regained normal neurological and cognitive function until the complete health recovery[20].

BOLA3 is a protein participating in the Fe/S cluster biogenesis that we found to interact with GLRX5 bridging a [2Fe–2S] cluster[22,23]. Recently we proposed that this hetero-complex works as a [4Fe-4S] cluster assembler on NFU1, a late-acting factor of the ISC pathway[24].

Spectroscopies studies and a structural model showed that an oxidized, ferredoxin-like $[2Fe\text{-}2S]^{2+}$ cluster is present in the BOLA3-GLRX5 complex, and the four residues acting as ligands for the bridged [2Fe-2S] cluster are His 96 and Cys 59 on BOLA3, together with

Cys 67 on GLRX5 and a GSH molecule[23]. Thus, the Cys 59 to Tyr mutation affects a highly conserved residue, involved in the [2Fe-2S] cluster binding.
To clarify whether this atypical phenotype for MMDS2 may be a mutation-specific phenotype, detailed studies on this mutant are needed. We have therefore characterized it and its interaction with GLRX5, exploiting various spectroscopic techniques, such as NMR, CD and UV-vis spectroscopies.

Here we show that the mutation does not affect the overall protein stability and its folding, neither drastically influence the protein-protein interaction with apo GLRX5. The higher stability of the [2Fe-2S] cluster bridged by C59Y BOLA3 mutant and GLRX5 might explain a milder MMDS2 phenotype and a functional recovery.

Results

Structural impact of the single point mutation Cys59Tyr on BOLA3

The pathogenic mutation of Cys 59 to Tyr (C59Y) does not significantly affect the stability of BOLA3 protein. The ^{1}H ^{15}N HSQC spectrum of ^{15}N labelled C59Y BOLA3 mutant (^{15}N C59Y BOLA3 hereafter) showed a well folded, cluster-free protein, since all the cross-peaks show wide dispersions and sharp linewidths. The NMR spectrum experiences some differences with respect to those of the wild-type protein (wt BOLA3), but the overall protein fold is maintained (**Fig.1 A, B**). The NMR backbone chemical shift differences between wt and C59Y BOLA3 proteins indicated that the C59Y mutation in BOLA3 affects some residues of the loop containing the mutation and the close, highly conserved, His 96 (**Fig. 1 C**). On the contrary when Cys 59 is mutated into Ala the chemical shifts differences are limited only to the region around the mutation[23].
A structural model of C59Y BOLA3 was obtained by MODELLER (see Material and Methods for details) and the Tyr 59, that introduces a bulkier sidechain in the loop region between the β1 and β2 sheets, resulted to be spatially closer to the C-terminal His 96, thus determining the observed small chemical shifts differences also in this region (**Fig. 1 D**).

The wt and C59Y BOLA3 did not co-elute in the same fractions, but the analytical gel filtration showed different elution profiles, (two peaks at 18.7 and 18.4 ml respectively) (**Fig S1**). C59Y BOLA3 eluted as a molecule of smaller size and shape respect to the wt protein, though a cysteine residue (121 Da) was mutated into a bulky tyrosine (181 Da). This confirms a conformational change of the flexible loop induced by C59Y mutation that shortens the distance between Tyr 59 and His 96, respect to wt (**Fig. 1 D)**. Intermolecular aromatic π-π stacking interactions between the Tyr residue and the close His might explain the slightly lower hydrodynamic radius of C59Y BOLA3, respect to wt, as shown by size exclusion chromatography[25–27].

Collectively, these data showed that this point mutation does not affect the overall protein stability and its folding, but the tyrosine results to be closer, with respect to wt, to the C-terminal His 96, that are both Fe/S cluster ligand candidates.

C59Y BOLA3 variant preserves its interaction with apo GLRX5

To perform its function, BOLA3 interacts with GLRX5, both in the apo- and holo-forms, forming a hetero-dimeric complex composed by one GLRX5, one BOLA3 and one GSH molecules[22,23].

To test whether the C59Y mutation may affects protein-protein interactions, apo GLRX5 was stepwise added to ^{15}N C59Y BOLA3, or vice versa, in presence of 5 mM GSH and the interaction was followed through ^{1}H ^{15}N HSQC experiments. Spectral changes occurred and were completed at the 1:1 protein ratio. The NMR signals of the free and the bound proteins are in fast and intermediate exchange regimes relative to the NMR time scale (**Fig 2 A, B**).

Thus, the mutant forms with apo GLRX5 a 1:1 heterocomplex similarly to the wt protein, having a GSH molecule bound to it (**Fig 2 A, B**), as also shown by analytical gel filtration data (**Suppl 1)**.

Chemical shift perturbations and line broadening analyses were performed by overlaying the ^{1}H-^{15}N HSQC spectrum of the ^{15}N wt BOLA3 or ^{15}N C59Y BOLA3 with the one in presence of equimolar apo GLRX5, forming the 1:1 apo hetero-complex (**Fig 3 A,B left panels**). The spectral changes between the isolated BOLA3 proteins (wt and C59Y mutant) and their 1:1 complex with GLRX5 were mapped on the solution structure of wt BOLA3 (PDB 2NCL) and the structural model of C59Y BOLA3 (**Fig 3 A, B right panels**). Similar

interacting region are identified on BOLA3 proteins (wt and C59Y mutant), with the further involvement on C59Y BOLA3 of the loop region containing Tyr 59, which experiences line broadening (**Fig 3B right panel**). Indeed, in the ^{1}H ^{15}N HSQC spectrum of ^{15}N C59Y BOLA3 more NH cross-peaks broadened beyond detection upon partner addition than in wt, possibly due to conformational exchange.

The same kind of analysis was performed on apo GLRX5 side for its interaction with wt BOLA3 or C59Y BOLA3, by mapping the chemical shift changes on its solution structure (PDB 2WUL) (**Fig 4 A, B**). Similar interaction regions were also identified on the apo GLRX5 structure for the two BOLA3 proteins, but more line broadening beyond signal detection was observed in the interaction with the C59Y mutant than for the wt protein (**Fig 4 A, B**).

To discriminate if apo GLRX5 has a greater affinity for one of the two proteins, i.e. wt BOLA3 vs C59Y BOLA3, a 1:1 ^{15}N wt BOLA3-^{15}N C59Y BOLA3 mixture was titrated with unlabeled apo GLRX5. Apo GLRX5 is equally partitioned between the two proteins upon its addition, and once a 1:1:2 ^{15}N wt BOLA3-^{15}N C59Y BOLA3-GLRX5 ratio was reached, both apo 1:1 heterodimeric complexes were completely formed (data not showed). Collectively, we can conclude that similar heterocomplexes with same affinity are formed by wt or C59Y BOLA3 proteins with GLRX5, in absence of the bridged-[2Fe-2S] cluster.

Structural models of apo wt BOLA3-GLRX5 and apo C59Y BOLA3-GLRX5 complexes

The structural models of apo wt BOLA3-GLRX5 and apo C59Y BOLA3-GLRX5 complexes were calculated following the standard protocol of HADDOCK 2.2 docking program and using the experimental chemical shift mapping data, which define the interacting residues in the complex, and imposing a GSH molecule involved in the interaction (**Table S1 and S2**, and see Material and Methods for details). The calculated models have been clustered on the basis of common contacts following standard HADDOCK scoring approach[28].

Superimposition of the structures of isolated wt and C59Y BOLA3 with those in the two best structural models of the heterocomplex (**Suppl 2**), indicates that for wt BOLA3 there are no meaningful structural variations. On the contrary, structural rearrangement are observed in C59Y BOLA3 that involves the loop region between β1 and β2 sheet, where

Tyr 59 is present, and the one between α2 helix and β3 strand, where His 96 is located, so that the Tyr 59 and His 96 are pushed apart when the protein is complexed with GLRX5 (distance from 11.19 C59Y BOLA3 alone to 11.81 Å in complex with GLRX5).

Once the GLRX5 structure in the two heterocomplexes is superimposed it appears that C59Y BOLA3 has a different orientation respect to the wt protein and the wt BOLA3-GLRX5 complex is more compact than the C59Y BOLA3-GLRX5 one (**Fig 5 A and B**). Overall, the interaction with GLRX5 drives Tyr 59 of C59Y BOLA3 closer to the [2Fe-2S] cluster ligand Cys 67 on GLRX5, respect to wt (20.09 Å for Cys 59 in wt BOLA3, to 8.97 Å for Tyr 59 in C59Y BOLA3), this agrees with the line broadening that affects the C59Y loop region observed in the apo interaction.

The interaction surface in wt BOLA3-GLRX5 complex mainly involves the α2 helix, part of the β3 strand and the β1/ β2 loop region on wt BOLA3 and α3, α4 helices, and β4 strand on GLRX5, where key electrostatic (i.e. Lys 89, Arg 99, in wt BOLA3 with Asp 102 and Asp 123 in GLRX5 respectively) and hydrophobic (Val 78, Phe 101 in wt BOLA3 with Phe 118, and Ile 124 in GLRX5, respectively) contacts are present.

Looking at C59Y BOLA3-GLRX5 complex, the interaction involves the α2 helix, α2/ β3 and β1/ β2 loop regions on C59Y BOLA3 and α2, α3, α4 helices on GLRX5, that is similarly driven by electrostatic (i.e. Lys 93 in C59Y BOLA3 with Asp 102 in GLRX5 respectively) and hydrophobic (Met 62 in C59Y BOLA3 with Phe 69 in GLRX5, respectively) contacts.

This different orientation and closer contacts between the Fe/S cluster ligand candidates in C59Y BOLA3-GLRX5 complex could favor the holo heterocomplex formation.

C59Y BOLA3 mutant shares a more stable $[2Fe\text{-}2S]^{2+}$ cluster with GLRX5

Wt BOLA3 cannot bind an Fe/S cluster on its own, it binds a [2Fe-2S] one through Cys 59 and His 96 residues when complexed with GLRX5[23]. To address whether the Cys 59 to Tyr mutation affects this cluster coordination and so its function, resulting in a MMDS2 milder phenotype, we next investigated the interaction of holo GLRX5 with C59Y BOLA3 by chemically reconstituting a [2Fe-2S] cluster on equimolar GLRX5 and C59Y BOLA3 mixture.

^{1}H ^{15}N HSQC spectra were acquired for the co-reconstituted C59Y BOLA3-GLRX5 complex by ^{15}N labelling the two proteins alternatively, and they resulted superimposable

to that of the apo heterocomplexes with slightly, no meaningful spectral variation, either as chemical shift changes and or line-broadenings beyond signal detection (**Fig 6 A, B**). Moreover, they resulted similar to spectra obtained by mixing C59Y BOLA3 with [2Fe-2S] GLRX5 homodimer (data not shown).

UV-vis and CD spectroscopy showed that C59Y BOLA3-GLRX5 heterocomplex was still able to bind a [2Fe-2S] cluster (**Fig 7 A, B**). Indeed, the UV-vis spectrum maintained all the absorption bands of biological oxidized $[2Fe\text{-}2S]^{2+}$ centers between 300 and 600 nm, all attributable to S□Fe(III) charge-transfer (CT) transitions[29]**,** but showed several differences from those of the wt one (**Fig 7 A).**

The absorption bands at 394, 440 and 510 nm in the [2Fe-2S] wt BOLA3-GLRX5 heterocomplex were shifted to ~ 413, 460 and 520 nm in the [2Fe-2S] C59Y BOLA3-GLRX5, and the peak near 593 nm decreased (**Fig 7 A)**. Likely, once cysteine residues in [2Fe-2S] ferredoxin like proteins are replaced by serine or aspartate residues, that are all O-based ligands, similar absorption bands with slightly shifts are observed respect to wt proteins [30,31]. Moreover, the UV-vis spectrum of [2Fe-2S] C59Y BOLA3-GLRX5 is very similar to that of the Cys 59 to Ala mutant[23], that has been already characterized and proposed to be similar to human BOLA2-GLRX3 and yeast Fra2-Grx3 complexes, in which the coordination pattern is composed by one His from Fra2/BOLA2, one Cys from Grx3/GLRX3, one GSH molecule and an undefined N/O ligand[32–35].

The CD spectrum of the [2Fe-2S] C59Y BOLA3-GLRX5 heterocomplex also characteristically differed from that of the wt one in a negative versus positive ellipticity around 394 nm and 40% increase of the ~460 nm peak (**Fig 7 B**). These differences in the Uv-vis and CD spectra suggest different structures of the [2Fe-2S] chromophores and of their environment.

Paramagnetic ^{1}H NMR spectrum showed the presence of broad signals at 28 and 23 ppm and a sharper one at 13 ppm, all of them typical of an oxidized [2Fe-2S] cluster[36] (**Fig 7 C**). Like Ser coordination, ligation of a Tyr to an Fe/S cluster is extremely rare and previously detected in few systems[37–39], in particular in a Tyrosine-coordinated P-Cluster in *G. diazotrophicus* Nitrogenase the importance of O-based ligands has been demonstrated to stabilize the oxidative state[39].

Thus, the cluster stability of [2Fe-2S] C59Y BOLA3-GLRX5 vs [2Fe-2S] wt BOLA3-GLRX5 upon oxygen exposure was investigated by UV-vis spectroscopy, exposing the holo protein samples to air and collecting UV-vis spectra every 30 min for 12 h (**Fig 8 A, and B upper panels**). It resulted that the Fe/S cluster in [2Fe-2S] wt BOLA3-GLRX5 is

gradually degraded over a period of ~3 h, indicating that it is oxidatively labile (**Fig 8 A lower panel)**. On the contrary, the one in [2Fe-2S] C59Y BOLA3-GLRX5 degraded slowly over a period of ~12 h, suggesting a role for tyrosinate in stabilizing the Fe/S cluster (**Fig 8 B lower panel)**.

These data indicate that C59Y BOLA3 is still able to coordinate a $[2Fe\text{-}2S]^{2+}$ cluster together with GLRX5 and that Cys 59 to Tyr mutation stabilizes it upon oxygen exposure.

Material and methods

Protein expression and purification

Site-directed mutagenesis (QuickChange Site-directed Mutagenesis Kit, Agilent Technologies) was used to obtain recombinant BOLA3 mutants. Wild type pETG20A-BOLA3 expression vectors were modified by using primers containing the required single mutations (C59Y).

Escherichia coli BL21(DE3) -Gold (Agilent) competent cells were transformed with pETG20A plasmid containing N-terminal tagged C59Y BOLA3 (N-terminal TRX-6His-tag). Cells were cultivated at 37°C in 1 L of Luria-Bertani (LB) media adding ampicillin (100 μg/mL), until the OD600 reached 0.6-0.8. The protein expression was induced by adding 0.5 mM of isopropyl β-D-1-thiogalactopyranoside (IPTG) and shaking for 5 hours at 30°C, 200 rpm. The cells were harvested by centrifugation at 5000 rpm for 20 min (JA-10, Beckman Coulter). The cell pellet was resuspended in the binding buffer (50 mM phosphate buffer, 300 mM NaCl, 20 mM imidazole, pH 8.0), and the cells were lysed by sonication (30 minutes, 2'' ON and 9.9'' OFF). The N-terminal TRX-6His-tag C59Y BOLA3 protein was purified from the lysate using a HisTrap HP column (GE Healthcare). The TRX-6His-tag was cleaved by tobacco etch virus protease over-night at room temperature in 50 mM phosphate buffer, 300 mM NaCl, 20 mM imidazole, pH 8. His-trap chromatography column was equilibrated with the binding buffer and performed to separate the digested C59Y BOLA3 from TRX-6His-tag and from TRX-6His-tag C59Y BOLA3 undigested. The final yield of apo C59Y BOLA3 was ~40 mg per liter of LB culture. Recovered C59Y BOLA3 was pure enough to be used for spectroscopic and biochemical studies. All the expression and purification steps were performed in aerobic conditions. ^{15}N-labeled C59Y BOLA3 was expressed in Escherichia coli grown in M9 minimal medium supplemented with $^{15}NH_4Cl$ and purified as indicated for E. coli in

LB medium. The expression and purification of human GLRX5 in its apo monomeric forms and in its homo-dimeric [2Fe-2S]$^{2+}$ cluster-bound forms were obtained as previously described[40].

BOLA3 C59Y and GLRX5 hetero-dimer with [2Fe-2S]$^{2+}$ cluster bound were chemically Fe-S cluster reconstituted in anaerobic conditions in 50 mM Tris-HCl, 100 mM NaCl, 5 mM DTT buffer at pH 8.0 with four-fold of $FeCl_3$ and Na_2S for 16 h at room temperature. Fe-S cluster chemical reconstitution was performed with complex concentrations of ~40-80 μM. Anaerobic conditions were obtained performing the chemical reconstitution in glovebox with less than 2 ppm of oxygen and by using all buffers degassed.

UV-visible and CD spectroscopy

UV/vis and CD absorption spectra were acquired to follow cluster transfer and assembly on the heterocomplex. All the experiments were performed under anaerobic condition by degassing the buffers and using gas-tight UV-vis cuvette. UV-visible and CD spectra were purchased at room temperature in 50 mM phosphate buffer, 5 mM DTT, 5 mM GSH, 150 mM NaCl, pH 7.0 on a Cary 50 Eclipse spectrophotometer and JASCO J-810 spectropolarimeter, respectively. Each experiment was successfully repeated three times.

SEC-MALS for protein-protein interaction studies

Analytical gel-filtration experiments were conducted using a Superdex^{TM} 200 Increase 10/300 GL column attached to a DAWN HELEOS system with a continuous flow rate of 0.6 mL/min. The column was equilibrated with phosphate buffer 50 mM, 150 mm NaCl, 5 mM DTT and pH 7.0. Degassed buffers were used for the experiments under anaerobic conditions.

NMR spectroscopy

NMR spectra were acquired at 298 K in 50 mM phosphate buffer pH 7, 150 mM NaCl and 10% (v/v) D_2O. All NMR spectra were recorded on Bruker AVANCE 700 and 950 MHz, processed using the standard Bruker software (Topspin) and analyzed with CARA program.

1D ^1H paramagnetic NMR experiments of the chemically reconstituted [2Fe-2S] GLRX5-C59Y BOLA3 were performed at 400 MHz with a ^1H optimized 5 mm probe at temperatures ranging from 280 K and 307 K, with protein samples in 50 mM phosphate

buffer pH 7.0, 5 mM DTT and 150 mM NaCl, 99% (v/v) D_2O . These spectra were acquired by means of the super-WEFT sequence with a recycle time of 50 ms. The protein concentration was 0.5-1 mM and the spectra were acquired adding different reducing compounds, i.e. DTT and GSH. To monitor formation of apo GLRX5- C59Y BOLA3 hetero-complex, ^{15}N labeled C59Y BOLA3 or apo GLRX5 were titrated with increasing amounts of unlabeled partner, until was reached the 1:1 ratio. Chemical shift changes followed by ^{1}H ^{15}N HSQC NMR spectra were compared with chemical shift of labelled protein in the free state. These NMR data were also compared with the ^{1}H ^{15}N HSQC spectra of wild type ^{15}N wt BOLA3-GLRX5 and ^{15}N GLRX5-wt BOLA3.

Molecular docking

Structural models of the apo wt BOLA3-GLRX5 and apo C59Y BOLA3 mutant-GLRX5 complexes were calculated using the protein-protein docking program HADDOCK 2.2 (high ambiguity driven protein-protein docking) by following the standard HADDOCK procedure[41–43]. Specifically, the structural models of the apo heterodimers were built from the structures of individual proteins (GLRX5 with GSH bound PDB entry 2WUL and BOLA3 PDB entry 2NCL). The structure of the C59Y BOLA3 was obtained with Modeller 9.20 [44] (https://salilab.org/modeller/) using as template the existing NMR solution structure of BOLA3. The NMR chemical shift mapping data, already available for the wt heterocomplex[22] and here performed for the C59Y mutant heterocomplex, were used to define ambiguous interaction restraints for the residues at the interface. The “active” residues were defined as those having a chemical shift perturbation upon complex formation larger than the average of Δavg(HN) plus 1σ (Δavg(HN) = (((ΔH)2 + (ΔN/5)2)/2)1/2, where ΔH and ΔN are chemical shift differences for backbone amide ^{1}H and ^{15}N nuclei, respectively) and with a solvent accessibility higher than 50%; the “passive” residues were defined as those being surface neighbors to the active residues and with a solvent accessibility higher than 50%.

Center of mass restraints between the various molecules to enforce contact between them, that are only active during it0 and it1, have been used and automatically defined in HADDOCK. The center of mass restraint is defined between each molecule as an ambiguous distance restraint with center averaging between all CA of one molecule and all CA of the other molecule.

The ensemble of 200 solutions was analyzed and clustered based on the pair-wise RMSD matrix calculated over the backbone atoms of the interface residues of GLRX5 after fitting on the interface residues of wt BOLA3 or C59Y BOLA3.

This way of calculating RMSD values in HADDOCK results in high values that emphasize the differences between docking solutions. For this reason, clustering was performed using a 7.5 Å cut-off. The water-refined models were clustered based on the default fraction of common contacts, FCC=0.75, with the minimum number of elements in a cluster of 4. The clusters were ranked based on the averaged HADDOCK score of their top four members and plotted against RMSD from lowest energy structure. NACCESS is the program used to calculate the atomic and residue accessibilities from a PDB format file. The models were rendered with Chimera program.

References:

1. Andreini, C., Banci, L. & Rosato, A. Exploiting Bacterial Operons To Illuminate Human Iron–Sulfur Proteins. *J. Proteome Res.* **15**, 1308–1322 (2016).
2. Ciofi-Baffoni, S., Nasta, V. & Banci, L. Protein networks in the maturation of human iron-sulfur proteins. *Met. Integr. Biometal Sci.* **10**, 49–72 (2018).
3. Przybyla-Toscano, J., Roland, M., Gaymard, F., Couturier, J. & Rouhier, N. Roles and maturation of iron-sulfur proteins in plastids. *J. Biol. Inorg. Chem. JBIC Publ. Soc. Biol. Inorg. Chem.* **23**, 545–566 (2018).
4. Lill, R. From the discovery to molecular understanding of cellular iron-sulfur protein biogenesis. *Biol. Chem.* **401**, 855–876 (2020).
5. Baussier, C. *et al.* Making iron-sulfur cluster: structure, regulation and evolution of the bacterial ISC system. *Adv. Microb. Physiol.* **76**, 1–39 (2020).
6. Lill, R. & Mühlenhoff, U. Iron-sulfur-protein biogenesis in eukaryotes. *Trends Biochem. Sci.* **30**, 133–141 (2005).
7. Maio, N. & Rouault, T. A. Outlining the Complex Pathway of Mammalian Fe-S Cluster Biogenesis. *Trends Biochem. Sci.* **45**, 411–426 (2020).
8. Lill, R. & Freibert, S.-A. Mechanisms of Mitochondrial Iron-Sulfur Protein Biogenesis. *Annu. Rev. Biochem.* **89**, 471–499 (2020).
9. Shukla, A., Narayanan, D. L., Kaur, P. & Girisha, K. M. ISCA1-Related Multiple Mitochondrial Dysfunctions Syndrome. in *GeneReviews®* (eds. Adam, M. P. et al.) (University of Washington, Seattle, 1993).
10. Rouault, T. A. Biogenesis of iron-sulfur clusters in mammalian cells: new insights and relevance to human disease. *Dis. Model. Mech.* **5**, 155–164 (2012).

11. Eidi, M. & Garshasbi, M. A novel ISCA2 variant responsible for an early-onset neurodegenerative mitochondrial disorder: a case report of multiple mitochondrial dysfunctions syndrome 4. *BMC Neurol.* **19**, 153 (2019).
12. Uzunhan, T. A., Çakar, N. E., Seyhan, S. & Aydin, K. A genetic mimic of cerebral palsy: Homozygous NFU1 mutation with marked intrafamilial phenotypic variation. *Brain Dev.* (2020) doi:10.1016/j.braindev.2020.07.009.
13. Meldau, S. *et al.* Pitfalls of relying on genetic testing only to diagnose inherited metabolic disorders in non-western populations - 5 cases of pyruvate dehydrogenase deficiency from South Africa. *Mol. Genet. Metab. Rep.* **24**, 100629 (2020).
14. Hartman, T. G. *et al.* Expanding the genotype-phenotype spectrum of ISCA2-related multiple mitochondrial dysfunction syndrome-cavitating leukoencephalopathy and prolonged survival. *Neurogenetics* (2020) doi:10.1007/s10048-020-00611-8.
15. Cameron, J. M. *et al.* Mutations in Iron-Sulfur Cluster Scaffold Genes NFU1 and BOLA3 Cause a Fatal Deficiency of Multiple Respiratory Chain and 2-Oxoacid Dehydrogenase Enzymes. *Am. J. Hum. Genet.* **89**, 486–495 (2011).
16. Baker, P. R. *et al.* Variant non ketotic hyperglycinemia is caused by mutations in LIAS, BOLA3 and the novel gene GLRX5. *Brain J. Neurol.* **137**, 366–379 (2014).
17. Nikam, R. M., Gripp, K. W., Choudhary, A. K. & Kandula, V. Imaging phenotype of multiple mitochondrial dysfunction syndrome 2, a rare BOLA3-associated leukodystrophy. *Am. J. Med. Genet. A.* **176**, 2787–2790 (2018).
18. Haack, T. B. *et al.* Homozygous missense mutation in BOLA3 causes multiple mitochondrial dysfunctions syndrome in two siblings. *J. Inherit. Metab. Dis.* **36**, 55–62 (2013).
19. Yu, Q. *et al.* BOLA (BolA Family Member 3) Deficiency Controls Endothelial Metabolism and Glycine Homeostasis in Pulmonary Hypertension. *Circulation* **139**, 2238–2255 (2019).
20. Stutterd, C. A. *et al.* Severe Leukoencephalopathy with Clinical Recovery Caused by Recessive BOLA3 Mutations. *JIMD Rep.* **43**, 63–70 (2019).
21. Imai-Okazaki, A. *et al.* Cardiomyopathy in children with mitochondrial disease: Prognosis and genetic background. *Int. J. Cardiol.* **279**, 115–121 (2019).
22. Uzarska, M. A. *et al.* Mitochondrial Bol1 and Bol3 function as assembly factors for specific iron-sulfur proteins. *eLife* **5**, (2016).
23. Nasta, V., Giachetti, A., Ciofi-Baffoni, S. & Banci, L. Structural insights into the molecular function of human [2Fe-2S] BOLA1-GRX5 and [2Fe-2S] BOLA3-GRX5 complexes. *Biochim. Biophys. Acta Gen. Subj.* **1861**, 2119–2131 (2017).
24. Nasta, V., Suraci, D., Gourdoupis, S., Ciofi-Baffoni, S. & Banci, L. A pathway for assembling [4Fe-4S]2+ clusters in mitochondrial iron-sulfur protein biogenesis. *FEBS J.* **287**, 2312–2327 (2020).
25. Cockroft, S. L., Hunter, C. A., Lawson, K. R., Perkins, J. & Urch, C. J. Electrostatic Control of Aromatic Stacking Interactions. *J. Am. Chem. Soc.* **127**, 8594–8595 (2005).
26. Boehr, D. D., Farley, A. R., Wright, G. D. & Cox, J. R. Analysis of the π-π Stacking Interactions between the Aminoglycoside Antibiotic Kinase APH(3')-IIIa and Its Nucleotide Ligands. *Chem. Biol.* **9**, 1209–1217 (2002).
27. Liao, S.-M., Du, Q.-S., Meng, J.-Z., Pang, Z.-W. & Huang, R.-B. The multiple roles of histidine in protein interactions. *Chem. Cent. J.* **7**, 44 (2013).
28. Rodrigues, J. P. G. L. M. *et al.* Clustering biomolecular complexes by residue contacts similarity. *Proteins Struct. Funct. Bioinforma.* **80**, 1810–1817 (2012).

29. Noodleman, L. & Baerends, E. J. Electronic structure, magnetic properties, ESR, and optical spectra for 2-iron ferredoxin models by LCAO-X.alpha. valence bond theory. *J. Am. Chem. Soc.* **106**, 2316–2327 (1984).
30. Cheng, H., Xia, B., Reed, G. H. & Markley, J. L. Optical, EPR, and 1H NMR Spectroscopy of Serine-Ligated [2Fe-2S] Ferredoxins Produced by Site-Directed Mutagenesis of Cysteine Residues in Recombinant Anabaena 7120 Vegetative Ferredoxin. *Biochemistry* **33**, 3155–3164 (1994).
31. Feinberg, B. A., Lo, X., Iwamoto, T. & Tomich, J. M. Synthetic mutants of Clostridium pasteurianum ferredoxin: open iron sites and testing carboxylate coordination. *Protein Eng. Des. Sel.* **10**, 69–75 (1997).
32. Banci, L., Camponeschi, F., Ciofi-Baffoni, S. & Muzzioli, R. Elucidating the Molecular Function of Human BOLA2 in GRX3-Dependent Anamorsin Maturation Pathway. *J. Am. Chem. Soc.* **137**, 16133–16143 (2015).
33. Li, H., Mapolelo, D. T., Randeniya, S., Johnson, M. K. & Outten, C. E. Human Glutaredoxin 3 Forms [2Fe-2S]-Bridged Complexes with Human BolA2. *Biochemistry* **51**, 1687–1696 (2012).
34. The yeast iron regulatory proteins Grx3/4 and Fra2 form heterodimeric complexes containing a [2Fe-2S] cluster with cysteinyl and histidyl ligation. - Abstract - Europe PMC. https://europepmc.org/article/med/19715344.
35. Histidine 103 in Fra2 is an iron-sulfur cluster ligand in the [2Fe-2S] Fra2-Grx3 complex and is required for in vivo iron signaling in yeast. - Abstract - Europe PMC. https://europepmc.org/article/med/20978135.
36. Banci, L., Camponeschi, F., Ciofi-Baffoni, S. & Piccioli, M. The NMR contribution to protein–protein networking in Fe–S protein maturation. *JBIC J. Biol. Inorg. Chem.* **23**, 665–685 (2018).
37. Belmonte, L. & Mansy, S. S. Patterns of Ligands Coordinated to Metallocofactors Extracted from the Protein Data Bank. *J. Chem. Inf. Model.* **57**, 3162–3171 (2017).
38. Nicolet, Y., Rohac, R., Martin, L. & Fontecilla-Camps, J. C. X-ray snapshots of possible intermediates in the time course of synthesis and degradation of protein-bound Fe4S4 clusters. *Proc. Natl. Acad. Sci. U. S. A.* **110**, 7188–7192 (2013).
39. Owens, C. P., Katz, F. E. H., Carter, C. H., Oswald, V. F. & Tezcan, F. A. Tyrosine-Coordinated P-Cluster in G. diazotrophicus Nitrogenase: Evidence for the Importance of O-Based Ligands in Conformationally Gated Electron Transfer. *J. Am. Chem. Soc.* **138**, 10124–10127 (2016).
40. Banci, L. *et al.* [2Fe-2S] cluster transfer in iron–sulfur protein biogenesis. *Proc. Natl. Acad. Sci.* **111**, 6203–6208 (2014).
41. Dominguez, C., Boelens, R. & Bonvin, A. M. J. J. HADDOCK: A Protein−Protein Docking Approach Based on Biochemical or Biophysical Information. *J. Am. Chem. Soc.* **125**, 1731–1737 (2003).
42. The HADDOCK2.2 Web Server: User-Friendly Integrative Modeling of Biomolecular Complexes - ScienceDirect. https://www.sciencedirect.com/science/article/pii/S0022283615005379?via%3Dihub.
43. HADDOCK: A Protein−Protein Docking Approach Based on Biochemical or Biophysical Information | Journal of the American Chemical Society. https://pubs.acs.org/doi/10.1021/ja026939x.
44. Sali, A. & Blundell, T. L. Comparative protein modelling by satisfaction of spatial restraints. *J. Mol. Biol.* **234**, 779–815 (1993).

Figures

Figure 1. C59Y mutation effect on BOLA3 and chemical shift differences between the wild type and the C59Y BOLA3 mutant A) Overlay of the $^{1}H^{15}N$ HSQC spectra of the wild type (wt) (blue) and the C59Y BOLA3 mutant (red), measured at 298K, 950 MHz. **B**) Insets of the above-mentioned overlayed spectra, G60 and C59, M62 NH cross-peaks in wt and C59Y BOLA3 spectra, in blue and red respectively. **C)** Plot of the normalized chemical shift differences between the wt and the C59Y BOLA3 mutant. Backbone weighted average chemical shift differences was calculated by the equation, $\mathbf{\Delta}avg(HN)= (((\mathbf{\Delta}H)^2 + (\mathbf{\Delta}N/5)^2)/2)^{1/2})$. The indicated threshold 0.061 values (obtained by averaging $\mathbf{\Delta}avg(HN)$ values plus 1 σ) were used to define meaningful chemical shift differences. **D**) Structural distances between C59 or A59 or Y59 and the invariant H96, 11.60 Å in wt, 13.12 Å in C59A mutant and 11.19 Å in C59Y mutant, respectively. C59 is depicted in yellow stick on the solution structure of BOLA3 (PDB 2NCL), A59 and C59 are depicted in red together with the residues affected by the mutation, on the structural models obtained with Modeller 9.20. The distances were calculated in Chimera.

Figure 2. Apo GLRX5- C59Y BOLA3 protein-protein interaction. A) Overlay of the $^{1}H^{15}N$ HSQC spectra of ^{15}N C59Y BOLA3 (red), 1:1 ^{15}N C59Y BOLA3-apo GLRX5 (blue) both in presence of 5 mM GSH. **B**) Overlay of the $^{1}H^{15}N$ HSQC spectra of ^{15}N apo GLRX5 (red), 1:1 ^{15}N apo GLRX5- C59Y BOLA3 (blue) both in presence of 5 mM GSH. The spectra were acquired at 950 MHz at 298K in buffer Pi 50 mM, pH 7, DTT 5 mM, NaCl 150 mM, GSH 5 mM.

Figure 3. Comparison between wt ^{15}N wt BOLA3-GLRX5 and ^{15}N C59Y BOLA3-GLRX5 complexes formation. A) Backbone chemical shift changes of ^{15}N wt BOLA3 upon complex formation with apo GLRX5 in Pi 50 mM, pH 7, 5 mM DTT, 5 mM GSH and 150 mM NaCl (**left panel**). Meaningful chemical shift differences were mapped on the solution structure of wt BOLA3 (PDB 2NCL) (**right panel**). **B**) **B**ackbone chemical shift changes of ^{15}N C59Y BOLA3 upon complex formation with apo GLRX5 (**left panel**). Meaningful chemical shift differences were mapped on the structural model of C59Y BOLA3 (**right panel**).
In green proline residues or unassigned NHs. Backbone weighted average chemical shift differences was calculated by the equation, $\mathbf{\Delta}avg(HN)= (((\mathbf{\Delta}H)^2 + (\mathbf{\Delta}N/5)^2)/2)^{1/2})$. The indicated threshold 0.046 in wt-BOLA3 and 0.06 in C59Y BOLA3 values (obtained by averaging $\mathbf{\Delta}avg(HN)$ values plus 1σ) were used to define meaningful chemical shift differences. In the mapping the NHs broaden beyond detection are depicted as red spheres, in yellow NHs having chemical shifts above the thresholds. C59, Y59 and H96 are in green sticks.

Figure 4. Comparison between wt ^{15}N apo GLRX5-wt BOLA3 and ^{15}N apo GLRX5-C59Y BOLA3 complexes formation. A) Backbone chemical shift changes of ^{15}N apo

GLRX5 upon complex formation with wt BOLA3 in Pi 50 mM, pH 7, 5 mM DTT, 5 mM GSH and 150 mM NaCl (**left panel**). Meaningful chemical shift differences were mapped on the solution structure of apo GLRX5 (PDB 2WUL) (**right panel**). **B**) Backbone chemical shift changes of ^{15}N apo GLRX5 upon complex formation with C59Y BOLA3 (**left panel**). Meaningful chemical shift differences were mapped on the solution structure of apo GLRX5 (**right panel**). In green proline residues or unassigned NHs. Backbone weighted average chemical shift differences was calculated by the equation, $\mathbf{\Delta}$avg(HN)= $(((\mathbf{\Delta}H)^2 + (\mathbf{\Delta}N/5)^2)/2)^{1/2}$). The indicated threshold 0.068 for the interaction with wt-BOLA3 and 0.061 for the one with C59Y BOLA3 values (obtained by averaging $\mathbf{\Delta}$avg(HN) values plus 1σ) were used to define meaningful chemical shift differences. In the mapping the NHs broaden beyond detection are depicted as red spheres, in yellow NHs having chemical shifts above the thresholds. C67 is represented as green stick and GSH as grey spheres.

Figure 5. Haddock structural models of wt BOLA3-GLRX5 and C59Y BOLA3 mutant-GLRX5
Structural models of apo wt BOLA3-GLRX5 (**A**) and C59Y BOLA3-GLRX5 (**B**) hetero-complexes are shown and orientated once GLRX5 structure is superimposed in the two heterocomplexes. Zoom in of Cys 69/ Tyr 59 region after the superimposition of the proteins alone (orange) with the one in complex with GLRX5 to identify structural rearrangement. GLRX5, wt BOLA3 and C59Y BOLA3 mutant structures in the structural model are in red, cyano and green, respectively. The invariant C-terminal His 96, Cys 59 in BOLA3, and Tyr 59 in C59Y BOLA3 mutant, Cys 67 in GLRX5 residues and GSH are shown.

Figure 6 [2Fe-2S] C59Y BOLA3-GLRX5 formation monitored by NMR. (**A**) Overlay of the ^{1}H ^{15}N HSQC spectra of apo ^{15}N C59Y BOLA3-GLRX5 (blue) and ^{15}N [2Fe-2S] C59Y BOLA3-GLRX5 (red). **B**) the ^{1}H ^{15}N HSQC spectra of apo ^{15}N GLRX5-C59Y BOLA3 (blue) and ^{15}N [2Fe-2S] GLRX5-C59Y BOLA3 (red).

Figure 7 Effect of C59Y mutation on cluster binding monitored by UV/vis, CD and paramagnetic NMR spectroscopy. UV-vis (**A**) and CD (**B**) spectra of chemically reconstituted [2Fe-2S] C59Y BOLA3 C59Y-GLRX5 (black) compared with the [2Fe-2S] wt BOLA3-GLRX5 (green), acquired in the same buffer conditions: Pi 50 mM, NaCl 150 mM, pH 7, DTT 5 mM, GSH 5 mM.
(**C**) Paramagnetic ^{1}H NMR spectra of chemically reconstituted [2Fe-2S] C59Y BOLA3-GLRX5 recorded at 400MHz, 298K in Pi 50mM. NaCl 150 mM. pH 7. DTT 5 mM. GSH 5 mM.

Figure 8 Cluster stability of [2Fe-2S] C59Y BOLA3-GLRX5 vs [2Fe-2S] wt BOLA3-GLRX5 upon oxygen exposure. Cluster oxidation of wt BOLA3-GLRX5 (A) and C59Y BOLA3-GLRX5 (B) was performed at room temperature under aerobic conditions, followed by UV-vis absorption spectroscopy for 12 h of oxygen-exposure. The proteins were in sodium phosphate buffer 50 mM and NaCl 150 mM at pH 7.0. The exponential decrease in absorbance was then fit by Origin Software with a mono exponential function to obtain the rate constant of decay.

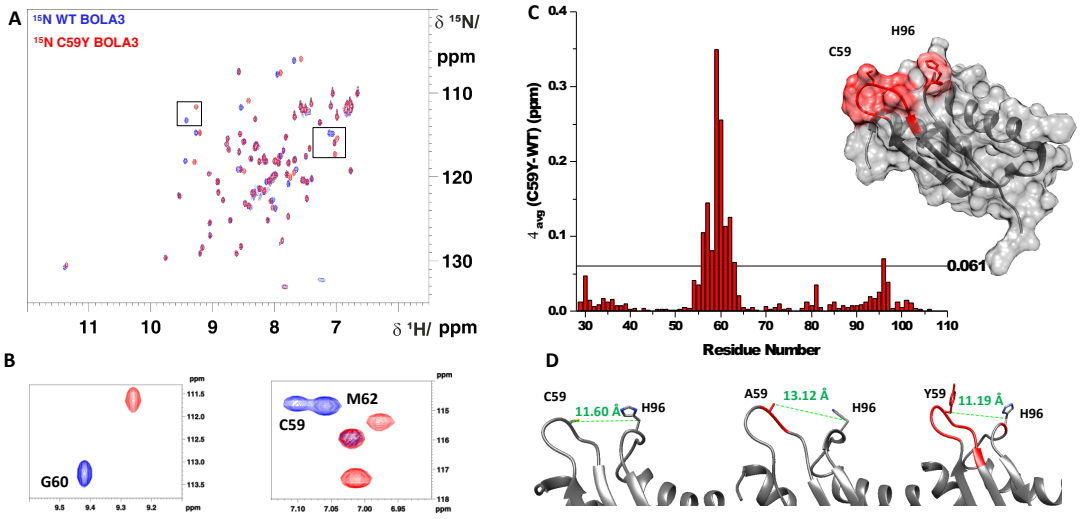
A
15N WT BOLA3
15N C59Y BOLA3
δ 15N/ ppm
110
120
130
11
10
9
8
7
δ 1H/ ppm
B
G60
M62
C59
C
4 avg (C59Y-WT) (ppm)
0.4
0.3
0.2
0.1
0.0
0.061
30
40
50
60
70
80
90
100
110
Residue Number
H96
C59
D
C59
11.60 Å
H96
A59
13.12 Å
H96
Y59
11.19 Å
H96

Fig 1

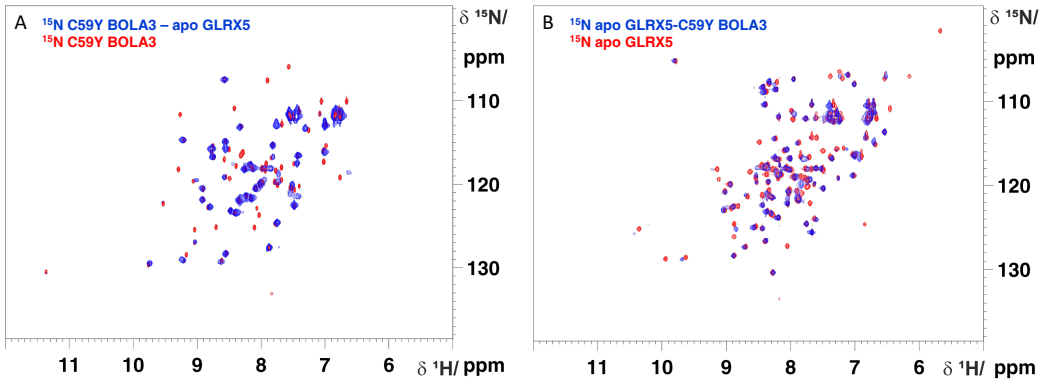
A
15N C59Y BOLA3 – apo GLRX5
15N C59Y BOLA3
δ 15N/ ppm
110
120
130
11
10
9
8
7
6
δ 1H/ ppm
B
15N apo GLRX5-C59Y BOLA3
15N apo GLRX5
δ 15N/ ppm
110
120
130
11
10
9
8
7
6
δ 1H/ ppm

Fig 2

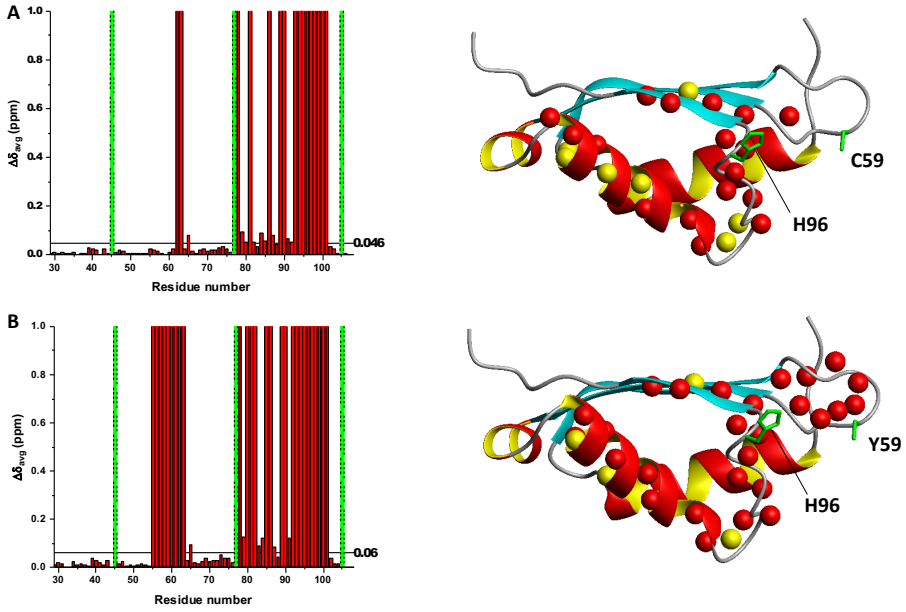
A
B
Residue number
0.046
0.06
C59
H96
Y59
H96

Fig 3

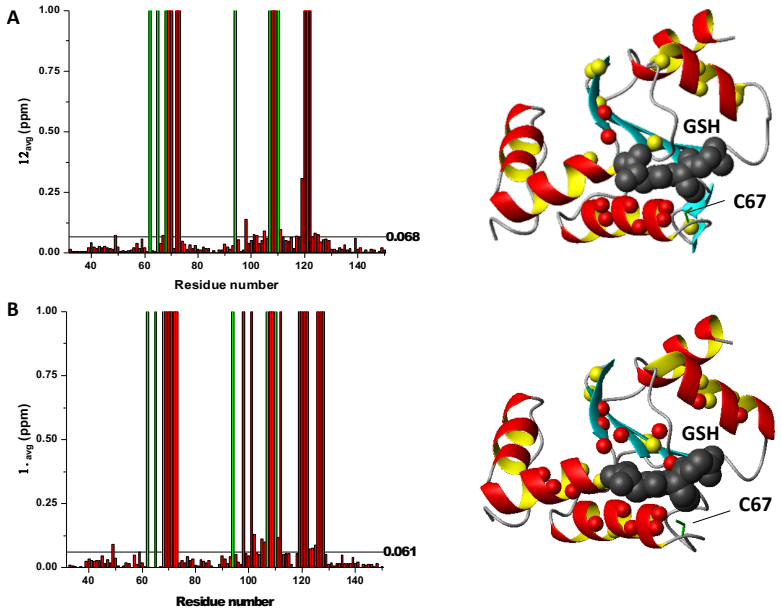
A
B
Residue number
0.068
0.061
GSH
C67
GSH
C67

Fig 4

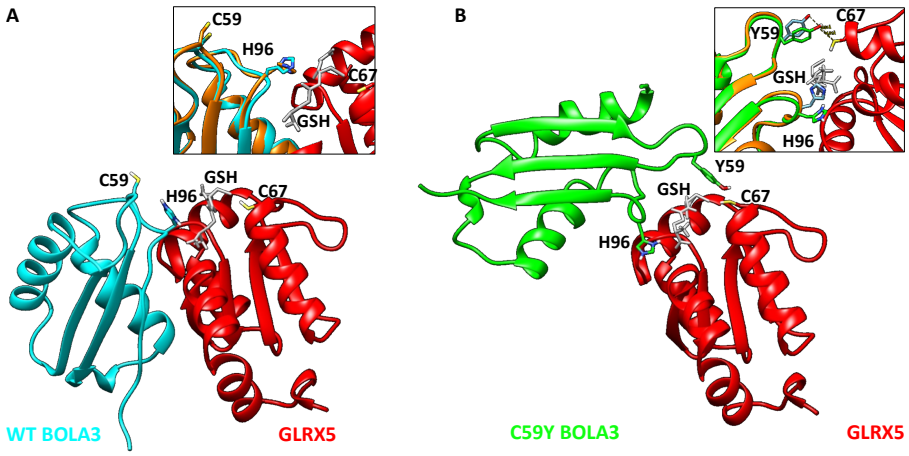
A
C59
H96
C67
GSH
C59
GSH
H96
C67
WT BOLA3
GLRX5
B
C67
Y59
GSH
H96
Y59
GSH
C67
H96
C59Y BOLA3
GLRX5

Fig 5

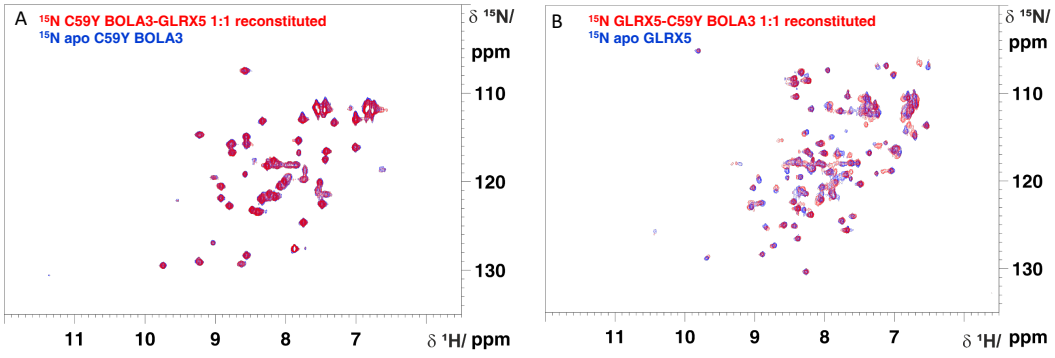
A
15N C59Y BOLA3-GLRX5 1:1 reconstituted
15N apo C59Y BOLA3
δ 15N/ ppm
110
120
130
11
10
9
8
7
δ 1H/ ppm
B
15N GLRX5-C59Y BOLA3 1:1 reconstituted
15N apo GLRX5
δ 15N/ ppm
110
120
130
11
10
9
8
7
δ 1H/ ppm

Fig 6

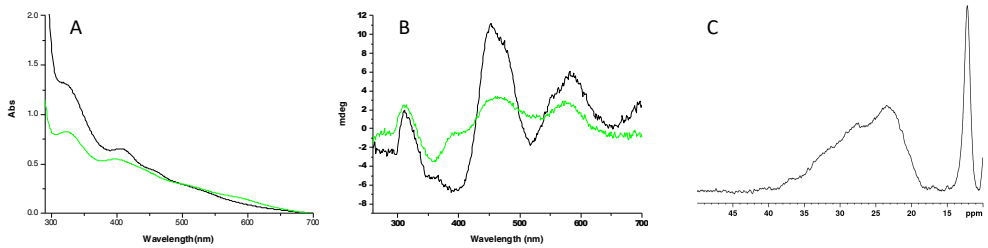
A
Abs
Wavelength(nm)
B
mdeg
Wavelength (nm)
C
ppm

Fig 7

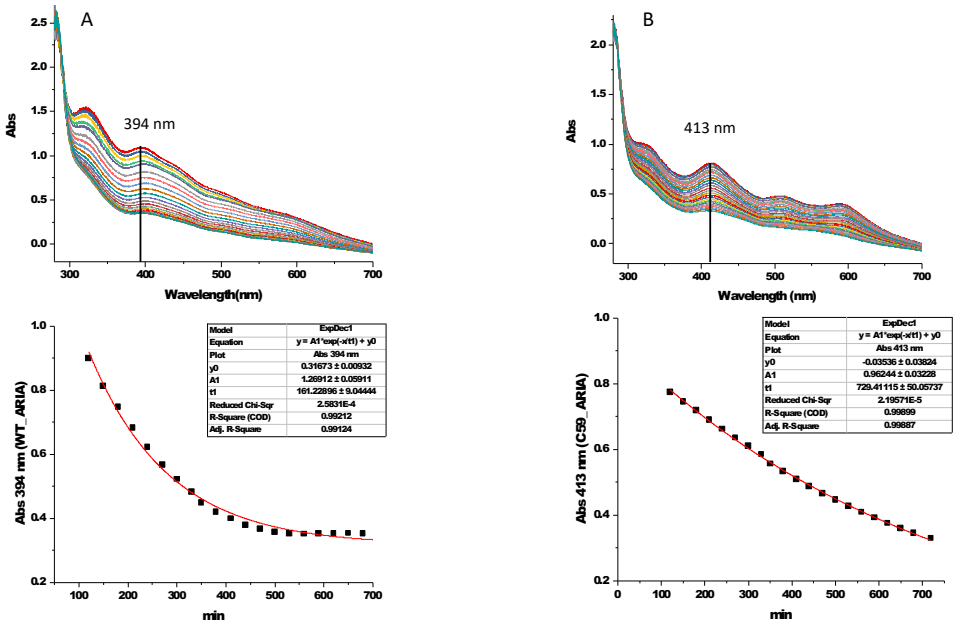
A
394 nm
Abs
Wavelength(nm)
Abs 394 nm (WT_ARIA)
min
Model ExpDec1
Equation y = A1*exp(-x/t1) + y0
Plot Abs 394 nm
y0 0.31673 ± 0.00932
A1 1.28912 ± 0.05911
t1 161.22896 ± 9.04444
Reduced Chi-Sqr 2.5831E-4
R-Square (COD) 0.99212
Adj. R-Square 0.99124
B
413 nm
Abs
Wavelength (nm)
Abs 413 nm (C59_ARIA)
min
Model ExpDec1
Equation y = A1*exp(-x/t1) + y0
Plot Abs 413 nm
y0 -0.03536 ± 0.03824
A1 0.96244 ± 0.03228
t1 729.41115 ± 50.05737
Reduced Chi-Sqr 2.19571E-5
R-Square (COD) 0.99899
Adj. R-Square 0.99887

Fig 8

3 METHODOLOGICAL ASPECTS

3.1 PROTEINS EXPRESSION AND PURIFICATION

After bioinformatics characterization and the choice of the cloning strategy, several conditions for the target protein expression have to be tested in order to obtain a high yield of soluble protein. The variables, which affect the expression of a recombinant protein, are host strain, growth medium and induction parameters (temperature, IPTG concentration and duration of induction step). A preliminary expression test is performed in a small-volume scale using at least:

- three different *E.coli* strains (e.g.: Bl21(DE3)pLysS a protease deficient strain, Rosetta(DE3) for rare codons containing genes and Origami(DE3) for disulphide containing proteins);
- three different expression vectors (containing different tags and/or fusion partners);
- three expression temperatures (37-25-17°C);
- three inducer (IPTG) concentrations and different induction times (4-6-16h).

Expression results are checked on SDS polyacrylamide gels (SDS-PAGE). This approach allows to explore a large set of expression conditions and to evaluate which one gives the best yield of soluble protein. A second expression test is performed to better refine the expression conditions before the scale-up. On the basis of these preliminary results, the expression protocol will be optimize and, in case of negative results, it is possible to change the cloning strategy, the construct or the expression system. With such an approach it is possible to find good expression conditions for many proteins. Anyway some proteins can be difficult to obtain, since *E.coli* is a prokaryote and lacks intracellular organelles, such as the endoplasmic reticulum and the Golgi apparatus, which are responsible for post-translation modifications of the produced proteins.

In case of negative results, variables like bacterial strain, induction time, the kind of vectors and expression promoters can be modified. If the main fraction of the protein is produced in the insoluble fraction, another approach is to try an *in vitro* refolding screening with different additives in order to get a folded and soluble protein. The last choices are to redesign the expressed domains or to switch to other expression system[1].

Depending on the investigating spectroscopic technique, protein expression is performed in differently composed media. In fact, when large amounts of proteins must be isolated for techniques that do not require isotopic labelling, the culture is usually

performed in a so-called rich or complex medium. Complex media contain water-soluble extracts of plant or animal tissue (e.g., enzymatically digested animal proteins such as peptone and tryptone), and for this reason are rich in nutrients and minerals, assuring a fast bacterial growth and a high expression level. Their exact composition is unknown and this can impair the reproducibility of cultures. Chemically defined (or minimal) media are composed of pure ingredients in measured concentrations, dissolved in milliQ water; in this way the exact chemical composition of the medium is known, allowing high reproducibility of protein yields and grade and type of interferents. Typically, this class of media is composed of a buffering agent to maintain culture pH around physiological values, a carbon and energy source like a simple sugar (glucose) or glycerol, and an inorganic nitrogen source, usually an ammonium inorganic salt. the bacterial strain and of the expressed proteins, various mineral salts can be added and, if necessary, growth factors such as purified amino acids, vitamins, purines and pyrimidines. Chemically defined media are easier to isotopically enrich, simply using ^{15}N and ^{13}C enriched nitrogen and carbon sources in its composition, even if isotopically enriched complex media are also commercially available.

Basically, protein purification is a series of processes intended to isolate a single type of protein from a complex mixture. Protein purification is vital for the characterization of the function, structure and interactions of the protein of interest. Separation of one protein from all others is typically the most laborious aspect of protein purification. Separation steps exploit differences in protein size, physico-chemical properties and binding affinity.

The location of expressed protein within the host will affect the selection of methods for its isolation and purification. Bacterial host may secrete the protein into the growth media, transport it to the periplasmic space, express a cytosolic protein or store it as insoluble inclusion bodies within the cytoplasm. For insoluble proteins, the first purification step is the extraction from inclusion bodies. Indeed, most of the bacterial proteins are removed by different extraction steps with native buffer conditions, while the recombinant protein is extracted from inclusion bodies with a denaturing buffer.

One of the most popular techniques for purification, which can be adopted for denatured and native state proteins, is immobilized metal ion affinity chromatography (IMAC). It is based on the specific coordination of amino acids, particularly histidine, to metals. This common technique involves engineering the sequence in such a way that 6 to 12 histidines are added to the N- or C-terminus of the protein. The polyhistidine binds strongly to divalent metal ions such as nickel. The protein can be loaded on a column

containing immobilized nickel ions, which binds the polyhistidine tag. All untagged proteins pass through the column. The protein can be eluted with imidazole, which competes with the polyhistidine tag for binding to the column, or by a decrease in pH (typically to 4.5), which decreases the affinity of the tag for the resin (**Fig 1**).

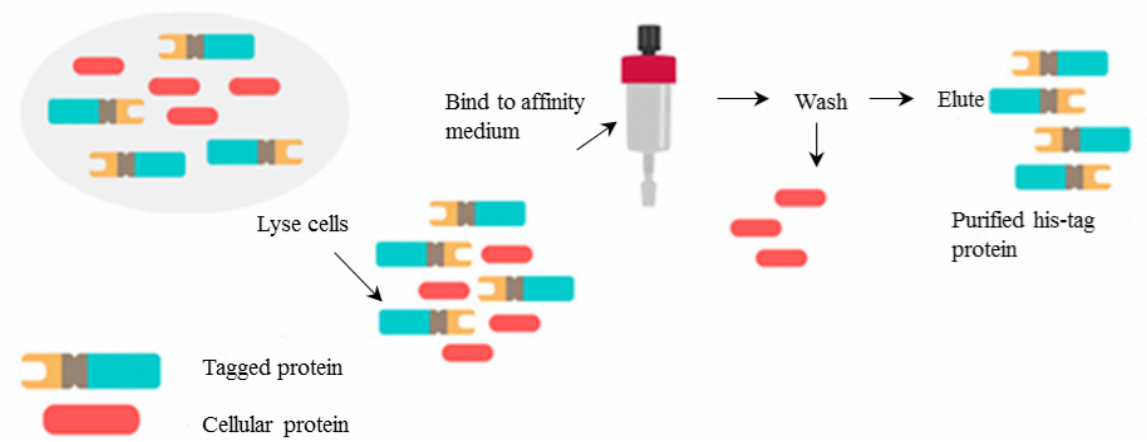

Figure 1. General purification procedure of a typical His-tagged proteins
Reprinted from Qiagen handbook for expression and purification of His-tagged proteins

After the affinity purification, the fusion-tag must be removed from the recombinant protein. Indeed, many expression vectors are engineered to express a protease clevage site between the fusion-tag and the protein. Tobacco Etch Virus (TEV), Factor Xa, Thrombin, Prescission Protease, recombinant Enterokinase are some examples of proteases that are normally used for the cleavage of tags. A second IMAC is generally performed in order to separate the fusion from the target native protein. However, if the fused protein is expressed in inclusion bodies, it must be refolded before performing the tag cleavage. This is not always possible, since fusion tags may interfere with protein folding.

Analytical size exclusion chromatography (SEC) and SEC-MALS

Gel filtration (GF) chromatography is the most common used purification step. GF is the simplest and mildest of all the chromatographic techniques; the gel in GF chromatography is composed of beads, which contain pores of given sizes. Larger molecules, which cannot penetrate the pores, move around the beads and migrate through the spaces, which separate the beads faster than the smaller molecules, which may penetrate the pores. Size exclusion can be performed on a "rough" level, separating the components of a sample in major groups to remove for example high or low molecular weight contaminants or to exchange buffers, while high resolution fractionation of bio- molecules allows to isolate one or more components of a protein mixture, to separate monomers from aggregates and to determine molecular weights or to perform a molecular weight distribution analysis, provided that suitable standards are available. Liquid chromatography (LC, SEC), may employ standard concentration detectors, such as refractive index (RI), UV absorbance, fluorescence detectors and/or light scattering detectors, in order to monitor the elution process. SEC separates according to the hydrodynamic size of the sample components and used in combination with light scattering detectors (e.g., multi-angle light scattering, MALS), enhance the analytical information by accurately determining the MW of the protein aggregates, either soluble or insoluble[2]. Static light scattering detection, usually in the multi-angle light scattering (MALS) version, is often used in a multitude of application fields. MALS detection can provide the absolute MW of proteins and protein aggregates, and the size (rms radius) can be obtained without any approximation on particle shape. Another interesting possibility is the recently developed online coupling of SEC with dynamic light scattering (DLS). Online DLS provides immediate information regarding the hydrodynamic size or the diffusion coefficient of the separated proteins and aggregate populations. In SEC, the upper size limit of detectable protein aggregate is dictated by the column characteristics; larger aggregates can be filtered out by frits in the system or by the column itself, therefore large protein aggregates may be disrupted and be overlooked in the analysis[3].

Gateway® cloning technology

The entry clones were created using two different pENTR/D-TOPO vector cloning systems; the pETG20A and the pDEST-His MBP vectors were used for generation of the expression clones. Detailed description of Gateway cloning technology is presented on the web site of Invitrogen (http://www.invitrogen.com/).

Site-directed mutagenesis

Site-directed mutagenesis was used to obtain the N-terminal domain of NFU1 and BOLA3 C59Y genes. These genes were generated using the Stratagene XL QuikChange Mutagenesis Kit. The mutations were confirmed by DNA sequencing. Amino acid substitutions were confirmed through ^{1}H-^{15}N heteronuclear single-quantum coherence (HSQC) NMR spectra.

BOLA3, GLRX5, ISCA2, expression and purification

The cDNAs coding for human glutaredoxin 5 (GLRX5), human BOLA3 and human ISCA2 were already available in our laboratory. Proteins expression and purification was performed as previously reported[4,5].BOLA3 C59Y mutant was expressed and purified following the wild type protocol.

NFU1 expression and purification

Mitochondrial human NFU1 is a 254 amino acid residues protein, containing a mitochondrial targeting signal in the N-terminal part of the sequence. Based on bioinformatic anlalysis, we cloned NFU1 full-length construct where the N-terminal 58 residues constituting the targeting signal were removed. The gene encoding the mature version of NFU1 (residues 59-254) (UniProt: Q9UMS0) was inserted into pETG20A vector, using the Gateway technology (Invitrogen), and transformed into BL21 (DE3) Gold *E.coli* strain for the expression of N-terminal His(x6)-tagged protein. Protein purification by affinity chromatography was performed in aerobic conditions and led to a soluble and pure apo-NFU1. Cells were cultivated at 37°C in 1 L of Luria-Bertani (LB) media adding ampicillin (100 μg/mL), until the OD_{600} reached 3-5. The cells were spun down (3000 rpm for 20 min) and re-suspended in 1 L of fresh LB or minimal media (with 1 g $(^{15}NH_4)_2SO_4$ and 3 g glucose) containing ampicillin (100 μg/mL). The culture was left at 37°C, 160 rpm for approximately 1 h, and then, protein expression was induced by adding 1 mM of

isopropyl β-D-1-thiogalactopyranoside (IPTG), shaking over-night at 30°C, 160 rpm. The cell paste was dissolved in the binding buffer (20 mM phosphate buffer, 500 mM NaCl, 30 mM imidazole, pH 7.8), and the cells were lysated using the CelLytic Express (C1990) (Sigma-Aldrich). The N-terminal TRX-6His-tag NFU1 protein was purified from *E. coli* using a HisTrap HP column (GE Healthcare). The TRX-6His-tag was cleaved by tobacco etch virus protease over-night at room temperature in 20 mM phosphate buffer, 500 mM NaCl, 500 mM imidazole, pH 7.8. The buffer was exchanged to binding buffer and a second His-trap chromatography column was performed to separate the digested mNFU1 from TRX-6His-tag NFU1 and TRX-6His-tag. Recovered NFU1 was pure enough to be used for spectroscopic and biochemical studies. The final yield of apo mNFU1 was ~60 mg per liter of LB culture. 2.5 mM tris (2-carboxyethyl) phosphine (TCEP) was added in all the purification steps to avoid disulfide bond formation.

C- and N- terminal NFU1 domain cloning, expression and purification

The pETG20A plasmid containing N-domain of mNFU1 (UniProt: Q9UMS0, residues 59-155 with N- terminal TRX-6His-tag; after tag cleavage the N-domain sequence contains N-terminal GSFT residues similarly to the full-length protein) was obtained by a site directed mutagenesis with a prokaryotic codon stop. The protein expression was performed likewise full length NFU1, in BL21-GOLD(DE3) cells. Cells were cultivated at 37°C in 1 L of LB or minimal media adding ampicillin (100 μg/mL), until the OD_{600} reached 0.6-0.8 and then protein expression was induced by adding 1 mM of IPTG, shaking over-night at 20°C, 160 rpm. Protein purification steps were performed following the protocol of NFU1, except that, during TEV protease cleavage, a dialysis step in the binding buffer (20 mM phosphate buffer, 500 mM NaCl, 30 mM imidazole, pH 7.8) was performed. The C-domain of NFU1 (UniProt: Q9UMS0, residues 162-247 with N-terminal GIDPFTM residues) was cloned by a TOPO cloning reaction (Invitrogen). The gene was inserted in the pET151/D-TOPO (Invitrogen) vector that present a polyhistidine (6x His) region, a TEV recognition site and a TOPO cloning site. Protein expression and purification steps do not differ from the previously described for the N-domain, and the apo form of C-domain was purified. The final yields of N- and C-domain of mNFU1 were ~60 mg per liter of LB culture. 2.5 mM TCEP was added in all the purification steps to avoid disulfide bond formation.

ISCA1 expression and purification

ISCA1 gene (UniProt: Q9BUE6) in a pDONR221 plasmid was purchased by Genescript. Gateway cloning technology (Invitrogen) was then applied to clone full-length ISCA1 gene into pDEST-HisMBP plasmid to express N-terminal Histag-MBP tagged ISCA1. The plasmid was use to transform *Escherichia coli* BL21-Gold(DE3) (Agilent) competent cells, cultivated at 37°C in Luria-Bertani (LB) media adding ampicillin (100 μg/mL), 4 mL of Solution Q and 250 μM of $FeCl_3$ per liter of sterile LB until OD_{600} reached 0.8-1. Protein expression was induced with 0.2 mM isopropyl IPTG at 18°C for 16 hours. The cells were harvested by centrifugation and resuspended in binding buffer (50 mM Tris-HCl, 500 mM NaCl, 15 mM Imidazole, pH 8.0), then lysed by sonication. The N-terminal 6Histag-MBP-ISCA1 protein was purified from the lysate using a HisTrap HP column (GE Healthcare) and then the MBP-6His-tag was cleaved by TEV treatment over-night at room temperature in binding buffer. His-trap column followed by amylose resin column were performed to separate the digested ISCA1 from MBP-6His-tag and from undigested MBP-6His-tag ISCA1. The final yield of ISCA1 was ~15 mg/L of LB culture. Apo ISCA1 was obtained performing all the purification steps under aerobic conditions, while a mixture of apo and $[2Fe\text{-}2S]^{2+}$ ISCA1 was purified under anaerobic conditions.

Determination of protein concentrations

Protein concentrations were either estimated from measuring the absorbance at 280 nm (A280) or using Bradford Reagent (Bio-Rad). Theoretical molar extinction coefficients were obtained from ProtParam analysis (http://ca.expasy.org/tools/protparam.html). Bradford reagent was used as described in the manufacturer's manual and protein concentrations were calculated using a BSA standard curve.

Chemical reconstitution

Full length [4Fe-4S] NFU1, [4Fe-4S] NFU1 C-domain and [4Fe-4S] ISCA2-ISCA1 complex were chemically Fe-S cluster reconstituted in anaerobic conditions in 50 mM Tris-HCl, 100 mM NaCl, 5 mM DTT buffer at pH 8.0 with eight-fold $FeCl_3$ and Na_2S for 16 h at room temperature. [2Fe-2S] BOLA3-GLRX5 and [2Fe-2S] BOLA3 C59Y-GLRX5 were reconstituted as previously reported for the wild type complex[6]. Chemical Fe-S cluster reconstitution was performed with protein concentrations of ~40-80 μM. Anaerobic

conditions were obtained by degassing all buffers and performing the chemical reconstitution in anaerobic chamber (**Fig. 2**) with less than 5 ppm of oxygen.

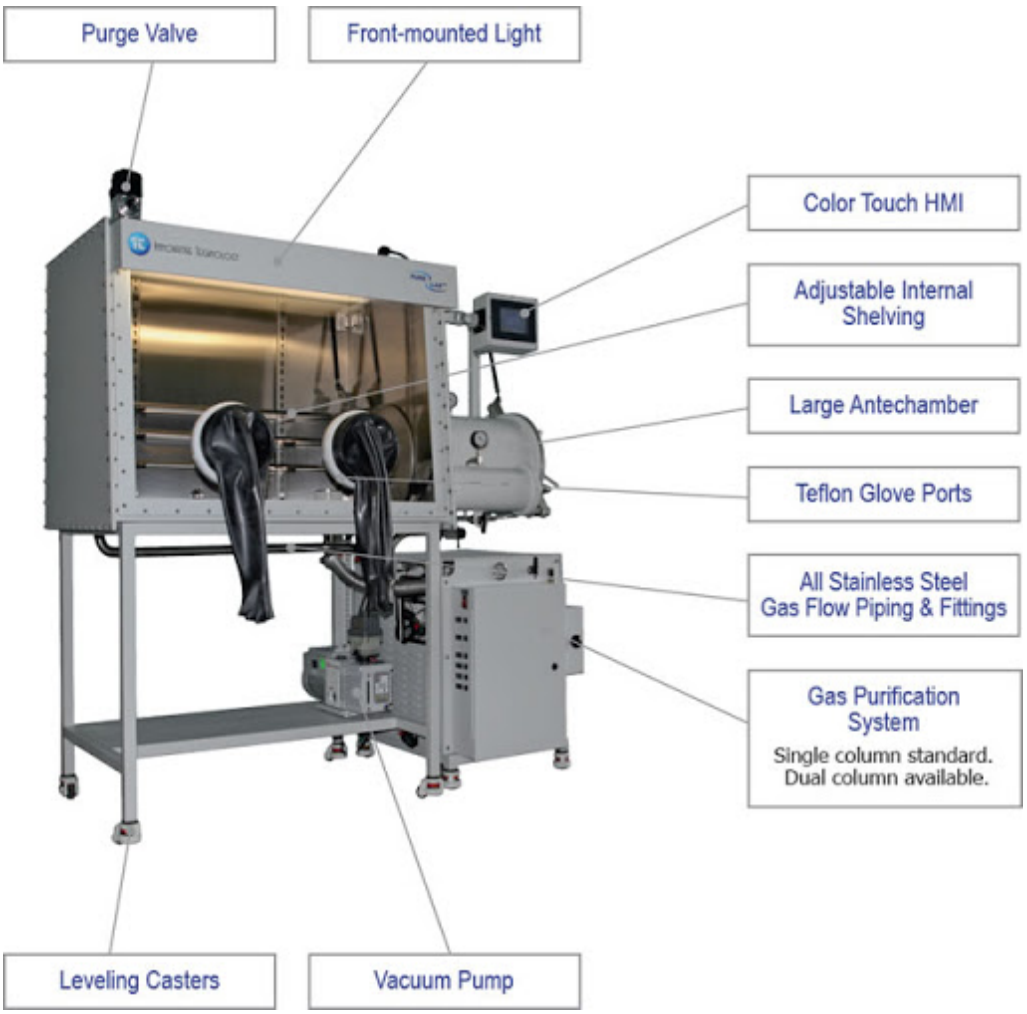

Figure 2. Schematic representation of an anaerobic chamber (glovebox)

3.2 PROTEIN CHARACTERIZATION

3.2.1 UV/VIS SPECTROSCOPY

UV/vis spectroscopy is routinely used in analytical chemistry for the quantitative determination of various types of molecules, such as transition metal ions, highly conjugated organic compounds, and biological macromolecules. The UV/vis spectrophotometer measures the intensity of light adsorbed by a sample containing the molecule(s) of interest, compared to same buffer or solvent without dissolved molecules. Solutions of transition metal ions can be colored (i.e., absorb visible light) because d-d electrons within the metal atoms can be excited.

UV-visible spectra of apo- BOLAs, holo- GLRX5, holo- GLRX5-BOLAs, holo-ISCA2, holo-ISCA2-ISCA1, holo- NFU1 in degassed 50 mM phosphate buffer at pH 7.0, 5 mM DTT, GSH5 mM or 100 mM Tris-HCl buffer and 100 mM NaCl at pH 8 were performed on a Cary 50 Eclipse spectrophotometer in the range 750-250 nm.

3.2.2 CIRCULAR DICHROISM

Circular dichrism (CD) in the middle UV range is an excellent method to analyze protein and nucleic acid secondary structure in solution and it can be used to follow the changes in folding as a function of temperature or denaturant[7,8]. CD is a phenomenon occurring when chiral molecules interact with circularly polarized light, thus absorbing left and right hand circularly polarized light with different absorption coefficients. In proteins the major optically active chiral groups are the amide bonds of the peptide backbone. Their electronic transitions adsorb differently the left vs the right polarized light, depending on the chirality of the peptide bond. Consequently, the various secondary structure motives, characterized by different backbone dihedral angles give rise to different CD spectra.

Circular dichroism spectroscopy is particularly good to:

- Determine whether a protein is folded and, if so, characterize its secondary structure;
- Compare the structures of a protein obtained from different sources (e.g. species or expression systems) or compare structures of different mutants of the same protein;
- Study the conformational stability of a protein under stress (thermal stability, pH stability, and stability to denaturants) and how this stability is altered by buffer composition or addition of stabilizers;

- Determine whether protein-protein interactions alter the conformation of the protein.

Middle UV CD analyses of the proteins (10-70μM) were performed in 50 mM phosphate buffer, NaCl 150 mM, pH 7.0 with the addition of different amounts of DTT. Spectra were acquired at 298K using a 1-mm path-length cell and a Jasco J-810 spectropolarimeter. All spectra were recorded with an average of 5 accumulations at a scan speed of 100 nm/min and at a response time of 1 s.

3.3 NMR

Nuclear magnetic resonance (NMR) spectroscopy has become established as an essential method for structural characterization in chemistry, biology, and the materials sciences[9]. The power of NMR technique with respect to other spectroscopies is due to its resolution at atomic level. Indeed, each NMR active nucleus gives rise to an individual signal in the spectrum that, when molecules contain hundreds of atoms such as proteins, can be resolved through multi-dimensional NMR experiments. Resolution becomes more difficult for larger molecules (more than 50 kDa) and puts a practical limit to the molecular size that can be studied in detail by solution NMR. The standard protocol includes the preparation of homogeneous and pure samples of the protein solution, the recording and processing of the NMR datasets, and their interpretation of the NMR data. In general, protein NMR techniques are continually being used and developed. Improvements in NMR hardware (magnetic field strength, cryoprobes) and NMR methodology, combined with the availability of molecular biology and biochemical methods for preparation and isotope labeling of recombinant proteins, have dramatically increased the use of NMR for the characterization of structure and dynamics of biological molecules in solution.

In NMR experiments, nuclear magnetic moments are oriented in accordance with a strong static magnetic field (B_0 field) in an equilibrium state until a RF (radio frequency) pulse perturb this state. The processes leading to the system returning to its equilibrium orientation are termed relaxation. As we detect only components of the magnetization transverse to the B_0 field the signal declines as the system moves back to its equilibrium state with spins in longitudinal orientation. The presence of paramagnetic species, i.e. unpaired electrons, increases in the sample the relaxation rate of nearby nuclei. This

phenomenon creates spectra annoying, i.e. the overall signal reduction, but it can also be used to obtain important structural information.

Heteronuclear Single Quantum Correlation (^{1}H-^{15}N HSQC)

1D 1H NMR spectra of biological macromolecules contain hundreds or even thousands of resonance lines which cannot be resolved with this type of spectra. So, analysis and assignment of the NMR spectra require correlations between different nuclei, which are implicitly contained in 1D spectra but often difficult to extract. Multidimensional NMR spectra provide both, increased resolution and correlations which are easy to analyze. The crucial step in increasing the dimensionality of NMR experiments lies in the extension from one to two dimensions. A higher dimensional NMR experiment consists of a combination of two-dimensional (2D) experiments.

The ^{1}H-^{15}N HSQC (Heteronuclear Single Quantum Correlation) experiment is probably the first and the most frequently recorded experiment in protein NMR[9–11]. In this experiment we have the correlation between the proton and the nitrogen. During the condensation reaction between the amino acids, the carboxyl group (-COOH) react with the amino group ($-NH_2$) to form the peptide bond (-CO-NH) with the release of a water molecule. Each residue of the protein (except proline and the NH_2 of the last amino acid at the C-terminal) has an amide proton attached to nitrogen in the peptide bond, so with the ^{1}H-^{15}N HSQC experiment we can correlate the proton with the nitrogen (^{15}N-labeled) of the amide group. If the protein is folded, the peaks are usually well dispersed in the proton/nitrogen dimension, and most of the individual peaks can be distinguished. The number of peaks in the spectrum should match the number of residues in the protein (though side chains with nitrogen-bound protons will add additional peaks). In order to analyze the nuclear magnetic resonance data, it is important to get a resonance assignment for the protein. That is to find out which chemical shift corresponds to which atom. This is typically achieved by sequential walking using information derived from several different types of NMR experiment. This barrier can be overcome with 3D NMR techniques and uniformly ^{13}C and ^{15}N labelled proteins. In the case of labelled proteins, it is possible to record an experiment that transfers magnetization over the peptide bond, and thus connects different spin systems through bonds.

3.3.1 PARAMAGNETIC NMR SPECTROSCOPY

Paramagnetic systems are defined as molecules or materials that contain one or more 'paramagnetic centers', which are atoms or ions with at least one unpaired electron. From the point of view of NMR spectroscopy the important property of these systems is that there is a hyperfine interaction between the unpaired electrons and the observed nucleus, which is the origin of the paramagnetic shift and shift anisotropy (SA), the paramagnetic relaxation enhancement (PRE), and additional sources of substantial broadening due to large magnetic susceptibility effects. These interactions potentially yield important information about the system:

- the bonding between the atoms and ions and their spatial arrangement.
- the delocalization of the unpaired electrons onto the coordinating atoms and ligands.
- the dynamics of the system
- details about the crystal-field splitting and consequent optical properties (particularly relevant in the case of lanthanide ions)

However, the paramagnetism can also cause problems when attempting to both acquire and interpret the NMR data. The problem of acquisition arises because the paramagnetic shifts and SAs are often very large, with the result that excitation of the nuclei with practicable radio-frequency (RF) powers can be both inefficient and not sufficiently broad banded, and the large PREs cause the coherences to decay rapidly once they have been excited. The interpretation of the NMR data is not always intuitive, and usually requires the availability of reliable theoretical models. Unpaired electrons are found in metal ions as well as organic radicals, both of which can be used to study proteins. There exists a variety of paramagnetic labels, which can be attached to the proteins in specific locations. The most common type of paramagnetic label is linked to cysteine residues using disulfide bonds[12,13]. In the case of Fe–S clusters, the magnetic coupling between the iron ions determines various electron spin energy levels whose separation depends on the magnetic coupling constants[14]. As already said, the coupling of the nuclear spins with these multiple electron spin levels significantly affect both the chemical shifts and the relaxation rates[15,16], and NMR signals results sharper than those observed for isolated iron ions. Due to these properties, NMR spectra

dramatically changes following oxidation state or cluster composition. The hyperfine shifts, their temperature dependencies and the relaxation rates of nuclei of cluster-bound residues allowed to elucidate the magnetic coupling patterns occurring in [2Fe–2S], [3Fe–4S] and [4Fe–4S] clusters[17,18].

3.3.2 SAMPLE PREPARATION

A soluble protein sample is required to perform the NMR experiments and to successfully solve the 3D structure of biological macromolecules. In fact, an inhomogeneous preparation and/or aggregation of the protein may severely compromise the structure determination. Therefore, the first step in every protein NMR study involves optimization of the experimental conditions such as pH, ionic strength, and temperature that can often be adjusted to mimic physiological conditions. The target macromolecule should be stable in the optimized conditions as long as possible. Proteins should be isotope enriched in ^{15}N and ^{13}C for an efficient structure determination because the most abundant carbon isotope (^{12}C) is not active and the most abundant nitrogen isotope (^{14}N) is quadrupolar and has undesired NMR properties. Triple labelled samples, ^{2}H, ^{13}C and ^{15}N, are necessary for protein with larger size (more than 30 kDa).

3.4 MOLECULAR DOCKING FOR THE STUDY OF PROTEIN-PROTEIN INTERACTION

Molecular docking have been investigated through the program HADDOCK 2.2[19,20]. In the latter the docking process is driven by ambiguous (AIRs) and unambiguous interaction restraints, which are ambiguous and unambiguous distances between all solvent exposed residues involved in the interaction. HADDOCK protocol defines active and passive residues. The active residues are all residues showing a significant chemical shift perturbation after the formation of the complex, with a solvent accessibility higher than 50%; the passive residues are the residues which are surface neighbors of the active and have a solvent accessibility usually higher than 50%.

The docking protocol consists of three consecutive steps:

- rigid body minimization driven by interaction restraints (it0), in which 1000 structures of the complex have been generated;
- the best 200 structures in terms of total intermolecular energy were further submitted to the semiflexible simulated annealing in which side-chains and backbone atoms of the interface residues are allowed to move (it1);
- final refinement in Cartesian space in an explicit solvent (water).

The 200 structures obtained are clustered using a threshold of 7.5 Å of RMSD among the structure of the cluster. Clusters containing at least 4 structures were considered and analyzed on the basis of HADDOCK score value (HADDOCK score: $1.0*E_{vdw}+0.2*E_{elc}+0.1*E_{dist}+1.0*E_{solv}$, where the four terms are respectively: van der Walls energy, electrostatic energy, distance restrains energy and desolvation energy), RMSD and Buried Surface Area.

REFERENCES

(1) Tsumoto, K.; Ejima, D.; Kumagai, I.; Arakawa, T. Practical Considerations in Refolding Proteins from Inclusion Bodies. *Protein Expression and Purification*. 2003. https://doi.org/10.1016/S1046-5928(02)00641-1.

(2) Mahler, H. C.; Friess, W.; Grauschopf, U.; Kiese, S. Protein Aggregation: Pathways, Induction Factors and Analysis. *Journal of Pharmaceutical Sciences*. 2009. https://doi.org/10.1002/jps.21566.

(3) Den Engelsman, J.; Garidel, P.; Smulders, R.; Koll, H.; Smith, B.; Bassarab, S.; Seidl, A.; Hainzl, O.; Jiskoot, W. Strategies for the Assessment of Protein Aggregates in Pharmaceutical Biotech Product Development. *Pharmaceutical Research*. 2011. https://doi.org/10.1007/s11095-010-0297-1.

(4) Banci, L.; Brancaccio, D.; Ciofi-Baffoni, S.; Del Conte, R.; Gadepalli, R.; Mikolajczyk, M.; Neri, S.; Piccioli, M.; Winkelmann, J. [2Fe-2S] Cluster Transfer in Iron-Sulfur Protein Biogenesis. *Proc. Natl. Acad. Sci. U. S. A.* **2014**. https://doi.org/10.1073/pnas.1400102111.

(5) Uzarska, M. A.; Nasta, V.; Weiler, B. D.; Spantgar, F.; Ciofi-Baffoni, S.; Saviello, M. R.; Gonnelli, L.; Mühlenhoff, U.; Banci, L.; Lill, R. Mitochondrial Bol1 and Bol3 Function as Assembly Factors for Specific Iron-Sulfur Proteins. *Elife* **2016**. https://doi.org/10.7554/eLife.16673.

(6) Nasta, V.; Giachetti, A.; Ciofi-Baffoni, S.; Banci, L. Structural Insights into the Molecular Function of Human [2Fe-2S] BOLA1-GRX5 and [2Fe-2S] BOLA3-GRX5 Complexes. *Biochim. Biophys. Acta - Gen. Subj.* **2017**. https://doi.org/10.1016/j.bbagen.2017.05.005.

(7) Kelly, S. M.; Jess, T. J.; Price, N. C. How to Study Proteins by Circular Dichroism. *Biochimica et Biophysica Acta - Proteins and Proteomics*. 2005. https://doi.org/10.1016/j.bbapap.2005.06.005.

(8) Banerjee, B.; Misra, G.; Ashraf, M. T. Circular Dichroism. In *Data Processing Handbook for Complex Biological Data Sources*; 2019. https://doi.org/10.1016/B978-0-12-816548-5.00002-2.

(9) Wüthrich, K. NMR with Proteins and Nucleic Acids. *Europhys. News* **1986**. https://doi.org/10.1051/epn/19861701011.

(10) Jeener, J.; Meier, B. H.; Bachmann, P.; Ernst, R. R. Investigation of Exchange Processes by Two-Dimensional NMR Spectroscopy. *J. Chem. Phys.* **1979**. https://doi.org/10.1063/1.438208.

(11) Kay, L. E.; Ikura, M.; Tschudin, R.; Bax, A. Three-Dimensional Triple-Resonance NMR Spectroscopy of Isotopically Enriched Proteins. *J. Magn. Reson.* **1990**. https://doi.org/10.1016/0022-2364(90)90333-5.

(12) Gayda, J. P.; Bertrand, P.; Theodule, F. X.; Moura, J. J. G. Three-Iron Clusters in Iron-Sulfur Proteins: An EPR Study of the Exchange Interactions. *J. Chem. Phys.* **1982**. https://doi.org/10.1063/1.444281.

(13) Hille, R.; Yoshida, T.; Tarr, G. E.; Williams, C. H.; Ludwig, M. L.; Fee, J. A.; Kent, T. A.; Huynh, B. H.; Münck, E. Studies of the Ferredoxin from Thermus Thermophilus. *J. Biol. Chem.* **1983**.

(14) Beinert, H.; Holm, R. H.; Münck, E. Iron-Sulfur Clusters: Nature's Modular, Multipurpose Structures. *Science (80-.).* **1997**. https://doi.org/10.1126/science.277.5326.653.

(15) Banci, L.; Bertini, I.; Turano, P.; Tient, M.; Kirko, T. K. *Proton NMR Investigation into the Basis for the Relatively High Redox Potential of Lignin Peroxidase*

(Horseradish Peroxidase/Cytochrome c Peroxidase/Lignin Blodegradation/Phanerochaete Chrysosporium); 1991.

(16) Lin, I. J.; Gebel, E. B.; Machonkin, T. E.; Westler, W. M.; Markley, J. L. Changes in Hydrogen-Bond Strengths Explain Reduction Potentials in 10 Rubredoxin Variants. *Proc. Natl. Acad. Sci. U. S. A.* **2005**. https://doi.org/10.1073/pnas.0505521102.

(17) Banci, L.; Camponeschi, F.; Ciofi-Baffoni, S.; Piccioli, M. The NMR Contribution to Protein–Protein Networking in Fe–S Protein Maturation. *Journal of Biological Inorganic Chemistry*. 2018. https://doi.org/10.1007/s00775-018-1552-x.

(18) Bertini, I.; Luchinat, C.; Piccioli, M. [15] Paramagnetic Probes in Metalloproteins. In *Methods in Enzymology*; 2001. https://doi.org/10.1016/S0076-6879(01)39320-5.

(19) Dominguez, C.; Boelens, R.; Bonvin, A. M. J. J. HADDOCK: A Protein-Protein Docking Approach Based on Biochemical or Biophysical Information. *J. Am. Chem. Soc.* **2003**. https://doi.org/10.1021/ja026939x.

(20) Van Zundert, G. C. P.; Rodrigues, J. P. G. L. M.; Trellet, M.; Schmitz, C.; Kastritis, P. L.; Karaca, E.; Melquiond, A. S. J.; Van Dijk, M.; De Vries, S. J.; Bonvin, A. M. J. J. The HADDOCK2.2 Web Server: User-Friendly Integrative Modeling of Biomolecular Complexes. *J. Mol. Biol.* **2016**. https://doi.org/10.1016/j.jmb.2015.09.014.

4 CONCLUSIONS AND PERSPECTIVES

4.1. CONCLUSIONS AND PERSPECTIVES

NFU1 is a late acting factor in iron sulfur cluster biogenesis, highly conserved from bacteria to humans. This protein evolved trough the tree of life to have specific physiological role and partners, in order to protect cells from oxidation and mitochondrial impairment. Previous studies classified human NFU1 as a [4Fe-4S] cluster *scaffold* protein. During my PhD I characterize apo and holo NFU1, highlighting new mechanisms by which NFU1 carries on its function.

First of all, data showed that the process of cluster transfer and assembly from $[2Fe\text{-}2S]^{2+}$ GLRX5-BOLA3 to NFU1 brings directly to the formation of a $[4Fe\text{-}4S]^{2+}$ cluster on NFU1. This mechanism might be alternative to the pathway involving the [4Fe-4S] cluster transfer from the ISCA1-ISCA2 complex to NFU1[2,3]. Considering the different yeast phenotypes on yeast BOLA3 and NFU1 (i.e. the defect in yeast lacking Bol3 is modest, while the defects are more pronounced in *nfu1*Δ cells), and that the yeast homologue of NFU1 has been implicated to work under oxidative metabolism, this second pathway might be mainly required under oxidative cellular conditions[4]. In conclusion, this new possible pathway establishes a role of NFU1 as an *assembler* and not only as a *scaffold* of the [4Fe-4S] clusters and may be alternative to the ISCA1-ISCA2 [4Fe-4S] assembly. Otherwise, our data do not support the previously proposed model defining BOLA3 as the assistant of the [4Fe-4S] cluster transfer from NFU1 to mitochondrial target proteins. No interaction between the two proteins has been detected in all tested conditions. According to this suggestion, *E. coli* NFU1 homologue, NfuA, efficiently transfers the [4Fe-4S] cluster to its target protein lipoyl synthase (LIAS) after each enzymatic turnover with any requirements of other proteins[5].

In our second work, we found the interaction between ISCA1 and NFU1. This interaction involves specifically the C-domain of NFU1 where the two helices of NFU1 encasing the cluster binding CXXC motif are involved in the interaction with ISCA1. The proposed molecular pathways orchestrated by ISCA1, ISCA2 and NFU1 to assemble and make available [4Fe-4S] clusters for mitochondrial apo client proteins fully rationalizes the *in vivo* data previously reported. Considering this molecular model, it resulted that ISCA1 is the crucial protein activating all [4Fe-4S] protein maturation pathways. Further analysis, for example, SAXS and ITC experiments may be used to better characterize the structural and thermodynamic properties of the observed complexes.

For what concerned the BOLA3 C59Y mutant, the protein present similar affinity for GLRX5 as the wild type does. Consequently, the mutant is also able to be complexed with its physiological partner, forming a stable hetero-complex.

From UV-vis spectroscopy investigation, it resulted that the [2Fe-2S] cluster on C59Y BOLA3-GLRX5 is not fully lost, once exposed to oxygen for 12h. Differently, after the same time of exposure of [2Fe-2S] BOLA3-GLRX5 to oxygen, cluster is completely undetectable. These data suggest that Cys 59 to Tyr mutation stabilizes the cluster, changing the distances between the cluster and the coordinating residues. Fluorescence data did not provide results about tyrosinate formation during the cluster binding. Further studies are needed to confirm this hypothesis, and to clarify how the substitution of cysteine 59 with a tyrosine inhibits the BOLA3 function in this specific side of the pathway. On the other hand, the milder patient phenotype presenting this protein variants, could be a consequence of genetic or environmental factors, that are able to modify the impact of these mutation[6].

Understanding the molecular mechanisms underline proteins interactions, cofactor assembly and transfer between partners, is essential to support *in vivo* data about human diseases.

REFERENCES

(1) Nasta, V.; Giachetti, A.; Ciofi-Baffoni, S.; Banci, L. Structural Insights into the Molecular Function of Human [2Fe-2S] BOLA1-GRX5 and [2Fe-2S] BOLA3-GRX5 Complexes. *Biochim. Biophys. Acta - Gen. Subj.* **2017**. https://doi.org/10.1016/j.bbagen.2017.05.005.

(2) Cameron, J. M.; Janer, A.; Levandovskiy, V.; MacKay, N.; Rouault, T. A.; Tong, W. H.; Ogilvie, I.; Shoubridge, E. A.; Robinson, B. H. Mutations in Iron-Sulfur Cluster Scaffold Genes NFU1 and BOLA3 Cause a Fatal Deficiency of Multiple Respiratory Chain and 2-Oxoacid Dehydrogenase Enzymes. *Am. J. Hum. Genet.* **2011**. https://doi.org/10.1016/j.ajhg.2011.08.011.

(3) Navarro-Sastre, A.; Tort, F.; Stehling, O.; Uzarska, M. A.; Arranz, J. A.; Del Toro, M.; Labayru, M. T.; Landa, J.; Font, A.; Garcia-Villoria, J.; Merinero, B.; Ugarte, M.; Gutierrez-Solana, L. G.; Campistol, J.; Garcia-Cazorla, A.; Vaquerizo, J.; Riudor, E.; Briones, P.; Elpeleg, O.; Ribes, A.; Lill, R. A Fatal Mitochondrial Disease Is Associated with Defective NFU1 Function in the Maturation of a Subset of Mitochondrial Fe-S Proteins. *Am. J. Hum. Genet.* **2011**. https://doi.org/10.1016/j.ajhg.2011.10.005.

(4) Melber, A.; Na, U.; Vashisht, A.; Weiler, B. D.; Lill, R.; Wohlschlegel, J. A.; Winge, D. R. Role of Nfu1 and Bol3 in Iron-Sulfur Cluster Transfer to Mitochondrial Clients. *Elife* **2016**. https://doi.org/10.7554/eLife.15991.

(5) McCarthy, E. L.; Booker, S. J. Destruction and Reformation of an Iron-Sulfur Cluster during Catalysis by Lipoyl Synthase. *Science (80-.).* **2017**. https://doi.org/10.1126/science.aan4574.

(6) Stutterd, C. A.; Lake, N. J.; Peters, H.; Lockhart, P. J.; Taft, R. J.; Van Der Knaap, M. S.; Vanderver, A.; Thorburn, D. R.; Simons, C.; Leventer, R. J. Severe Leukoencephalopathy with Clinical Recovery Caused by Recessive BOLA3 Mutations. In *JIMD Reports*; 2019. https://doi.org/10.1007/8904_2018_100.

Ringraziamenti

Rare sono le persone che usano la mente, poche coloro che usano il cuore e uniche coloro che usano entrambi

Rita Levi-Montalcini

Tre anni sono pochi nell'arco di una vita, tantissimi quando li vivi.
Ci sono stati momenti dolorosi, momenti di sconforto, di paura.
Tanti, tantissimi, di gioia, calore, vittoria e fame di conoscenza.
La mia più grande fortuna sono state le persone che ho conosciuto e con le quali ho avuto l'occasione di lavorare. Come dice Rita Levi-Montalcini, ho trovato persone rare, persone che usano la mente in modo brillante e ispirante, come la mia tutor, Lucia Banci, che qui ringrazio. Lo stesso posso dire di Simone Ciofi, insegnante e ricercatore eccezionale.
Sono innumerevoli le persone piene di cuore che hanno costellato il mio percorso, Giovanni, Domenico, Sara, Alessio, Pan, Gaia. Le ragazze di stanza 2, Silvia, Anna, Deborah che mi hanno accompagnato non solo nelle gioie e i dolori, ma anche in laute merende e pause sigaretta.
I miei primissimi compagni di viaggio, Lucia, Matteo, Cristina e Nihar. Le ricercatrici Ferro-zolfiste, Francesca e Veronica, sempre disponibili a sistemare qualche pasticcio. Il team di Genexpress, con tutta la loro accoglienza e premura.
Agnese che non finirò mai di ringraziare, compagna di pianti e tisane, ad oggi vera amica e compagna di vita.

Un ringraziamento speciale alle mie amiche storiche, Giorgia e Federica alle quali posso dire soltanto: *Senti come mi batte forte il tuo cuore*.
A Gaia, che c'è da 15 anni in tutto quello che faccio.
Ringrazio Sara e Benedetta, sempre accanto a me ad ogni esame, ad ogni gradino di questo percorso, lontane ma mai nel cuore.
Alla splendida donna che sta diventando mia sorella, ringrazio ogni giorno di poter crescere mano nella mano con lei.
Ringrazio mia nonna e i suoi continui incoraggiamenti, senza i quali arrivare qui non sarebbe stato possibile.
Ringrazio mia madre, che mi ha insegnato a vivere con determinazione e coraggio, e quando mi scordo come si fa, viene sempre a ricordarmelo.

Ringrazio infinitamente le maestre Labodif, Gianna e Gio, per la loro prospettiva rivoluzionaria. Grazie a loro ho definito il paesaggio. Ringrazio tutte le compagne di classe della H e della C, con le quali condivido parte di questo paesaggio.

In ultimo ringrazio gli altri e le altre, le persone che sono passate, quelle che se ne sono andate, quelle che anche solo per un po', hanno aperto una porta di se stessi con me ed io con loro.